THE BOUNDARY LAYER WIND REGIME OF A REPRESENTATIVE TROPICAL AFRICAN REGION, CENTRAL SUDAN

E. H. ABU BAKR

THE BOUNDARY LAYER WIND REGIME OF A REPRESENTATIVE TROPICAL AFRICAN REGION, CENTRAL SUDAN

THE BOUNDARY LAYER WIND REGIME OF A REPRESENTATIVE TROPICAL AFRICAN REGION, CENTRAL SUDAN

PROEFSCHRIFT

DOOR

EIMAN HASSAN ABU BAKR

GEBOREN TE ATBARA (SUDAN)

They that sow in tears,

shall reap in joy.

CONTENTS

1. GENERAL INTRODUCTION

2. THEORETICAL BACKGROUND

3. PRELIMINARY SURVEY OF THE PHYSICAL ENVIRONMENT AND THE WIND POTENTIAL IN THE SUDAN

4. DATA BASE

5. A BOUNDARY LAYER MODEL FOR THE DETERMINATION OF HOURLY SURFACE WIND CHARACTERISTICS IN A REPRESENTATIVE TROPICAL AFRICAN REGION

6. CHARACTERISTICS OF THE DIURNAL COURSE OF THE UPPER AIR WIND IN CENTRAL SUDAN

Notation

C H A P T E R 1

GENERAL INTRODUCTION

CHAPTER 1

GENERAL INTRODUCTION

1.1 Background and purpose

During the last decade several methods have been developed for temperate latitudes (in Europe) to determine the wind potential (e.g. Petersen et al., 1981, Wieringa and Rijkoort, 1983, Duchêne-Marullaz, 1977). For determination of the potential wind in developing (tropical) countries, however, the situation is different. Many mechanisms governing the air flow in the tropics, such as the extreme stable climate and the monsoon phenomena, are different from the air flow mechanisms in temperate latitudes. The standard methods developed for temperate latitudes are therefore not necessarily applicable in tropical countries. Moreover, no methods or theories exist which can accurately predict the wind potential in low latitudes.

One of the major difficulties one encounters with respect to the application of wind energy in developing countries is the problem of accurately assessing the wind potential. The problem is mainly due to the scarcity and unreliability of the available wind data. For a number of reasons the general situation with respect to these data can be indicated by the following items:

1. The purpose of meteorological stations in tropical countries is not to determine the wind potential but mostly to supply information for agriculture (wind measurements at about 2 m height) or, in a few areas, for airports. The airport stations are expected to give relatively reliable data; the maintenance of the measuring equipment is usually reasonable and the time interval of measurements is acceptable.
2. It often occurs that anemometers are situated in areas which later became more populated. A consequence of the increased density of buildings and trees is that the magnitude of the measured wind data is influenced dramatically.

2

3. At many stations only the wind direction is measured (using a simple vane at a height of 10 m above the ground) and the wind speed is only roughly estimated according to the Beaufort scale (visual estimation of wind speed), which is insufficiently accurate for wind energy assessment studies.

4. The frequency of measurements is mostly too low for estimating the wind energy potential.

5. Maintenance of wind measuring equipment is generally very poor. Also the time interval of anemometer calibration is mostly not satisfactory.

6. The density of stations is very low (compare for instance the 57 stations over an area of 3.6×10^4 km^2 in the Netherlands with the 53 stations over 2.5×10^6 km^2 in the Sudan).

The above points clearly indicate the need for a method to determine the wind potential in tropical regions. However, these very points also show the problems of the development of such a method. In this thesis we made a first step towards the solution of the outstanding problem of wind speed estimation by choosing a representative tropical region for a detailed study of the wind sources. Central Sudan was taken for this purpose for the following reasons:

1. Sudan is the largest tropical country in Africa and it comprises three different vast climatological areas (desert, savannah and tropical forest, the latter being of secondary importance for wind energy application) which are very representative for other regions in the African Sahel zone.

2. Central Sudan is land locked, which eliminates the problem of considering the effect of the energy input from tropical seas.

3. The topography of the surroundings of the region is very homogeneous (flat savannah over large distances).

4. The application of wind energy is feasible since the average wind speed is about 4 m/s (which is sufficient for wind pumps) and the country is flat with a very low population density. During the dry seasons and during the periodical occurrence of drought there is a large demand for water pumping for irrigation and drinking water. The irrigation with wind pumps is estimated to be four times cheaper than irrigation by means of diesel pumps. This is concluded from the water pumping project in the Khartoum area, see Costa 1985 (Netherlands-Sudan bilateral aid program).

5. In the Sudan there are meteorological data available, including wind data, over a period of at least 30 years. Also upper air data have been collected since 1930. In the Central Sudan region the station density and observation frequency is relatively high compared to other regions in the Sudan.

1.2 *Survey of the contents of the thesis*

The background theory concerning certain topics of the PBL of Central Sudan is discussed in chapter 2.

Chapter 3 provides an overview of the climatological and geographical characteristics of the region.

In chapter 4 we discuss the quality of the data and the data base constructed. Since the quality of the obtained data could have been questionable, a detailed study of the stations history was carried out by means of visiting some of the stations to investigate the station surroundings, checking the measuring equipment and the quality of the obtained routine meteorological data (about 330×10^3 observations, kindly supplied by the Sudanese Meteorological Department in Khartoum with support of the WMO). In this chapter we also deal with a qualitative data analysis. Among other topics, we discuss the frequency distribution of the wind velocity. It was found that the monthly distribution is much more important than the annual distribution in considering wind energy application in tropical regions.

In chapter 5 we describe one of the major results of this research: the development of a transposition boundary layer model which computes the average diurnal cycle of the surface wind speed for an arbitrary location where no wind data are available. The applicability of wind energy at an arbitrary location in Central Sudan can therefore be estimated. The basic assumptions of this model are concluded from the stationary character of the climate and the flat topography of the region. We also show in this chapter that the model results are in good agreement with the measured data.

In chapter 6 a preliminary study is presented of important aspects of the PBL, which contribute to the understanding of the diurnal wind course behaviour. The diurnal course of the height of the PBL is computed using only the measured surface data and the midday temperature profile. The computational results are in good agreement with the estimated values from the upper air data. In this chapter we also investigate the veering of the wind

with height over the region. The thermal advection shows a considerable variation over the region in the nighttime while during daytime it shows homogeneity over the region.

C H A P T E R 2

THEORETICAL BACKGROUND

CHAPTER 2

THEORETICAL BACKGROUND

2.1 *Introduction*

In this chapter we give a theoretical introduction to some selected topics in planetary boundary layer (PBL) physics for tropical regions. Our discussion is focussed on the theory used in the analysis of chapter 4, 5 and 6. This chapter may be of special interest to readers who are not completely familiar with this field and may provide them with some theoretical background information for the above mentioned chapters. For more detailed information about this chapter see e.g. Monin and Yaglom 1971, Holton 1972, Oke 1978, Plate 1982, and Dutton 1986.

In section 2.2 we describe the equation of motion and its application to tropical regions. Then, in section 2.3, the potential temperature and the atmospheric stability are dealt with and in section 2.4 the geostrophic and thermal wind are discussed. Section 2.5 and 2.6 review the surface heat flux and the surface layer wind profile, respectively. Section 2.6 also contains an introduction to the Monin-Obukhov similarity theory. Finally, in section 2.7, the planetary boundary layer structure is shortly discussed.

2.2 *The momentum equation*

The momentum equation usually used for the atmospheric PBL is a version of the Navier-Stokes equation for an incompressible fluid with constant viscosity plus a term arising from the acceleration of the reference system due to the earth's rotation. If the z-axis is the vertical axis and the x and y axis are the coordinates of the horizontal plane (the y-axis northwards and x-axis eastwards), then the equation of motion is given by:

$$\frac{d\vec{V}}{dt} = -\frac{1}{\rho} \nabla P + \nu \nabla^2 \vec{V} - g\vec{k} - f (\vec{k} \times \vec{V}), \qquad (2.1)$$

where $f = 2\Omega\sin\phi$ is the Coriolis parameter, ϕ is the latitude (or the angle the horizontal plane makes with the axis of rotation of the earth), Ω is the

earth's angular speed of rotation and $\vec{k}$ is the vertical unit vector. The meaning of the other notations are listed in appendix A.

Since the atmospheric boundary layer (ABL) is turbulent, we write all parameters according to Reynolds approximation as a mean value plus a time dependent value:

$$\vec{V} = \overline{\vec{V}} + \vec{V}', \quad \overline{\rho} = \overline{\rho} + \rho', \quad P = \overline{P} + P'.$$

Substituting this in equation (2.1) and taking the mean and further omitting the averaging sign of $\vec{V}$, $\overline{\rho}$, and $\overline{P}$ we get the well-known equation

$$\frac{d\vec{V}}{dt} = -\frac{1}{\rho} \nabla P + \nu \nabla^2 \vec{V} - g\vec{k} - f(\vec{k} \times \vec{V}) - \overline{(\vec{V}.\nabla)\vec{V}'} \ . \tag{2.2}$$

Since in the ABL the horizontal length scale (which is of the order of 100 km) is much larger than the vertical length scale (order of 1 km), the momentum equation (2.2) can be simplified to the following formulae for the horizontal wind vector components u (along wind) and v (cross wind):

$$\frac{du}{dt} = -\frac{1}{\rho} \frac{\partial P}{\partial x} + fv + \frac{1}{\rho} \frac{\partial \tau_x}{\partial z} \ , \tag{2.3}$$

$$\frac{dv}{dt} = -\frac{1}{\rho} \frac{\partial P}{\partial y} - fu + \frac{1}{\rho} \frac{\partial \tau_y}{\partial z} \ , \tag{2.4}$$

where

$$\tau_x = -\rho \overline{u'w'} + \rho\nu \frac{\partial u}{\partial z} \ , \tag{2.5}$$

$$\tau_y = -\rho \overline{v'w'} + \rho\nu \frac{\partial v}{\partial z} \ . \tag{2.6}$$

For the vertical component equation usually only the static part is used, resulting in the hydrostatic equation:

$$\frac{\partial p}{\partial z} = -\rho g \ . \tag{2.7}$$

In equations 2.5 and 2.6 τ_x and τ_y are the turbulent stress components and $\overline{u'w'}$ and $\overline{v'w'}$ are called Reynolds stresses; they are formally the result of Reynolds' separation of the fluctuations (u',v',w') from the averages. Their significance is that they describe vertical transport of horizontal motion by

turbulence. If we assume the direction of the surface stess τ_s, at the level $z = z_0$, to be along the x-axis, equation 2.5 and 2.6 will be $\tau_y = - \rho \overline{v'w'} = 0$ and $\tau_x = \tau_s = - \rho \overline{u'w'} = \rho u_*^2$. Here u_* is called the friction velocity and is an important parameter for describing effects of turbulence on wind profiles (see section 2.6).

2.3 *Potential temperature and atmospheric stability*

The potential temperature (θ) is defined as the temperature a parcel of air would have if it were expanded or (compressed) adiabatically from its present state (P and T) to a pressure of 1000 mb;

$$\theta = T \left(\frac{1000}{P}\right)^{R/c_p} . \tag{2.8}$$

Differentiating equation (2.8) as a function of height we obtain

$$\frac{\partial \theta}{\partial z} = \frac{\theta}{T} \left(\frac{\partial T}{\partial z} + \Gamma_d\right) , \tag{2.9}$$

where Γ_d ($= \frac{g}{c_p}$ = 10 K/km) is known as the dry adiabatic lapse rate.

In equation (2.9) the term $\partial \theta / \partial z$ is an important criterion for the stability of a dry atmosphere. In a stable atmosphere ($\frac{d\theta}{dz} > 0$) an air parcel displaced adiabatically upward will have a lower temperature than its surrounding and thus will be displaced downward again. In an unstable atmosphere ($\frac{\partial \theta}{\partial z} < 0$) an air parcel displaced from its equilibrium will tend to move away from its original position. In a neutral atmosphere ($\frac{\partial \theta}{\partial z} = 0$) an air parcel displaced adiabatically will remain at the temperature of the surrounding and thus remains at the level to which it is displaced since the temperature gradient balances the adiabatic rate.

In a convective PBL the potential temperature is approximately constant due to turbulent mixing, while above the PBL it shows a sharp increase (with large values of $\frac{\partial \theta}{\partial z}$), due to the non-turbulent stable air aloft. The transition layer, where the cold air from the PBL entrains to the warmer upper air, is referred to as an inversion (see chapter 6). Consequently the potential temperature gradient is an important parameter for indicating the height of the PBL.

In the Sahel region the lapse rate ($\frac{\partial \theta}{\partial z}$) above the inversion is very large

due to the cumulative large scale subsidence (which is related to the downward branch of the Hadley cell). This results in a large stability aloft and a substantially lower PBL height compared to other regions at similar latitudes.

2.4 *Geostrophic wind and thermal wind*

When the atmospheric flow is frictionless, horizontal and with zero acceleration, the existing wind is said to be geostrophic. A parcel of air which is initially at rest starts to move due to the pressure forces. The earth rotation (Coriolis force) will deflect the parcel to the right of the original direction of motion (northern hemisphere) and turn it away from the direction that originally was perpendicular with the isobars (see fig. 2.1). As the speed increases the Coriolis force increases, until the motion is finally parallel to the isobars with the Coriolis force and the pressure gradient forces equal in magnitude and opposite in direction. In the final state the only acting forces are the Coriolis force, pressure gradient and gravity. In such a geostrophic equilibrium the momentum equation is:

$$fv_g = \frac{1}{\rho} \frac{\partial P}{\partial x} \, , \tag{2.10}$$

$$fu_g = -\frac{1}{\rho} \frac{\partial P}{\partial y} \, , \tag{2.11}$$

$$g = -\frac{1}{\rho} \frac{\partial P}{\partial z} \, . \tag{2.12}$$
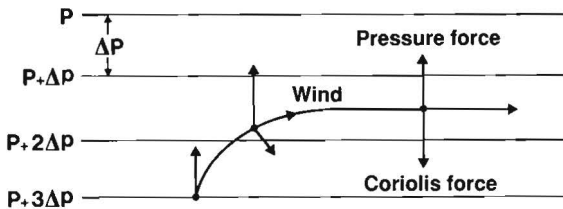
Fig. 2.1
Gradient adjustment towards
geostrophic wind equilibrium

It is obvious from equations 2.10 and 2.11 that the concept of the geostrophic wind is not valid at the equator, where f = 0 and the horizontal

Coriolis force vanishes. However, in Sudan this concept is still considered
applicable for regions at latitudes above 10°N.

The thermal wind is the variation of the geostrophic wind with height due
to the large-scale horizontal temperature gradient (∇T). To determine the
thermal wind we differentiate equations (2.10) and (2.11) with respect to z,
which results in

$$\frac{\partial u_g}{\partial z} = -\frac{g}{fT}\frac{\partial T}{\partial y} - \frac{1}{T}\frac{\partial T}{\partial z}\left(\frac{1}{\rho f}\frac{\partial P}{\partial y}\right) , \qquad (2.13)$$

$$\frac{\partial v_g}{\partial z} = \frac{g}{fT}\frac{\partial T}{\partial x} + \frac{1}{T}\frac{\partial T}{\partial z}\left(\frac{1}{\rho f}\frac{\partial P}{\partial x}\right) . \qquad (2.14)$$

In Central Sudan the ratio between the second and third term in these
equations is larger than 20, since ∇T is 7°C/1000 km and ∇P is 6 mb/1000 km.
The third term in equations 2.13 and 2.14 can therefore be neglected. Thus,
the thermal wind in differential form is given by

$$\frac{\partial \vec{v}_g}{\partial z} = \frac{g}{f}\left(\vec{k} \times \frac{\nabla T}{T}\right) . \qquad (2.15)$$

From equation (2.15) we see that the change of the wind with height is
determined by the horizontal gradient of the temperature in such a way that
the vector ($\partial \vec{v}_g/\partial z$) is directed along the isotherm with the cold air on the
left. By way of the thermal wind equation we can obtain the horizontal
temperature gradient from the vertical change of geostrophic wind speed and
vice versa. In practice, the thermal wind can be obtained from a so called
hodograph of the measured wind vector if we assume that the wind is
geostrophic, which is an acceptable assumption for wind speed at heights above
1 km.

A hodograph is a curve connecting the endpoints of the wind vectors which
are obtained from a sounding. They are plotted with a common origin (see fig.
2.2). The vectors connecting successive endpoints represent the wind shear
through the different layers and are approximately identified as the thermal
wind vectors of successive layers. These vectors will be along the approximate
thickness lines (isopachs), which are equivalent to the layer-averaged
isotherms. The main characteristic of the air flow indicated by a hodograph is
the disposition of warm and cold air relative to the station. The thermal wind
between two levels (in the northern hemisphere) blows in such a way that cold

air is on the left and warm air on the right when following the direction of
the thermal wind. For example, figure (2.2) shows that the thermal wind is
north-westerly and colder air is then north-east and warmer air is south-west.
Since the wind vector is north-east, it will transport (advect) colder air to
the station. (i.e. cold advection). Cold advection always occurs when the wind
backs (turns counter clockwise) with height while warm advection occurs when
the wind veers (turns clockwise) with increasing height. When the thermal wind
is parallel to the actual wind there is neither warm nor cold advection, which
means that $\nabla T = 0$.
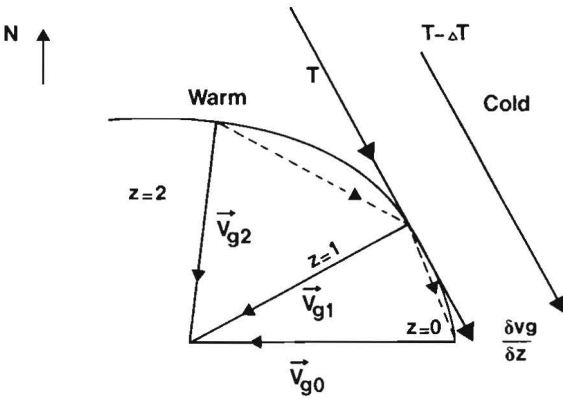
Fig. 2.2
An example of a hodograph showing
the relation between a geostrophic
wind and the thermal wind.

The direction of the geostrophic temperature advection (which is the
temperature change when the flow is horizontal and adiabatic) can also be
estimated from the hodograph. The temperature advection is defined by:

$$(\frac{\partial T}{\partial t})_{adv} = - \vec{v}_g \cdot \nabla T \ . \tag{2.16}$$

In case of warm advection $(\frac{\partial T}{\partial t})_{adv} > 0$ and in case of cold advection
$(\frac{\partial T}{\partial t})_{adv} < 0$.

2.5 Surface heat fluxes

The main parameters of the thermal energy balance equations for the
earth's surface are the short-wave radiation from the sun (Q_T), long-wave

radiation from the earth and sky ($Q_{L\uparrow}$, $Q_{L\downarrow}$), soil heat flux (Q_G), sensible heat flux (Q_H) and latent heat flux (Q_E). During the day there is a gain of radiant energy by the surface (Q_G is positive), while during the night there is a net loss of radiant energy by the surface (Q_G is negative) and Q_T is zero. Fig. (2.3) shows a schematic description of the received and reflected heat fluxes at the surface.

In arid regions such as Central Sudan, where the relative humidity is very low, the latent heat flux (Q_E) is negligible in comparison to the other radiant energy components. Thus the energy balance equation for Central Sudan can be written as

$$Q_H = Q_T + Q_{L\downarrow} - Q_{L\uparrow} - Q_G , \qquad (2.17)$$

where Q_H is the sensible heat flux and $Q_{L\uparrow}$ is the long wave radiation scattered by and reflected from the ground. $Q_{L\downarrow}$ is the direct longwave radiation received by the earth surface from the atmosphere (see also chapter 5).
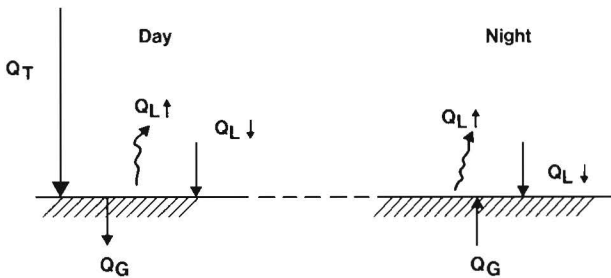
Fig. 2.3
Schematic diagram of the received and reflected heat fluxes at the earth's surface during the day.

2.6 Surface layer wind profile and Monin-Obukhov similarity theory

The wind flow in the surface layer is strongly dependent on the roughness length, which represents the dynamic effect of the surface on the wind profile. In general the surface BL wind varies logarithmically with height. The logarithmic wind profile can be obtained from a simplified relation between the shearing stress (τ) and the wind speed gradient:

$$\frac{\partial u}{\partial z} = \frac{1}{\kappa z} (\frac{\tau}{\rho})^{1/2} = \frac{u_*}{\kappa z} , \qquad (2.18)$$

where κ is the Von Kármán constant ($= 0.399 \pm 0.005$, see Zhang et al., 1988). This relation can be seen as an expression of constancy of turbulent mechanical flux in the surface layer. However, its validity does not depend on the assumption of constant flux but is more general (Tennekes, 1973b). Integrating eqn. (2.18) yields the well-known logarithmic wind profile for a neutral surface layer (about the lowest 20% of a neutral PBL):

$$\kappa \frac{u}{u_*} = \ln \left(\frac{z}{z_0}\right) , \qquad (2.19)$$

where z_0 is the roughness length, which is a constant of integration. The roughness length is strongly dependent on the characteristics of the surface. When the surface roughness is very large ($z_0 > 0.5$; in case of forests and urban areas) an additional empirical parameter is introduced; the zero-plane displacement (d). The wind speed in such rough terrains is approximately zero at height z_0+d (see fig. 2.4).

A practical first-order solution to the problem that most wind stations are not located in homogeneous terrain but have different roughness for different azimuths is the application of exposure correction procedure introduced by Wieringa (1986). The exposure correction procedure transforms the measured wind speed (U_M) to a potential wind speed (U_p). The potential wind is the maximum average surface wind (at 10 m) over open land for a given synoptic pressure field:

$$U_p = 0.76 \ U_M \ \ln\left(\frac{60}{z_0}\right)\left[\ln \frac{z}{z_0}\right]^{-1} \qquad (2.20)$$
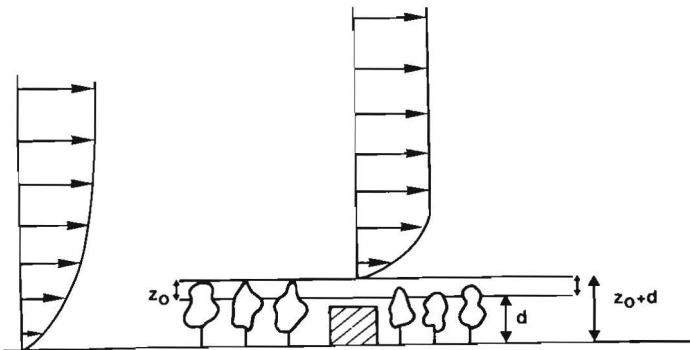
Fig. 2.4
Illustration of the influence of the terrain roughness on the wind profile.

15

The logarithmic wind profile, which is based on neutral stratification, is not always useful for the atmosphere since in most cases the buoyancy forces have to be taken into consideration. Monin and Obukhov introduced a solution for this problem in their similarity theory. Their basic hypothesis is that the surface layer wind profile and turbulence characteristics do not depend only on u_* and z, but also on the sensible heat flux (Q_H) and the term (T/g). As a result they modified the logarithmic-profile, multiplying equation (2.18) by a dimensionless function $\phi_M(\frac{z}{L})$:

$$\frac{\partial u}{\partial z} = \frac{u_*}{\kappa z} \phi_M(\frac{z}{L}) \ , \tag{2.21}$$

where $L = \dfrac{\rho c_p u_*^3 T}{\kappa g Q_H}$. $\tag{2.22}$

L is the Monin-Obukhov stability parameter. Similar to the wind gradient, the potential temperature gradient is expressed by:

$$\frac{\partial \theta}{\partial z} = \frac{\theta_*}{\kappa z} \phi_H(\frac{z}{L}) \ , \tag{2.23}$$

where $\theta_* = -Q_H/\rho c_p u_*$. $\tag{2.24}$

In the last two equations θ_* represents the friction temperature at the surface. According to Paulson (1970) and Dyer (1974) the empirical analytical formulae for the flux profile relationships ϕ_M and ϕ_H are given by:

$$\phi_M(\frac{z}{L}) = \begin{cases} (1 + 5 \frac{z}{L}) & \text{stable conditions} \\ (1 - 16 \frac{z}{L})^{-\frac{1}{4}} & \text{unstable conditions} \end{cases} \tag{2.25}$$

$$\phi_H(\frac{z}{L}) = \begin{cases} (1 + 5 \frac{z}{L}) & \text{stable conditions} \\ (1 - 16 \frac{z}{L})^{-\frac{1}{2}} & \text{unstable conditions} \end{cases} \tag{2.26}$$

The integration of the above equations yields (Paulson, 1970):

$$u_* = \kappa \ U(z)[\ln(\frac{z}{z_o}) - \psi_M(\frac{z}{L}) + \psi_M(\frac{z_o}{L})]^{-1} \tag{2.27}$$

16

$$\theta_* = \kappa \; \Delta T [\ln \left(\frac{z}{z_o}\right) - \psi_H\left(\frac{z}{L}\right) + \psi_H\left(\frac{z_o}{L}\right)]^{-1} \; , \qquad\qquad (2.28)$$

where

$$\psi_M \left(\frac{z}{L}\right) = 2 \; \ln\left(\frac{1 + \phi_M^{-1}\left(\frac{z}{L}\right)}{2}\right) + \ln\left(\frac{1 + \phi_M^{-2}\left(\frac{z}{L}\right)}{2}\right) \qquad\qquad (2.29)$$

$$- \; 2 \; \arctan \left(\phi_M^{-1}\left(\frac{z}{L}\right)\right) + \frac{\pi}{2} \; ,$$

$$\psi_H\left(\frac{z}{L}\right) = 2 \; \ln\left(\frac{1 + \phi_M^{-2}\left(\frac{z}{L}\right)}{2}\right) \; . \qquad\qquad (2.30)$$

2.7 *Planetary boundary-layer structure*

Unlike the laboratory boundary layers the atmospheric boundary layer is governed by the planet's rotation (Coriolis forces) and the buoyancy forces. The convective activities play an important role in determining the characteristics of the planetary boundary layer (PBL).

There are two distinctive types of tropical boundary layers. Firstly, the stationary tropical PBL where the trade wind regime is dominant. Secondly, the disturbed tropical PBL which is due to passage of the Inter Tropical Convergence Zone (see chapter 3). This study is devoted to the stationary tropical PBL, which occurs in the seasons when the demand of wind energy application in the Sahel region is high.

The general structure of the daytime tropical BL consists of three layers. At the bottom is the viscous layer, which extends at the most a few centimeters above the ground, where transfer of heat from the ground takes place by molecular conduction. Above this layer there is the friction layer or forced-convection layer, where heat transfer is caused by turbulent shear stresses. Some tens of meters above the ground this highly unstable super-adiabatic layer gradually changes to an adiabatic mixing layer (or free convection layer) where thermals (turbulent parcels of warm air) rise into colder regions causing downward motion of turbulent colder air parcels. This

mixing of air parcels becomes very strong in the course of the day, resulting
in nearly constant windspeed and potential temperature in the mixing layer.
The mixing layer is capped by a stable layer where the potential temperature
increases with height and the vertical heat flux becomes negative (see fig.
2.5).
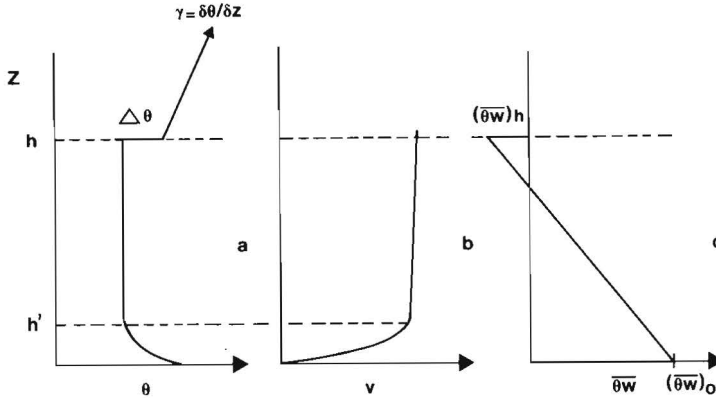
Fig. 2.5 Schematic representation of the convective boundary layer
a - Potential wind profile. b - Wind speed profile, c - The heat
flux profile (where $\overline{\theta w} = \frac{Q_H}{\rho c_p}$). The height of the mixing layer is
indicated by h while h' indicates the lower limit of the mixing
height.

Our calculation of the height of the mixing layer (h_d), discussed in
chapter 6, is based on the jump model of Tennekes (1973a). This model
describes the evolution of the height h_d and the strength $\Delta\theta$ of the capping
inversion as a function of surface fluxes and of the potential temperature
gradient $\gamma = (\partial\theta/\partial z)$ above the inversion. In the model the mixed layer is
considered as a uniform slab, which means that the density profile is linear.
Also $\partial\theta/\partial t$ is constant over the whole slab, and by way of the first law of
thermodynamics it then follows that $\partial(\overline{\theta w})/\partial z$ is height-independent too in a
dry layer with negligible radiation exchange. Consequently, in the mixed layer
the turbulent heat flux shows linear variation between its source levels, the
surface layer and the inversion.

Now there are two reasons why the inversion strength $\Delta\theta$ can change,
namely the inversion rise and the mixed layer heating. If the inversion rises

with a net amount $\partial h_d / \partial t$ (including subsidence), the inversion strength changes with an amount $\gamma \, \partial h_d / \partial t$. The total heating of the mixed layer due to a downward heat flux at the inversion, $(\overline{\theta w})_h$, and an upward heat flux from the surface layer, $(\overline{\theta w})_o$, is given by:

$$\frac{\partial \theta}{\partial t} = \frac{1}{h_d} \left[(\overline{\theta w})_o - (\overline{\theta w})_h \right] , \tag{2.31}$$

because of the linear variation of the turbulent heat flux in the mixed layer. This means that the inversion strength is given by the balance equation:

$$\frac{\partial}{\partial t} \Delta \theta = \gamma \frac{\partial h_d}{\partial t} - \frac{\partial \theta}{\partial t} . \tag{2.32}$$

The occurrence of the downward heat flux at the inversion level is due to the fact that the turbulence below it acts upon the stable layer above it by drawing in stable air and making it turbulent (entrainment). The entrained air will be warmer than the mixed layer, and will add excess heat to that layer, resulting in a downward heat flux given by:

$$- (\overline{\theta w})_h = \Delta \theta \frac{dh_d}{dt} . \tag{2.33}$$

To a first approximation the (unknown) turbulent heat flux at the inversion level can be estimated as the sum of a fixed fraction of the surface layer heat flux and a term related to the amount of mechanical turbulence in the mixed layer:

$$-(\overline{\theta w})_h = c_1 (\overline{\theta w})_o - c_2 \left(\frac{T}{g}\right) \frac{u_*^3}{h_d} , \tag{2.34}$$

where the empirical values of the constants are $c_1 = 0.2$ and $c_2 = 5$ (Driedonks, 1982). The upward heat flux from the surface layer follows from

$$(\overline{\theta w})_o = \frac{Q_H}{\rho \, c_p} . \tag{2.35}$$

If $(\overline{\theta w_o})$ and γ are known functions of time and the initial conditions are given, equation (2.31) can be solved using a standard numerical method (Driedonks, 1981). To calculate the stepwise increments of the height of the boundary layer a simplified method has been introduced by Van Dop et al. (1982) which is based on two conditions:

(a) $c_1 (\overline{\theta w})_o \gg \dfrac{c_2 \frac{T}{g} u_*^3}{h_d}$ or $h_d/|L| \gg k\, c_2/c_1$, in case of a daytime boundary
layer with not too strong wind. This implies that the second term of equation
(2.34) can be neglected and an analytical expression of $\dfrac{\partial h_d}{\partial t}$ is obtained:

$$\frac{\partial h_d}{\partial t} = \frac{1 + 2\,c_1}{\gamma} \frac{(\overline{\theta w})_o}{h_d} \, . \tag{2.36}$$

(b) $c_1 (\overline{\theta w})_o \ll c_2 (\dfrac{T}{g}) \dfrac{u_*^3}{h_d}$ or $0 < h_d/|L| \ll k\, c_2/c_1$, in case the mixed layer
growth is dominated by mechanical turbulence. This implies that the first term
of equation (2.34) can be neglected and the equation will be

$$\frac{\partial h_d}{dt} = [\frac{2c_2}{\gamma} (\frac{T}{g})\, u_*^3]/h_d^2 \, . \tag{2.37}$$

The general solution of equation (2.31) changes smoothly from equation
(2.36) to (2.37) where $h_d/|L|$ varies from very large to small values. As a
result an approximate solution is proposed by van Dop et al., 1982:

$$h_d(t+\Delta t) = h_d(t) + \Delta t\, \frac{\partial h_d}{\partial t} \, , \tag{2.38}$$

$$\frac{dh_d}{dt} = \frac{(\overline{\theta w})_o}{\gamma h_d[1 - (\frac{k\,c_2}{c_1})\frac{L}{h_d}]} [1 + 2\,c_1 + \frac{2k^2\,c_2^2}{c_1} (\frac{L}{h_d})^2] \, . \tag{2.39}$$

In practice, the initial value for this equation is normally taken as the PBL
height at the last hour of the night (just before sunrise).

During the nighttime the PBL consists of two layers, the viscous layer
and the friction layer. Just after sunset the surface cools rapidly and the
temperature of the air exceeds that of the ground, resulting in a downward
heat flux and a stable stratified temperature-gradient layer near the ground.
In other words, the low-level cooling diminishes the mechanical and buoyant
mixing and forms a much thinner boundary layer. This implies that the wind
shear is limited to a few hundred meters above the surface.

The shear stress during the evening can generate an inertial oscillation

component that adds vectorially to the geostrophic wind and produces a layer of maximum wind (low level jet). The period of oscillation is $\frac{\pi}{f}$, which implies that the inertial oscillation period depends on the latitude. Thus the position of the jet defines the height of the nocturnal boundary layer which is the maximum height for the vertical wind shear to be generated (Blackadar, 1957).

It is clear, that this jump-model cannot be used to calculate the height of the nocturnal boundary layer. In literature there are many simple parametric expression for calculating the height of nocturnal PBL (h_n); for a review see Nieuwstadt, 1981. The most important and well known equation has been given by Zilitinkevich (1972):

$$h_n = C_N \left(\frac{u_* L}{f}\right)^{1/2} \tag{2.40}$$

In literature different values are proposed for the proportionality constant C_N, which critically depends on the quality of the data used. In this dissertation we will use $C_N = 0.35$, which is the most recently published value on the basis of an accurate nocturnal boundary layer experiment (Nieuwstadt, 1984).

C H A P T E R 3

PRELIMINARY SURVEY OF THE PHYSICAL ENVIRONMENT
AND THE WIND POTENTIAL IN THE SUDAN

CHAPTER 3

PRELIMINARY SURVEY OF THE PHYSICAL ENVIRONMENT
AND THE WIND POTENTIAL IN THE SUDAN

3.1 Introduction

The interpretation of wind data requires general knowledge about the geographical and climatological characteristics of the region of investigation. Besides this knowledge one needs information about the quality of the measured data and the history of the meteorological stations in the region.

The necessity of this chapter is to give a background knowledge of the geography and climates of the Sudan and the station density in the region. Moreover, it highlights some practical problems of the evaluation of wind potential in such a tropical region.

The geographical and climatological characteristics are dealt with in section 3.2. Section 3.3 gives a survey of the station density and a preliminary analysis of the wind potential on the basis of the annual averages.

3.2 Geographical and climatological characteristics of the Sudan

Sudan, the largest African country, covers an area of about 2.51×10^6 km^2, which is about 70 times the area of the Netherlands. It represents 8.3% of the African continent and about 1.7% of the world's land. Its maximum length is about 2100 km from Nimule (near the border with Uganda) at 3.5° N to Bir Shalatin near the Red Sea at 23°N. Its maximum width is about 1800 km from El Geneina (near the border with Chad) at 21.75°E to the Red Sea coast near Tokar at 38.5°E (Barbour, 1961). Sudan shares frontiers with eight countries; Egypt, Libya, Chad, Central African Republic, Zaire, Uganda, Kenya and Ethiopia, see fig. 3.1.
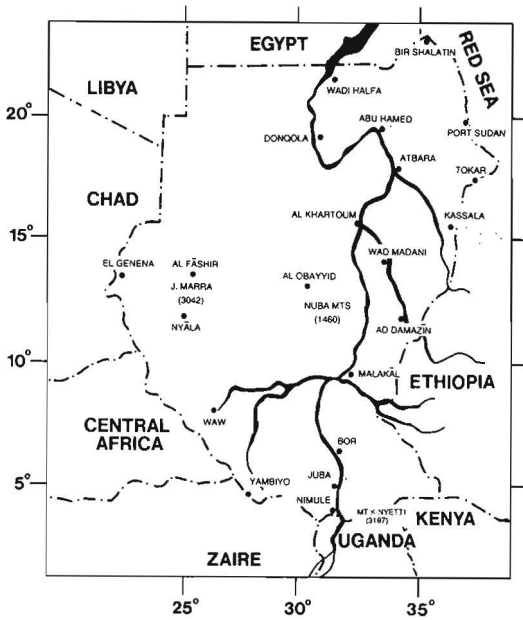
Fig. 3.1
Map of Sudan indicating
some regions and cities
mentioned in the text.

The relief of the country is generally flat, except for some hills (in the east and centre of the country) and mountains (in the west and south of Sudan). There is no exact relief map published for Sudan; it is estimated that 25% of the country is lower than 400 m above sea-level, about 20% lies between 400 and 500 m, about 50% lies between 500 and 1200 m and about 5% lies between 1200 and 3500 m. Fig. 3.2 shows the general relief of the country. The main source of water in the Sudan is the river Nile, which crosses the country from south to north. Its main tributaries are the White Nile, originating from lake Victoria (Kenya) and the Blue Nile, originating from lake Tana (Ethiopia). The Blue and the White Nile meet at Khartoum to form the river Nile (see figure 3.1).
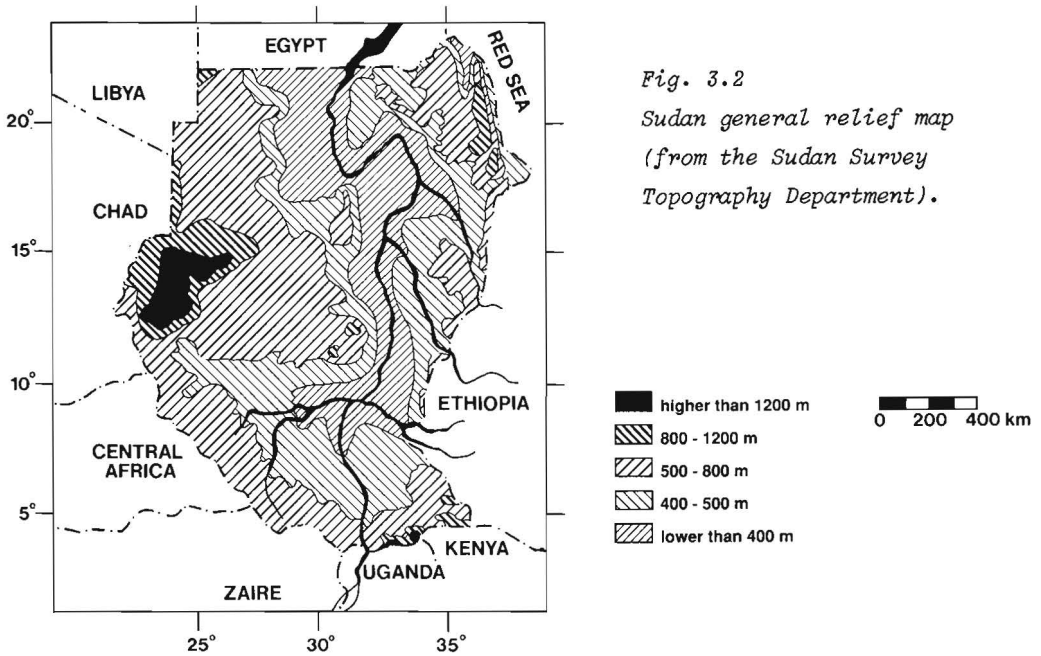
Fig. 3.2
Sudan general relief map
(from the Sudan Survey
Topography Department).

In the Sudan there are two types of climate: desert and tropical. In the northern region of the country the Sahara desert conditions are dominant: very large diurnal temperature variations and no rainfall. In the southern region (tropical climate) equatorial rainfall is dominant. Between these two regions, the temperature, rainfall and humidity decrease from south to north. Local variations are caused by the Nuba mountains of Central Sudan, Jebel Marra in the west, the Red Sea hills in the east and the Sudd swamps in southern Sudan. The Red Sea coast is the only region in the country affected by sea-breezes.

As a result of the two types of climate the length of the seasons in the Sudan varies according to the latitude. In Central and North Sudan there are four seasons; winter (Dec.-Feb.), advancing monsoon (March-May), monsoon (June-Sept.) and retreating monsoon (Oct.-Nov.). The south of the country experiences a rainy season for six months and a dry season for six months.

Physically we can explain the climate in Sudan by the motion of the high and low pressure belts in the north hemisphere at different times in the year. In the winter the pressure is high to the north of Sudan and in the Sahara. The north trade winds blow across Sudan towards the Inter Tropical Convergence Zone (I.T.C.Z.), which is south of the Sudan during the winter. The Inter Tropical Convergence Zone is a low pressure belt around the earth resulting from the intense heating of the earth by the sun in the tropical zone.
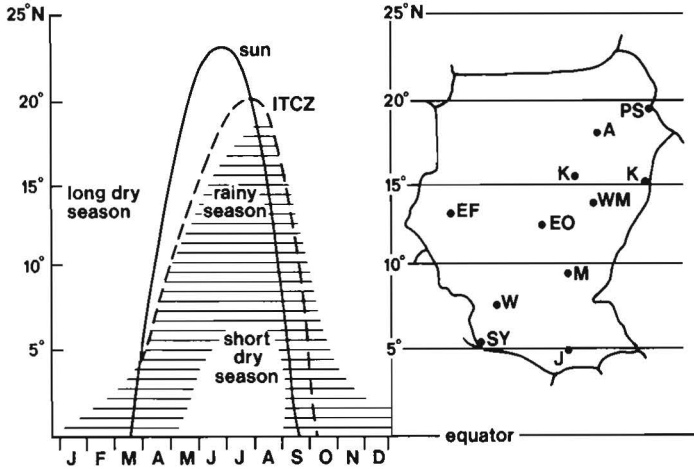
Fig. 3.3
The annual motion
of the I.T.C.Z. and
the sun versus
latitude (from
Noordwijk, 1984).

Fig. 3.3 shows the apparent yearly movement of the sun and of the
I.T.C.Z. with latitude in the northern hemisphere, with the resulting duration
of dry and rainy season (Noordwijk, 1984). In the advancing monsoon season the
I.T.C.Z. moves towards the north, associated with a low pressure area, known
as the Sudan Low, resulting in high horizontal temperature gradients. Usually
during this season the occurrence of sandstorms is high. In the monsoon season
the I.T.C.Z. gradually moves northwards, and the Sudan Low moves northwest as
a result of a south-west humid air stream which originates from the South
Atlantic Ocean. In the retreating monsoon the I.T.C.Z. reaches its maximum
northwards from Sudan (25°N) and starts to move back south in the end of
October. In this month the effective wind is northwards.

Concentrating on the large scale climate pattern of Central Sudan one
finds that the climate mainly depends on the following factors (Bhalotra 1963,
Griffiths 1972):

1. The Sahara High "pressure area", generally located in the western part of
   the Sahara, which is a rather persistent large-scale circulation feature,
   resulting in a large-scale subsidence.
2. The Arabian High, which occurs over the Arabian peninsula and has the same
   characteristics as the Sahara High.

3. The Red Sea Trough; a stationary front which results from the convergence in between the Sahara High and the Arabian High, combined with geographical features.
4. The Inter Tropical Convergence Zone (I.T.C.Z.).
5. The Equatorial Trough, which is an extended low pressure area over Central Africa.
6. The Mediterranean Depressions.
7. A homogeneous pressure area over the Turkish Peninsula and over South Central Asia (high in winter, low in summer).

The importance of these pressure fields in Central Sudan is dependent on the seasons; for instance in the winter and retreating monsoon the Sahara High and the Arabian High are the prevailing factors of the wind flow in the region. The I.T.C.Z. on the other hand has a strong influence on the wind flow during advancing and retreating monsoon. More details about the behaviour of these pressure fields during the seasons are summarized in Table 3.1.

Table 3.1

Winter season or dry season (Dec.-Feb.)	Advancing Monsoon season (March-May)	Rainy season Monsoon (June-Sept.)	Retreating Monsoon season (Oct.-Nov.)
1. The Sahara High (S.H.) controls the air circulation in this season and there is north-north easterly flow over the whole country, except for the southern part of the Red Sea area. The S.H. is dynamic in behaviour and the anticyclonic circulation associated with it extends to great heights. Therefore very dry air prevails over the country and the weather is fine with clear skies. The northerly wind is relatively cooler and becomes warmer as it moves south.	The S.H. in this season moves towards north-west Africa as a ridge of high-pressure.	The Thermal Low in the southern Sahara is replaced by deep Sahara anticyclonic circulation at a height less than 3 km. It results in anticyclonic circulation of winds over the north-west of Sudan.	S.H. is remarkable in this season and an anticyclonic circulation exists in the whole north-west Africa and adjoining parts of north-west Sudan.
2. The Arabic High (A.H.) produces anticyclones which induce north-easterly air stream. Over the Red Sea this air stream appears as a southerly wind. Approaching the coastal hills it gives showers and thunderstorms. It sometimes causes early morning fog or stratus cloud over the hills.	In this season the A.H. is weakened.	The A.H. gives place to a deep low pressure area over Arabia and Iraq. This low pressure system results in a weak wind flow over the north-east Sudan.	The A.H. starts to develop again forming anticyclonic circulation which affects the north-east Sudan.
3. The S.H. & A.H. converge towards each other to form a stationary front which is known as the Red Sea Trough (R.S.T.). The front normally lies along the Red Sea coast but may be displaced east or west depending on the intensity of the S.H. & A.H. The present of this front contributes in thunderstorms and showers in the Red Sea regions.	The R.S.T. results in occasional thunderstorm and showers in the Red Sea hills.	No effect.	The R.S.T. is very active in this season. Port Sudan area and the neighbouring Red Sea hills get the heaviest rainfalls of the year during this season.

4. During this season the I.T.C.Z. is south of Sudan.	In late April the I.T.C.Z. is usually about 10° N over eastern Sudan. Associated with the I.T.C.Z. there is low pressure area which is known as Sudan Low; it is a part of the thermal equator and oscillates north and south with the declination of the sun. As the season advances the I.T.C.Z. and the Low move northward.	In this season the I.T.C.Z. moves northward. It results in a south-west humid air stream.	In this season the I.T.C.Z. reaches its maximum northward and starts to move back southwards.
5. The low pressure over Central Africa forms part of the equatorial low pressure belt which is shallow and purely thermal in character. This low pressure has not much effect on the climate in this season.	No effect.	The low pressure over Central Africa in the winter is replaced by two ridges of high pressure which extend into central Africa from two large scale subtropical anti-cyclones; one into the south Indian Ocean and the other into the south Atlantic Ocean. This formation of anti-cyclones results in moist air stream which penetrates the Sudan as south westerly streams south of the I.T.C.Z.	No effect.
6. The Mediterranean depressions give rise to a strong cold front which sweeps along north Sudan causing wide spread blowing sand in its rear.	The effect of the low pressure is the same as in the winter season but the sandy winds are more frequent in this season because of the high lapse rate During the last part of the season the cyclonic activity in the Mediterranean decreases.	No effect.	No effect.
7. The intensification of the cold anti-cyclone over Central Asia and its displacement westwards causes a flow of cold air streams which move through south Russia and across the Mediterranean and streams over eastern north Sudan.	No effect.	No effect.	No effect.

Table 3.1 The behaviour of various pressure belts during the four seasons.

The most significant local climate phenomena in Central and North Sudan are the dust storms which consist of three kinds of storms (Bhalotra, 1963; Lawson, 1971):

1. Haboob (squalls), i.e. dust storms associated with Cb clouds (cumulonimbus clouds) which occur in the period April-September. Fig. 3.4 gives a schematic representation for the Haboob.
2. Dust storms caused by steep pressure gradients of south/southwesterly winds south of the intertropical front. They occur in the period May-October.
3. Dust storms caused by the continental polar air reaching Sudan as cold fronts associated with strong eastern depressions. They occur in the period February-April.
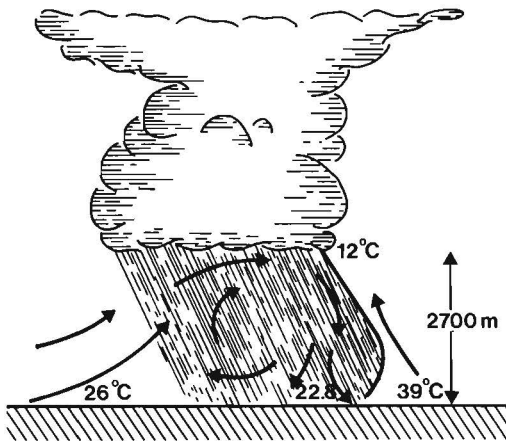
Fig. 3.4
A schematic representation of the sand storm (Haboob) (obtained from Khartoum Meteorological Office).

The most violent storms are the Haboob and the dust storms caused by steep pressure gradients. The minimum wind speed is about 10 m/s while the maximum gust may reach about 50 m/s. The duration of these storms varies between 1 and 4 hours; 80% lasts less than 2 hours. They occur usually between 15 and 23 hr. SLT (Sudan Local Time) (Lawson, 1971).

3.3 *Meteorological stations and wind potential*

In Sudan there are 53 meteorological stations where wind data are collected. At 22 stations: Wadi Halfa, Station No. 6, Abu Hamed, Port Sudan, Dongola, Karima, Atbara, Khartoum, Kassala, Wad Madani, El Gedaref, El Duim,

El Fasher, Sennar, El Geneina, El Obeid, Kosti, El Damazin, Gazala Gawazat, Malakal, Wau and Juba, the wind direction and speeds are measured by vanes and Dines pressure tube anemographs at a height of about 15 meter above ground level. At the others only Beaufort estimates are available. In fig. 3.5 the geographical position of all these stations are shown on a map.
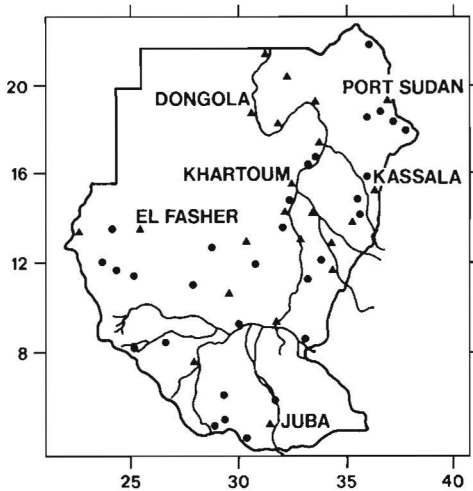
Figure 3.5   Geographical position of meteorological stations.

▲   represents stations where wind speed is recorded by Dines pressure-tube anemograph at a height of about 15 meters above the ground level.

●   represents the stations where the wind force is estimated by the Beaufort scale.

In the Sudan there are three radiosonde stations: Khartoum, El Fasher and Port Sudan. Radiosonde observations are recorded once every 24 hours at 1100 G.M.T. In Wadi Halfa, Abu Hamed, Dongola, Kassala, El Obeid, Juba, Wau, El Damazin and Malakal only pilot balloons are sent up twice every 24 hours: at 1100 G.M.T. and 2200 G.M.T.

The annual average wind speed and direction for the period (1970-80) for all stations in Sudan is summarized in Table 3.2. These data have been obtained from the Khartoum Meteorological Office. For review purposes we assume that these data are correct, and some useful conclusions can be obtained. However, some of these data may show some errors, which we will illustrate in the latter part of this section.

Station	lat.(N)	long.(E)	alt.(m) above sea level	Mean wind speed (m/s) and direction			
				Dec.-Feb.	March-May	June-Sept.	Oct.-Nov.
Halayib	22 5'	36 7'	350	3.1 W	3.1 NW	3.1 NW	3.1 NW
Wadi Halfa*	21 49'	31 21'	190	4.2 NNW	4.3 NNW	3.9 NNW	4.4 NNW
Gebeit	21	36	?	2.7 NE	2.7 NE	2.7 NE SW	2.7 NE
Station no. 6	20 45'	32 33'	470	2.7 NE	2.8 N	2.7 N	2.7 N
Dongola*	19 10'	30 29'	228	4.7 N	4.9 N	4.5 N	4.7 N
Port Sudan*	19 35'	37 13'	5	4.7 N	3.8 N	3.1 N	3.6 N
Abu Hamid*	19 32'	33 20'	315	5.8 N	4.6 N	3.7 N	4.9 N
Karima*	18 33'	31 51'	250	4.9 N	5.0 N	4.1 $NNW_{6,7}N$	4.7 N
Tokar	18 26'	37 44'	20	2.8 N	2.7 N	2.7 N_6SW	3.3 NE
Haiya	18 40'	36 40'	?	5.6 NE	4.7 NE	4.7 SW	4.4 NE
Atbara*	17 40'	33 58'	345	2.8 N	2.4 N	2.2 SW_6SSW	2.0 N
Hudeiba	17 34'	33 56'	350	2.9 N	2.8 N	2.8 NW_6,SW	2.7 N
Aqeq	18 2'	38	?	2.9 N	2.9 N	3.2 W	3.1 E
Shendi	16 42'	33 26'	360	2.7 NE	2.7 NE	2.7 SW	2.7 NE
Wadi Seidna	15 40'	32 33'	?	4.3 N	4.4 NE	5.4 SW	4.0 $SW_{10}N$
Aroma	15 50'	36 9'	430	2.7 NE	2.7 NE	2.9 SW_6S	2.7 NE
Shambot	15 40'	32 32'	380	3.1 N	2.8 N	2.8 SSW	2.9 NNW,N
Khartoum*	15 36'	32 33'	381	4.3 N	4 $N_{3,4}SSW_5$	3.8 SSW	3.3 N
Jebel Awelia	15 40'	32 33'	?	2.7 N	2.7 NE	2.7 SW	2.7 NE,N
Kassala*	15 28'	36 24'	500	1.8 NNE	1.8 $NNE_{3,4}S$	2.4 S	1.3 S,NNE
Halfa El Gadida*	15 40'	35 20'	?	3.0 NNW	2.8 $NNW_{3,4}S$	3.6 S	2 S,NNE
Wad Madani*	14 23'	33 29'	405	2.9 N	3.1 $N_{3,4}SW$	4.2 SSW_6S	2.3 S,NNW
El Shawak	14 24'	35 51'	510	2.7 N	2.7 $N_{3,4}SW$	2.7 $S_{6,9}SW$	2.7 S,N
Kutum	14 40'	24 50'	?	2.5 SE	2.7 SE_3SW	2.7 SW	2.7 NE
El Gedaref*	14 02'	35 24'	600	2.7 N	2.4 N	2.8 $SW_{6,7}S$	2.7 NNE
Ed Duim	13 59'	32 20'	380	2.8 N	2.7 N	2.7 S	2.7 N
El Obied*	13 10'	30 14'	570	3.9 N	2.8 N,SSW_5	3.1 SW	3.2 NNE,N
El Geneina*	13 29'	22 27'	805	4.0 NNE	3.0 NNE	2.1 W	2.7 NE
El Fasher*	13 38'	25 20'	730	2.2 NE	2.5 NE	2.3 SSE,ENE_9	2.2 NE
Sennar	13 33'	30 14'	570	2.7 NE	2.5 NE,SW_5	2.6 SW	2.7 SW
Kosti*	13 10'	30 14'	380	2.9 N	2.4 NNW	2.3 S	1.8 S,NNW
Zalingo	12 54'	23 19'	900	1.8 E	1.8 E	1.8 W	1.3 W,E
Abu Na'ama*	12 44'	34 8'	445	3.1 NNE	3.1 NNW	3.0 S	2.5 S,NNW
En Nahud*	12 42'	28 26'	565	3.0 NNE	2.0 NNE	2.0 SSW	2.5 NNE
Kas	12 5'	24 20'	?	2.7 E	2.7 E	2.9 SE_6SW_7NW	3.1 E
Nyala	12 04'	24 53'	655	2.9 NE	2.7 NE	2.5 SW	2.9 NE
Rashad	11 52'	31 03'	885	3.0 N	3.0 NE	2.9 $NE_{6,7}SW$	2.7 NE
El Damazin*	11 49'	34 24'	470	2.9 N	2.9 $W_{3,4}S$	2.6 S	2.2 S,N
Babanosa	11 20'	27 40'	543	2.8 NE	2.8 NE,S	2.7 S	2.7 SW,N
Er Renk	11 7'	33 10'	?	2.7 $N_{12,1}NW$	2.7 $NW SW_5$	2.0 S	2.0 S,NWE
Kadugli*	11 0'	29 43'	500	3.4 NNE	2.7 NE,SW	2.7 SW	2.7 NE
Malakal*	9 33'	31 39'	390	4.1 NNE	2.9 NNE	2.1 S	2 SW,NNE
Bentiu	9 14'	31 39'	390	2.7 $N_{12,1}NE$	2.9 NE_3S_4SW	2.7 SW	2.7 S,N
Aweil	8 8'	27 30'	?	2.7 $NW_{12,1}NE$	2.7 NE_3SW	2.7 SW	2.7 NE,NW
Nasir	8 7'	33 15'	?	4.0 N	3.9 N_3S	3.1 S	3.4 S,N
Roga	8 5'	25 50'	?	2.7 NE	2.7 NE_3SW	2.7 SW	2.7 SW,WE
Waw*	7 42'	28 01'	435	1.8 $N_{12}NNE$	1.8 E_3SSW	1.8 W	1.8 SW,NE
Bor	6 3'	31 45'	?	2.7 NW,SW	2.7 SW	2.7 SE	2.7 SE,NE
Rumbek	6 8'	29 45'	?	2.7 $N_{12}NE$	2.7 NE_3S	2.7 S_6SW	2.7 SW,N
Maridi	5 10'	29 30'	?	2.7 N	2.7 N_3SE	2.7 SE_6SW	2.7 S,SE
Juba*	4 52'	31 36'	460	1.5 NE	1.8 S	1.3 S	1.3 S
Yambio	4 34'	28 24'	650	2.7 NE	2.7 SW	2.7 SW	2.7 SW,NE
Yei	4 2'	30 50'	?	3.1 NE	2.7 SE	2.7 SE	2.7 SE

Table 3.2 Summary of the annual average wind speed and direction for period 1970-1980. The stations which have asterisk (*) are stations where wind speed is measured by Dines pressure tube anemograph. The index of the direction refers to the month.

The change in wind direction from the north of Sudan to the south in table 3.2 is related to the motion of the I.T.C.Z. From the table it can be concluded that the I.T.C.Z. is around Khartoum in the period March-May and around Karima in the period October-November. This estimation of the I.T.C.Z. motion is in agreement with fig. 3.3.

From the data in the table one also observes that the wind potential in Sudan is dependent on the latitude; the higher the latitude, the larger the wind potential. In other words, the region below 9°N (tropical region) has a lower wind potential than the region above 9°N. From a practical point of view it is advantageous that a relatively high wind potential is available in the north of the country, where there is a high demand for water pumping windmills.

From the annual averaged wind direction data for the period 1940-1970 (available in the Meteorology Office in Khartoum) we constructed wind roses for a number of stations, which are plotted in fig. 3.6. This figure shows the percentage of wind occurrence in the eight compass directions and also the calms percentage. From the figure we see that in the north of the country the prevailing wind is from the north and northeast directions and the percentage of calms does not exceed 10%. In the south of the country the effective wind is from the south and southwest and the percentage of calms exceeds 20%.

In the data shown in fig. 3.6 there are remarkable discrepancies to be observed, two of which will be treated in some detail:

1. When we compare the wind speed data from Kosti (13° N) with those from Malakal (9° N) (Kosti is at the same height above sea level as Malakal) during the winter when the northeast trade wind is dominant, we observe that the average of the recorded data at Kosti is about 2.9 m/s, whereas the average at Malakal is 4.1 m/s (see table (3.2)). Geographically, higher wind speeds are expected at Kosti. A possible explanation for this discrepancy could be provided by a publication of Hamid et al. (1980), where it is mentioned that the station in Kosti was affected by growth of some trees in the north east direction.

2. In Kassala independent measurements were done by Hamid et al. (1981) in a representative area 5 km east of the meteorological station at about 8 m above ground level. The average wind speed was 4.8 m/s, which is about 80% more than the data recorded at the same time at the meteorological station of Kassala.
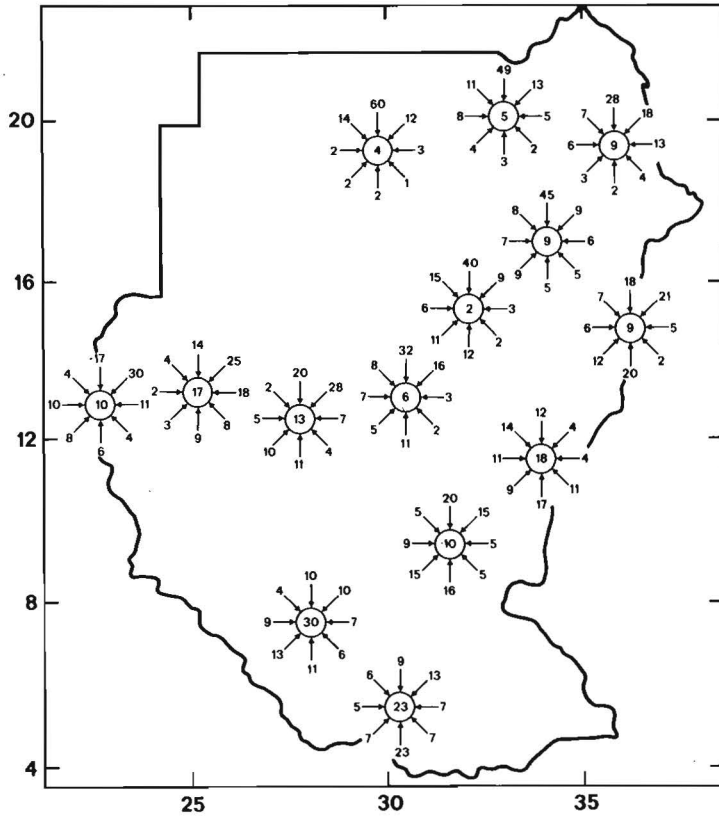
*Figure 3.6 Percentage frequency of wind direction (wind roses) for the period
1940-1970. The encircled numbers are the percentage of calms which
are highly dependent on the condition of the instrumentation. The
reliability of some of these calms percentages is questionable.*

These examples indicate some typical problems about the reliability of
the wind data in these regions. In general the most important reasons expected
for these uncertainties are the following:

a. The growth of trees and new buildings around the stations.
b. The less than perfect maintenance and calibration of the measuring
   equipment. An example of this is that in most stations the Dines air
   pressure tube anemographs are based upon an assumed air density of
   1.226 kg/m³. In fact, the actual air density (which is dependent on the
   seasons) at various stations is about 1.1 kg/m³ or less (Hamid et al.,
   1981).
c. Replacement of measuring equipment by another type, without registering the

time of replacement.

It is clear that from the annual averaged data only very limited
conclusions can be drawn because of the uncertainty problem, the large period
of averaging and the seasonal variation. For a better understanding of the
wind regime in Central Sudan hourly wind data are necessary and the history of
the stations should be investigated. To solve this problem we assembled hourly
wind data and visited some stations to investigate the station surroundings
and check the measuring equipment. In chapter 4 some important results from
four representative stations will be discussed.

3.4 Conclusions

Sudan is a very large country, about 2.51×10^6 km^2, with generally a
flat relief as shown in fig. 3.2. In Sudan there are two types of climates:
desert and tropical. These climates are strongly dependent on the I.T.C.Z.,
the high pressure belts and the low pressure belts. As a result the seasonal
wind regimes are controlled by these pressure fields.

The density of stations in Sudan is 53 stations over 2.51×10^6 km^2,
which is very low (compare: 57 stations over an area of 3.6×10^4 km^2 in the
Netherlands). At half of the Sudanese stations the wind speed is roughly
estimated using the Beaufort scale, which is insufficient for quantitative
evaluation of the wind potential.

In spite of the uncertainty observed in the data due to terrain
obstructions and the maintenance of the equipments, the discussion presented
in this chapter gives a qualitative description of the wind potential in
Sudan. South of 9°N the wind speed on the average is less than 3 m/s, while
north of 9°N it is larger than 3 m/s. From the wind roses constructed for the
whole country it is concluded that the prevailing wind in the north of the
country is north to northeasterly with a percentage of calms less than 10%,
while in the south of the country it is south to southwesterly with a
percentage of calms larger than 20%. The application of wind energy, specially
for water pumping, clearly shows to be more promising north of 9°N.

For understanding the wind flow in the region a reliable hourly data base
is necessary. The construction of such a data base will be discussed in the
following chapter.

C H A P T E R 4

DATA BASE

CHAPTER 4

DATA BASE

4.1 Introduction

For accurate evaluations of the wind potential and modelling of the
boundary layer wind flow a reliable data base is indispensable. In order to
achieve a reliable meteorological data base for tropical African countries it
is necessary to evaluate the quality of the data and the measuring equipment
and to have information about the close surroundings of the stations.

In the first part of this chapter (section 4.2-4.4) we concentrate on the
construction of a data base from unprocessed meteorological data from eight
stations in Central Sudan. The number of observations concerned are about
330×10^3 and the area involved covers about 560,000 sq km. around Khartoum.
The station surroundings and the quality of the measuring equipment was
investigated by visiting the stations (section 4.3). In section 4.4 some
procedures to obtain a homogeneous wind data base, such as reliability checks,
the azimuth-dependent exposure correction and the correction to a standard
height are discussed.

The second part of this chapter (section 4.5-4.7) deals with the way in
which the obtained data are represented together with a preliminary analysis
of the monthly wind frequency distribution and the diurnal cycles of the
different types of data. On the basis of the corrected data an evaluation of
the wind potential, presented as frequency distribution, is given in section
4.4. The behaviour of the diurnal course of the surface data is discussed in
section 4.6. Section 4.7 deals with the upper air data and their behaviour
across the region. In the last section, section 4.8, some general conclusions
about the data sets are drawn.

4.2 Assembled data

The unprocessed data described in this chapter were kindly supplied by
the Sudanese Meteorological Department in Khartoum with support from WMO. The
data are measured at the following stations:

a. Khartoum (Al Khurtum) airport (15°40'N, 32°32'E, 381 m a.s.l.).

b. Shambat agrometeorological station (8 km north of Khartoum airport, 380 m a.s.l.).

c. Wadi-Seidna airport (25 km NNE of Khartoum airport, 385 m a.s.l.).

d. Wad Madani (Wad Medani) agrometeorological station (14°23'N, 33°29'E, 405 m a.s.l.).

e. Atbara (Atbarah) station (17°40'N, 33°58'E, 345 m a.s.l.).

f. Dongola (Dunqulah) airport (19°10'N, 30°29'E, 228 m a.s.l.).

g. El Obeid (Al Ubayyid) airport (13°10'N, 30°14'E, 570 m a.s.l.).

h. El Damazin (Ad Damazin) station (11°49'N, 34°24'E, 470 m a.s.l.).

Table 4.1 reviews the available data. The data were processed by computer and corrected for obvious errors. The surface wind data were corrected for local exposure deficiencies by a method which will be discussed in the following section. Construction of a data base in this fashion is more economical than to install a new network of measuring equipment to estimate the wind potential over the region.

Type of the data	Stations	Years
1. Surface-wind hourly data measured by means of Dines pressure tube anemograph. The measurements are at 15 m above the ground level.	Khartoum Atbara Wad Madani El Obeid	1982, 83, 84 1982, 83, 84 1982, 83, 84 1984
2. Surface wind 3-hourly average data between 0500 and 1100 SLT, Dines pressure-tube anemograph (10 m above ground level) is used.	Wadi-Seidna	1984
3. Surface-wind 6 hours mean data. Cup anemometer measurements at 13 m.	Shambat Wad Madani	1984 1984
4. Surface temperature, hourly data.	Shambat Atbara Dongola Khartoum	1984 1984 1984 1983, 84
5. Surface pressure, 3 hourly data	Khartoum Atbara	1983, 84 1984
6. Soil temperature for different depths in the soil (recorded at 06, 12, 18 hours SLT).	Shambat	1984
7. Global radiation recorded hourly.	Dongola Shambat	1984 1984
8. Relative humidity recorded hourly.	Shambat Dongola Khartoum	1984 1984 1984
9. Radiosonde midday data (13 hr SLT). Wind speed, wind direction, temperature and humidity.	Khartoum	1983, 84
10. Pilot balloon midnight data (24 hr SLT). Wind speed and wind direction.	Khartoum	1984
11. Pilot balloon midday and midnight data. Wind speed and wind direction.	Dongola Kassala El Obeid El Damazin	1984 1984 1984 1984

Table 4.1 Tabulation of the data obtained from Khartoum Meteorology Office. The abbreviation SLT means Sudan local time.

4.3 *The characteristics of the stations surroundings and the surface wind measuring equipment*

To obtain sufficiently detailed information about the wind regime in Central Sudan, some stations were visited to investigate the maintenance of the measuring equipment and the close surroundings of the stations. The stations visited are the following: Khartoum airport, Shambat agrometeorological station (8 km north of Khartoum), Wad Madani agrometeorological station (190 km south of Khartoum) and Atbara station (280 km north of Khartoum). Fig. 4.1 shows the geographical position of the stations.
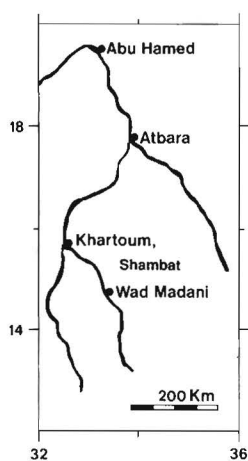
Fig. 4.1
An enlarged part of the Sudan map to show the position of the four stations; Atbara, Khartoum, Shambat and Wad Madani.

The Khartoum airport station (381 m a.s.l.) is located about three kilometers east of the centre of Khartoum. About one kilometer from the airport in the north and north-east directions there are a number of buildings with a height of about 6 to 10 m. Fig. 4.2. overviews the surroundings of the airport.

In order to have detailed information about the close surroundings, photos were taken of the airport surroundings for different azimuths (see fig. 4.3). The wind speed at about 15 m above ground level (a.g.l) is recorded hourly, using a Dines pressure tube anemograph. At this station the calibration and equipment maintenance is done every six months. The maintenance consists of cleaning the tubes of the anemograph and changing the distilled water. The history of the hourly data collection for Khartoum airport goes back to 1923.
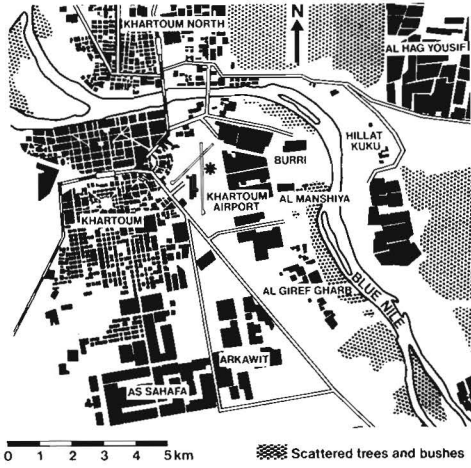
Fig. 4.2
A map to show the surroundings of Khartoum airport. The location of the meteorological station is indicated by *.
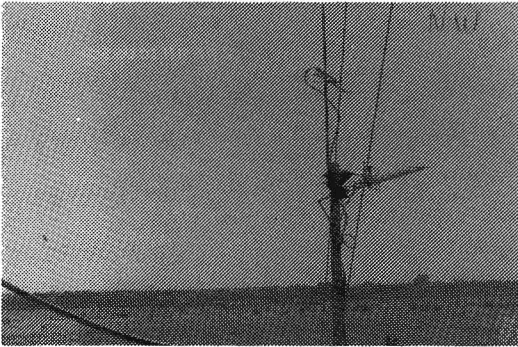
a - north-west azimuth
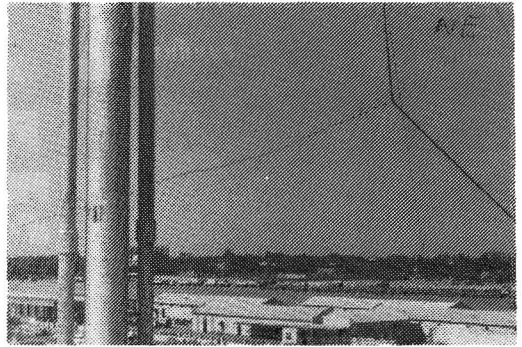
b - north-east azimuth
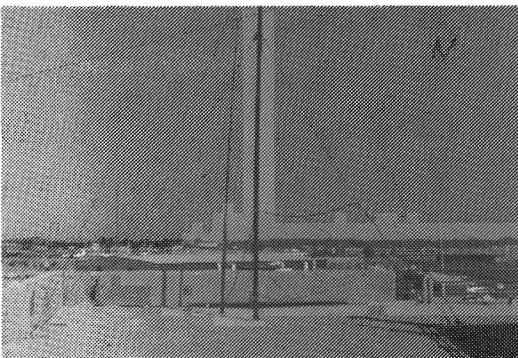
c - north azimuth

d - south azimuth

Figure 4.3 The close surroundings of the Khartoum airport station (the prevailing wind directions are north and north east).

Shambat is the main agrometeorological station in the Khartoum region.
The station is located at about 8 km north of Khartoum-Airport. Fig. 4.4 shows
the surroundings of the station.

Fig. 4.4
A map to show the surroundings
of Shambat station which is
indicated by * in the map.

The station has a mast which holds nine cup-anemometers (Casella-type,
with a mechanical counter that indicates the total run of the wind). The
anemometers are placed at different heights from 0.5 m to 13.0 m. Measurements
are collected every three hours in the period 6-18 hr. SLT. In this mast there
is also an arrangement for measuring the temperature at the different levels.
However, temperature measurements are not recorded during the last five years.

Fig. 4.5 shows photos of the close surroundings of the station.
Maintenance is hardly done for these cup-anemometers. Calibration is carried
out once every year and since there is no wind tunnel available in Sudan
calibration is performed by comparing the anemometer with a standard one.
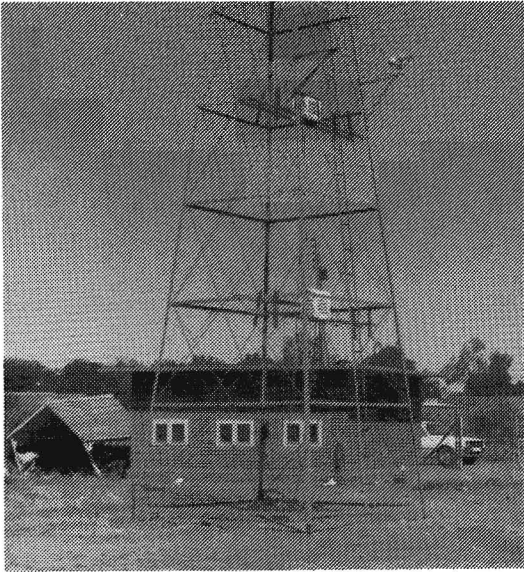
a - north-west azimuth
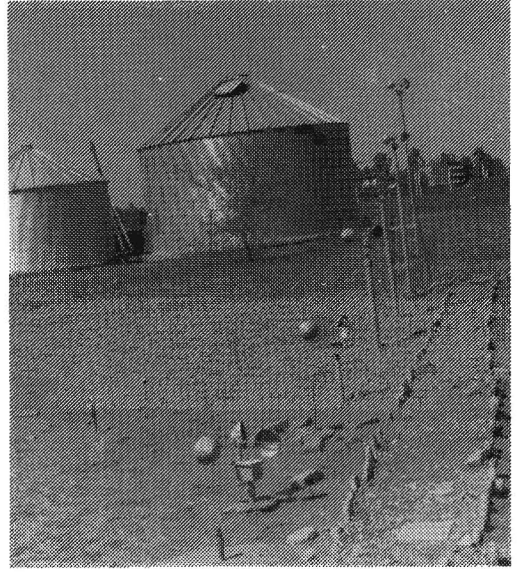
b - south-west azimuth
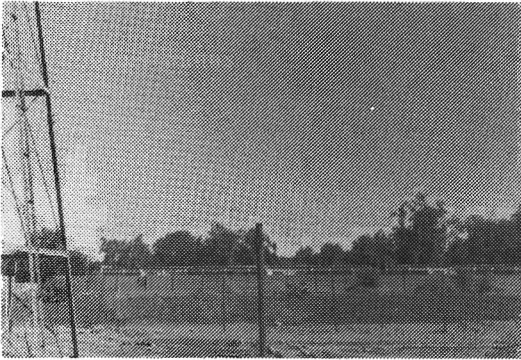
c - north azimuth

d - west azimuth

e - east azimuth
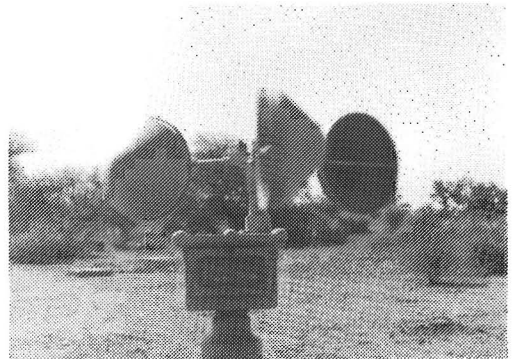
f - the anemometer used
(Casella type)

Figure 4.5   The close surroundings of Shambat station (the prevailing wind
directions are north and north-east).

To check the reliability of the data, the author measured the wind speed using a cup-anemometer (Maximum Anemometer with Aeolian Kinetics Windor Counter WP 4000, calibrated in the wind tunnel of the University of Eindhoven) which was borrowed from the Wind Energy group, University of Eindhoven. The Maximum Anemometer was placed near the station anemometer at 10 m. The two resulting sets of data are represented in table 4.2 and plotted in fig. 4.6. The figure shows that the station anemometer records lower wind speeds (about 0.3 m/s) than the calibrated (reference) anemometer which is probably caused by insufficient maintenance. On the average the percentage difference between the two sets of data is 13 ± 10%.

GMT	Wind speed measured by reference anemometer (U_r)	Wind speed measured by the available station anemometer (U_s)	Percentage difference $\left\lvert(\frac{U_r-U_s}{U_r})\times100\right\rvert$
5.30	3.2	2.5	22
6.30	3.1	2.7	13
7.30	2.8	2.8	0
8.30	3.6	3.9	6
9.30	4.1	3.7	10
10.30	4.4	4.0	9
11.30	3.6	3.3	8
12.30	3.6	2.8	22
13.30	2.3	2.1	9
14.30	2.4	2.5	4
15.30	1.5	1.0	33
16.30	1.4	1.0	29
17.30	2.8	2.5	11
18.30	3.3	3.2	3
19.30	2.9	2.6	10
20.30	1.4	1.0	29

Table 4.2   Wind speed (m/s) measured by the reference anemometer (U_r) compared with the wind speed (m/s) measured by the available anemometer (U_s) at Shambat station. Both anemometers are placed at 10 m above ground level. The averaging periods are 5 to 10 min.

Wad Madani station (405 m a.s.l.) is about 190 km south of Khartoum airport. It is an agrometeorological station which is equipped with a pressure tube Dines anemograph. There is a mast which holds nine cup-anemometers (Casella type), placed at different levels from 0.5 m to 9.14 m. The measurements at larger heights, 9.14 m and 6.10 m, are hourly but recorded only once a day as an average for the 24 hours. The anemograph is installed at about 15 m above ground level and it records hourly data. The distance between the anemograph and the mast is 30 m. Calibration and maintenance is done once

a year. Fig. 4.7 shows some photos of the close surroundings of the station.

Atbara station (345 m a.s.l.) is about 280 km north of Khartoum. Fig. 4.8 shows photos of the close surroundings of the station. The wind speed at about 15 m a.g.l. is recorded hourly, using a pressure tube Dines anemograph. Maintenance is done every six months. The history of hourly wind speed measurements goes back to 1940. At the north azimuth there are houses with a height of about 6 m at about 20 m from the anemograph position. At east azimuth houses and trees appear at about 40 m from the anemograph. At south-east and south-west azimuth there are buildings at about 40 m from the anemograph. At west azimuth, trees of 2 m height are at about 15 m from the anemograph. It is obvious that the surroundings of the station are very rough, resulting in a large aerodynamical roughness.

El Obeid airport station (570 m a.s.l.), about 370 km south west of Khartoum, was not visited because of transport difficulty from Khartoum to El Obeid at that time. However, the roughness of the close surroundings of the station is estimated at about 0.25 m from the description of the station surroundings provided by some members of the El Obeid airport meteorological staff. The wind speed at about 15 m a.g.l. is recorded hourly by using a pressure tube anemograph. The maintenance is done every six months.
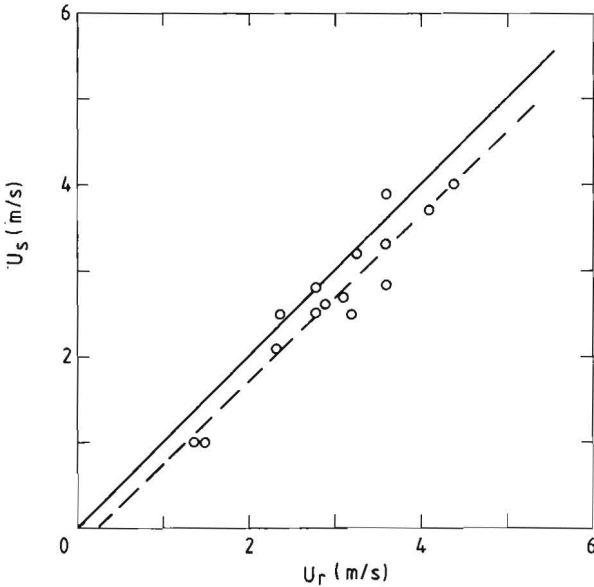
Fig. 4.6
The wind speed measured by the anemometer from Shambat stations (U_s) versus the wind speed measured by the reference anemometer (U_r).
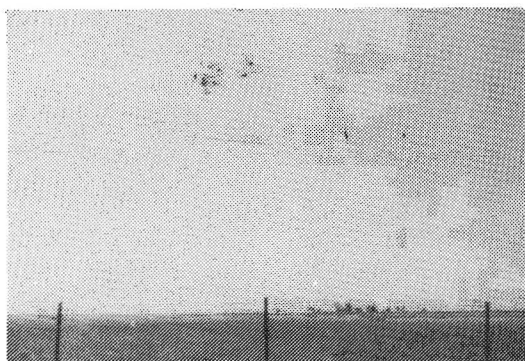
a - north azimuth
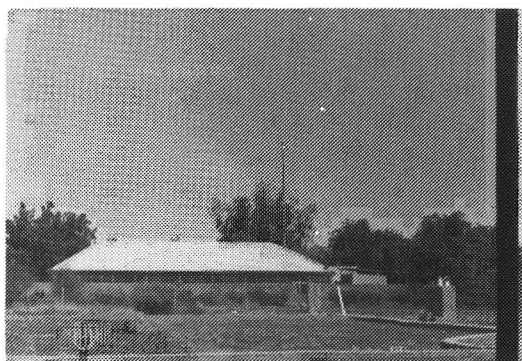
b - south-west azimuth

c - north-east azmimuth
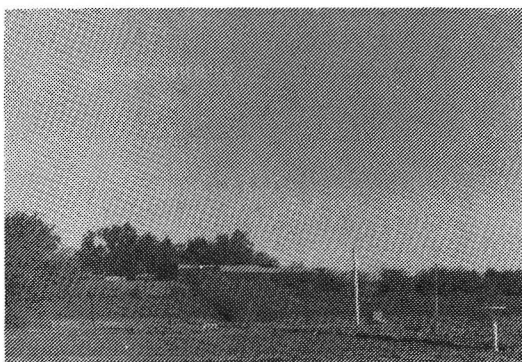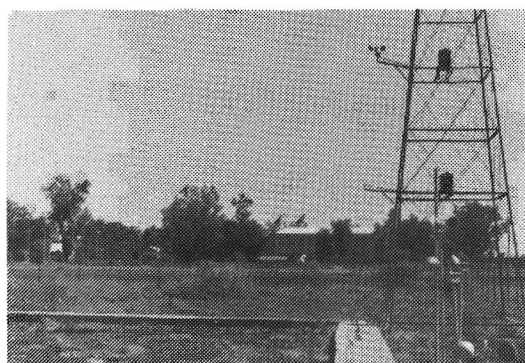
d - south azimuth

e - east azimuth

f - south-east azimuth

Figure 4.7 The close surroundings of Wadi Madani station (north and north-east are the prevailing wind directions).
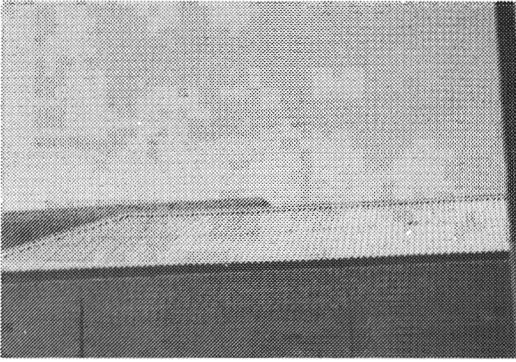
a - north
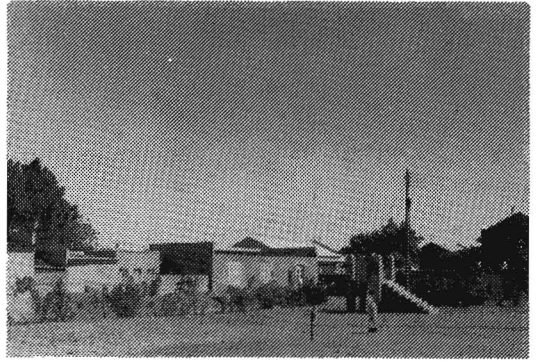
b - south-east
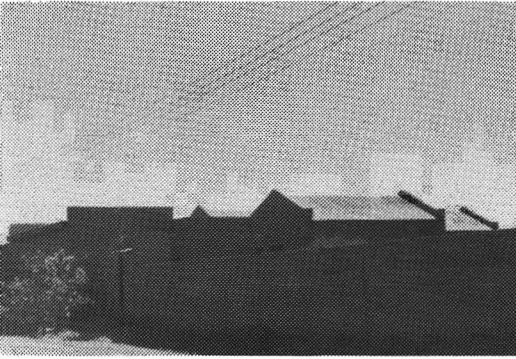
c - north-east
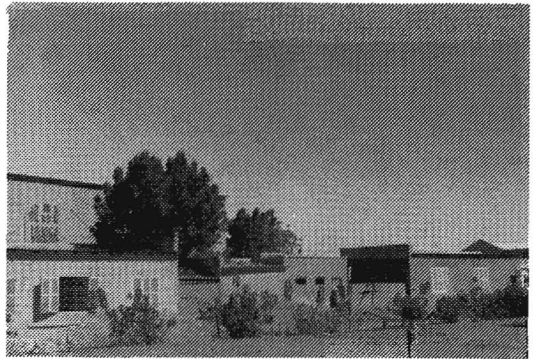
d - south-south-east
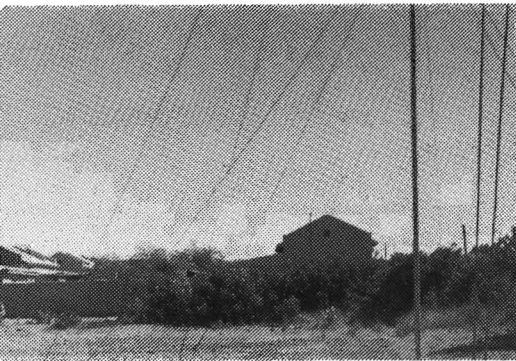
e - east
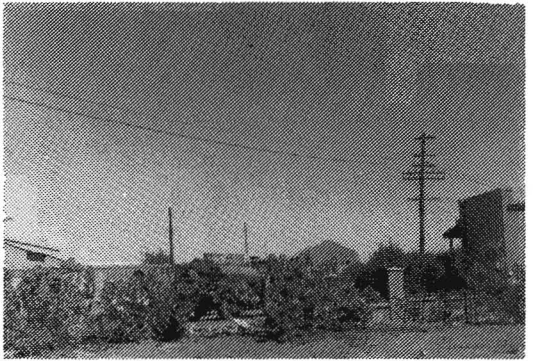
f - south-east

Figure 4.8 The close surroundings of Atbara station (the prevailing wind directions are north and north-east).

a – *Surroundings of Dongola*

b – *Surroundings of Kassala*

c – *Surroundings of Malakal*

d – *Surroundings of El Obeid*

Figure 4.9 Representative photos of the large scale landscape of the region.

To estimate the mesoscale roughness of the region, some photos of the landscape of the region (kindly supplied by Edgar Cleijne, private communication, 1987) were used in addition to the topography map of the region. Figure 4.9 shows some photos of the landscape of the region. The estimated mesoscale roughness length according to the Davenport (1960) terrain description is about 0.25 m.

4.4 *Surface wind data exposure correction and quality checks*

The data were first corrected for writing and systematic errors by comparison between two sets of data. The obviously erroneous data were subsequently removed. Secondly, data from nearby stations (e.g. Shambat station in case of Khartoum) are used to check the quality of the data. We finally estimated the roughness length from the characteristics of the surrounding of the stations (see section 4.3) using the terrain classification of Davenport (1960), presented in table 4.3.

Class	Terrain description	z_o(m)
1	Open sea, fetch at least 5 km	0.0002
2	Mud flats, snow; no vegetation, no obstacles	0.005
3	Open flat terrain; grass, few isolated obstacles	0.03
4	Low crops; occasional large obstacles, $x/H > 20$	0.10
5	High crops; scattered obstacles, $15 < x/H < 20$	0.25
6	Parkland, bushes; numerous obstacles, $x/H \sim 10$	0.5
7	Regular large obstacle coverage (suburb, forest)	1.0
8	City centre with high- and low-rise buildings	?

Table 4.3 Davenport roughness classification. Adapted from Davenport (1960), in z_o-form by Wieringa (1986).

Notes: x is a typical upwind obstacle distance and H the height of the corresponding major obstacles. For class 7, the applicability of logarithmic exposure corrections modelling is doubtful, and requires at any rate the substitution of $(z-d)$ for z in the formulae, where d is the displacement length ($d \sim 0.7$ x average obstacle height; see Brutsaert, 1975). Class 8 is analytically intractable and can better be modelled in a wind-tunnel.

The estimates of the roughness length are made in azimuth sectors of 45°. The roughness lengths obtained for Khartoum, Shambat and Wad Madani are tabulated in table 4.4.

Azimuth	roughness length		
sectors	Khartoum airport	Shambat	Wad Madani
0 - 45	0.3	0.4	0.2
45 - 90	0.3	0.4	0.3
90 - 135	0.4	0.5	0.3
135 - 180	0.5	0.5	0.3
180 - 225	0.4	0.5	0.3
225 - 270	0.3	0.6	0.3
270 - 315	0.2	0.6	0.2
315 - 360	0.2	0.5	0.2

Table 4.4 The estimated roughness length for the stations Khartoum, Shambat
and Wad Madani.

For Atbara the roughness (z_o) is estimated to be 1.0 m for all
directions, since from all directions the upwind obstacle distance (x) is less
than 6 times the height of the obstacle (H) (i.e. x/H < 6). The displacement
height (d) is estimated to be 4 m (d ~ 0.7 H). As a result of the large
aerodynamical roughness we substituted the mast height (z) by (z-d) before
using the logarithmic exposure correction.

Using the estimated roughness lengths z_o in table 4.4, and z_o = 0.25 m
for El Obeid, the data have subsequently been corrected for exposure. The
potential wind speed at a standard height (10 m) is determined using the
logarithmic wind profile equation (Wieringa, 1986):

$$U_p = 0.76 \ U_{15} \ \ln(\frac{60}{z_o}) \ / \ \ln(\frac{15}{z_o}) \ , \qquad (4.1)$$

where U_p is the potential wind speed (at 10 m) and U_{15} is the wind speed at
15 m (the height at which the original data are measured).

To check the reliability of the data from Khartoum and Wad Madani we used
data from nearby stations or data from the same station measured by means of
other equipment. In case of the Khartoum data we used data from the Shambat
agrometeorological station, which is 8 km north of Khartoum. The data from
Shambat are 6-hourly averaged data (cup anemometer measurements) which have
been corrected for terrain roughness. Fig. 4.10 shows the comparison of the

monthly averages of the potential wind for the two sets of data. The data are found to be reliable with a correlation coefficient r = 0.84.
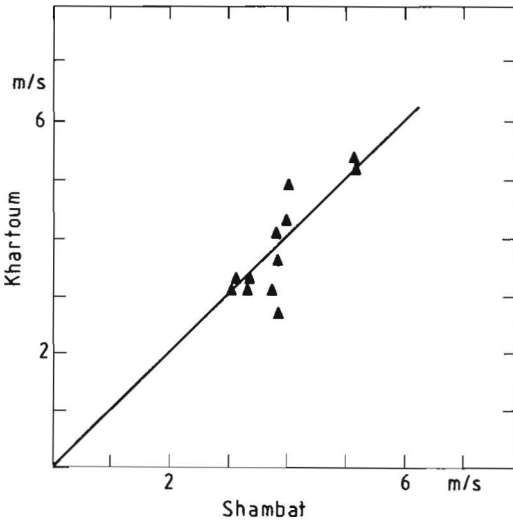
Fig. 4.10
Comparison of the monthly
averages of the potential
wind speed from Khartoum
and Shambat. The correlation
coefficient r = 0.84.
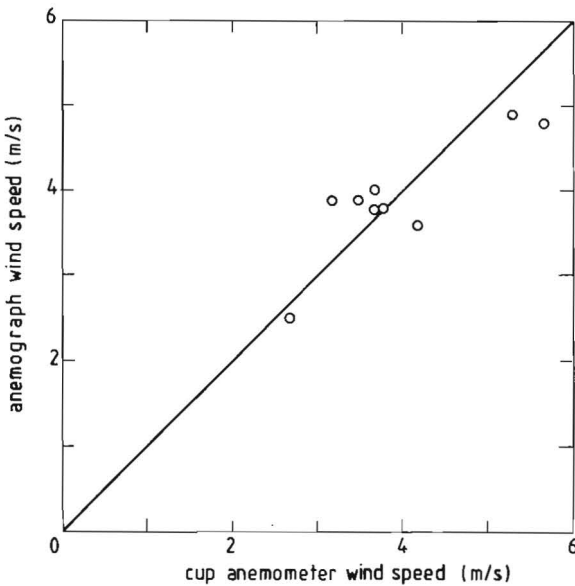
Fig. 4.11
Comparison between the
cup anemometer data and
the anemograph data from
Wad Madani for 1984. The
correlation coefficient
r = 0.86.

In case of Wad Madani we used independent data sets from the same
station, 6-hourly averaged data measured by a cup anemometer. Fig. 4.11 shows
the comparison between the sets of data. The data are on the average in good
agreement with each other, with a correlation coefficient of 0.86.

In conclusion we can say that the wind data from Khartoum and Wad Madani
are sufficiently accurate to be used both for wind energy potential estimates
and for model development. Hourly potential wind speed and wind direction data
from Khartoum and Wad Madani for 1983, '84 are given in Appendix B.
Unfortunately, to check the quality of the data from El Obeid and Atbara there
are no nearby stations and also no independent checks by other means. However,
qualitative checks indicated that El Obeid wind speed data are reliable, since
El Obeid records high wind speed in the order of magnitude of the Khartoum
wind speed, especially in the winter. The high wind speed is expected because
El Obeid is at high altitude (570 m a.s.l.) and in a semi-desert region facing
the Sahara from the north.

The Atbara data are low compared with the Khartoum data, especially in
the winter season. One would expect that the Atbara winter wind speeds are
higher or at least equal to those in Khartoum because the winter in Sudan is
characterised by a northern trade wind, which means that the more north the
region is, the higher is the winter wind speed, especially in the Nile valley
as discussed in Chapter 3. For example, the winter wind speed at Abu Hamed
(which is about 250 km north of Atbara) is higher than that at Khartoum (see
table 3.2). We therefore think that the actual winter wind speed in Atbara is
higher than what is measured.

4.5 *Potential wind variation and frequency distribution*

In order to find a measure for the monthly wind variation we introduce
the ratio σ_u/U (Abu Bakr et al., 1986) where U is the monthly average wind
speed for each hour of the day and σ_u the standard deviation. The value
of σ_u/U is a very good indication for the wind seasonal variation. Table 4.5
shows the values of σ_u/U for 1983 and 1984 for the Khartoum airport and Wad
Madani data. The Atbara data are not considered because of the high
uncertainty in the data.

It is observed that the winter season has the most steady wind speeds,
i.e. small σ_u/U ratio. The largest σ_u/U ratio is observed in May and
September. The diurnal wind directions in these months show large variations,

which are caused by the following reasons:

a. The low wind speed recorded in these months.

b. The influence of the I.T.C.Z. which passes over this region in May northwards and September southwards.

We conclude that the data of these two months are difficult material for basic physical modelling because of their large variation. They can be used, however, to indicate the passage of the I.T.C.Z.

The calculated values of σ_u/U for different seasons are in agreement with our expectations for the seasonal variation. In the winter σ_u/U has its lowest value, $(27\pm4)\%$, which is due to the steady north trade wind. In the advancing monsoon the value increases to $(44\pm11)\%$, which is due to the changing of the prevailing wind direction from north trade wind to a southwest humid wind originating from the South Atlantic Ocean. The monsoon shows the highest value, $(52\pm9)\%$, due to the interaction between the dry air stream from the north and the humid air stream from the south. In the retreating monsoon the value of σ_u/U decreases to $(35\pm9)\%$, due to the retreatment of the humid air stream to the south and a prevailing northeast trade wind.

Month	$(\sigma_u/U)\%$			
	Khartoum		Wad Madani	
	1983	1984	1983	1984
January	28	28	22	25
February	27	32	24	25
March	41	39	32	33
April	39	37	41	30
May	58	60	59	59
June	55	41	60	52
July	57	53	50	42
August	41	52	40	44
September	58	59	75	60
October	37	47	−	42
November	28	42	30	21
December	28	39	28	23

Table 4.5 The monthly values of $(\sigma_u/U)\%$ for 1983, 1984 for Khartoum and Wad Madani.

Since the conventional method for wind potential evaluation is the computation of the frequency distribution, calculated frequency distributions for the stations Khartoum and Wad Madani are presented in Appendix C. The frequency distribution of Atbara is not considered because of the high uncertainty in the data; For example at Atbara the measured percentage of

calms in 1984 is four times larger than at Khartoum which is improbable, see chapter 3. Fig. 4.12 shows the frequency distribution behaviour in Khartoum, which indicates substantial differences between the annual distribution and the different monthly distributions (Abu Bakr et al., 1986). Obviously, for wind energy application it is advisable not to restrict an analysis to the annual distribution. The application of wind energy will be more efficient in the winter than in other seasons. Fortunately, in the winter the demand for water pumping is very high for winter crop irrigation.
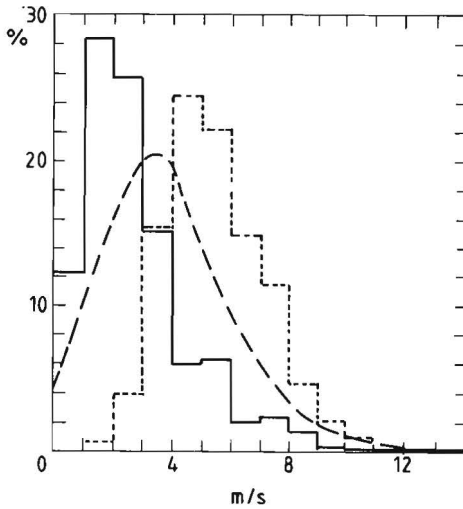
Figure 4.12 Percentage frequency distribution of the potential
wind speed at Khartoum for the 1983 and 1984 combined data.
---- Annual distribution with a Weibull distribution shape
factor (k) of 1.75.
.... January distribution with a shape factor (k) of 3.2.
____ May distribution with a shape factor (k) of 1.5.

We also used the Weibull cumulative distribution paper to represent the frequency distribution and to obtain the shape factor (k). The shape factor (k) is a good indicator of the type of wind regimes (Stevens and Smulders, 1979). Fig. 4.13 gives an example of the Weibull distribution plots. The k-values versus the months are plotted in fig. 4.14. High k-values (k ≥ 3) indicate a steady wind regime (i.e. trade wind regime) and low k-values (k ≤ 1.5) indicate large wind variations. From fig. 4.14 we see that the winter months show a steady trade wind characteristic, while the largest wind variations are observed in May and September.
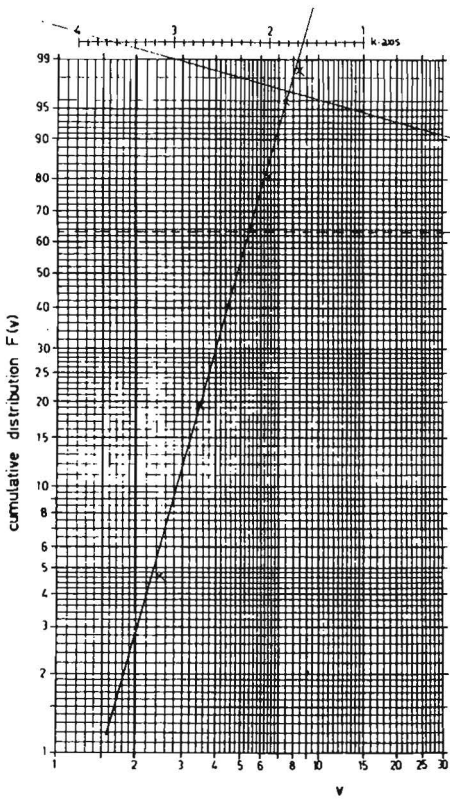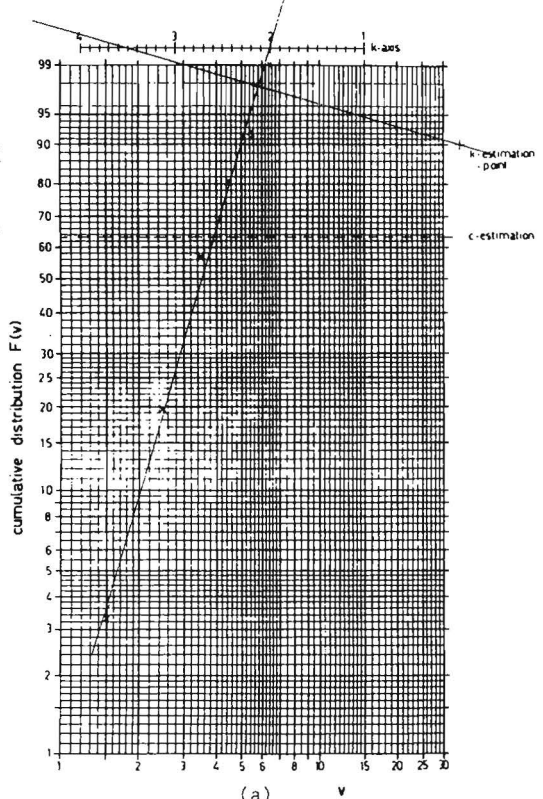
(b)   (a)

Figure 4.13 Weibull probability paper for wind energy studies
a - Wad Madani data for February 1984. Shape factor (k) = 3.5
b - Wad Madani data for January 1983. Shape factor (k) = 3.6
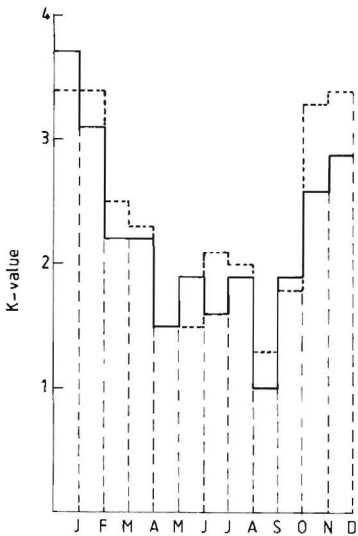
Fig. 4.14
The value of the shape factor k
versus month for 1983, 1984.
―――――― *Khartoum*
------ *Wad Madani*

56

4.6   Surface data diurnal course representation

4.6.1 Potential wind speed

To study the behavour of the wind speed during the 24-hour cycle we
calculated the average of hourly data for every month for the stations
Khartoum, Wad Madani, Atbara and El Obeid. The diurnal cycles of the different
stations and different months mostly do not show an identical behaviour. We
therefore divided, for ease of representation and possibly for future
interpretation, the diurnal cycles into a number of classes. In general four
groups, according to the behaviour of the wind diurnal cycle, can be distilled
from all data available. Of course, the classification into four groups is a
data simplification since there are also wind diurnal course data which are
difficult to be classified into one of these, but nevertheless it is a useful
qualitative tool for the representation of our data. Table 4.6 shows the
groups of the diurnal course and the range of the potential wind speed for
each month and station.

Group A shows an approximately constant wind speed during the night
hours. In the period 8-10 hr the wind speed shows a sharp increase (about 1.5
m/s per hour) reaching an absolute maximum around 10 hr. In the period 17-19
hr the wind speed shows a sharp decrease (about 0.8 m/s per hour). Fig. 4.15a
shows a representative diurnal cycle of group A.

Group B diurnal cycle is in general similar to the group A cycle, except
that the maximum around 10 hr is more pronounced and sharper, and the wind
speed between 14-18 hr is approximately constant. It shows a minimum at about
20 hr., after which it starts increasing to a secondary maximum around 23
hr. Fig. 4.15b shows a typical group B cycle.

Group C shows a slightly broader maximum (around 10 hr) than the group B
cycles with a steady decrease in the afternoon, and a more pronounced maximum
at midnight than that of group B; see figure 4.15c.

In group D the wind speed is approximately constant from the beginning of
the day until about 16 hr, after which it starts decreasing to a minimum at
around 20 hr. Figure 4.15d gives a typical example of the group D cycles.

From table 4.6a we observe that for all stations the diurnal cycles in
the winter can be represented, without exception, by groups A and B. In the

advancing monsoon (March and April) most of the cycles can be classified by group A and B while in May the majority of the diurnal cycles are represented by group C; see table 4.6b. The large majority of the diurnal cycles in the monsoon are represented by group C and D, while in the retreating monsoon they are mostly from groups B and C.

The diurnal cycle shows a remarkable variable character during the day. The sharp increase (decrease) of the wind speed coincides with the sunrise (sunset), which indicates that the source of the wind is thermal due to the high sensible heat flux received in the cloudless atmosphere of Central Sudan. In most cases in the monsoon the magnitude of the wind increase or wind decrease is smaller in comparison to the winter cycles, which can be observed from the wind speed range in table 4.6c. A reasonable explanation for this difference in magnitude is the presence of cloud-cover in the monsoon season.
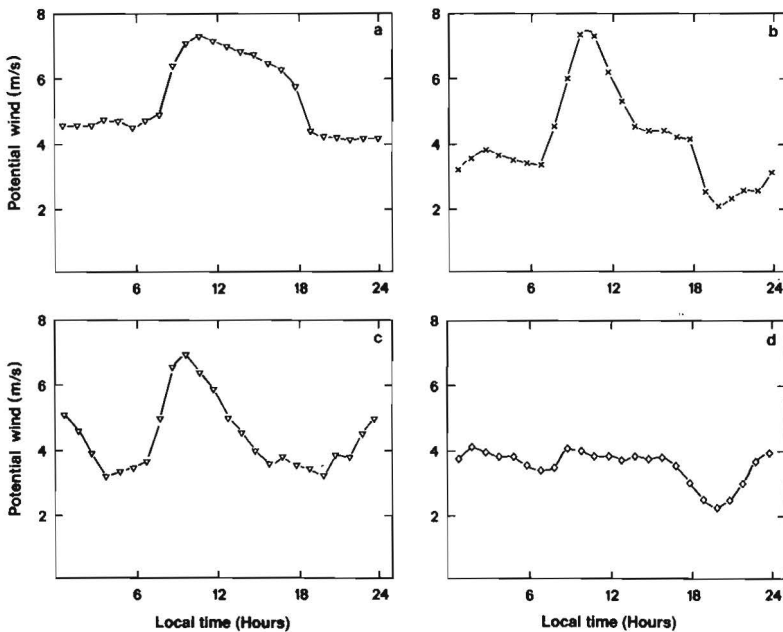
Figure 4.15 Potential wind diurnal cycle classification.
a - Group A, b - Group B, c - Group C, d - Group D.

The general shape of the wind speed diurnal cycle in Central Sudan does not resemble those usually observed at temperate latitudes, since in Sudan the

wind speed decreases from the morning to the afternoon, while in temperate
latitudes the wind speed increases from the morning to the afternoon. This
phenomenon will be discussed in more detail in the chapters 5 and 6.

In addition to the wind speed in table 4.6, we also tabulated the wind
direction range for all seasons for the four stations. Table 4.6a shows the
wind direction variation during the winter season. In the winter the wind
direction from the four stations varies from NNW-NNE. For all stations the
wind direction cycle in the winter shows a similar pattern. Figure 4.16 shows
a representative wind direction diurnal cycle (WDC) for the winter. This
constant WDC is due to the north trade wind in this season. In the advancing
monsoon the WDC (see table 4.6b) normally varies between NE and NW, except for
some May months which show variations larger than 180° during the 24-hours
cycles. In the monsoon the WDC (see table 4.6c and 4.6d) varies over the
azimuths S-W-N; some September months, however, show variations larger than
180°.
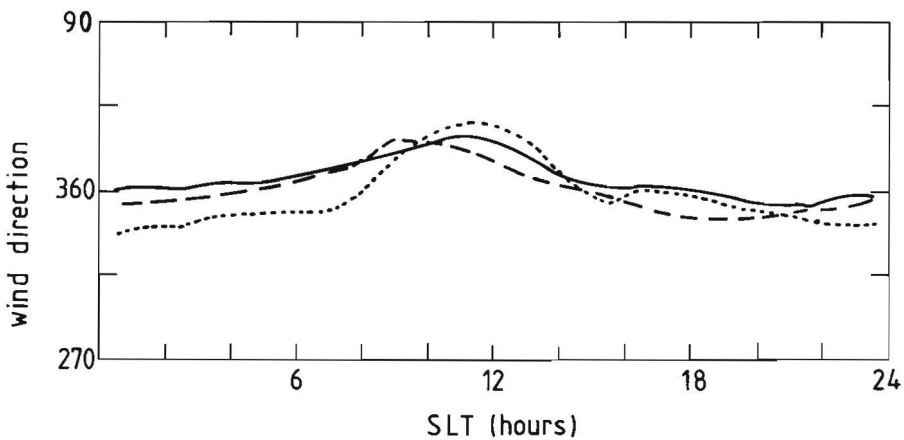
Figure 4.16 The wind direction course of January 1984.
——— Atbara, ... Khartoum, --- Wad Madani

Figure 4.17 gives an example of the diurnal wind direction behaviour for
May and September. The WDC of the retreating monsoon is similar to that of the
advancing monsoon: it varies between NE and NW. However, for Wad Madani
(November 1982) the WDC varies over azimuths W-NW but this exceptional
variation could very well be caused by uncertainties in the data.
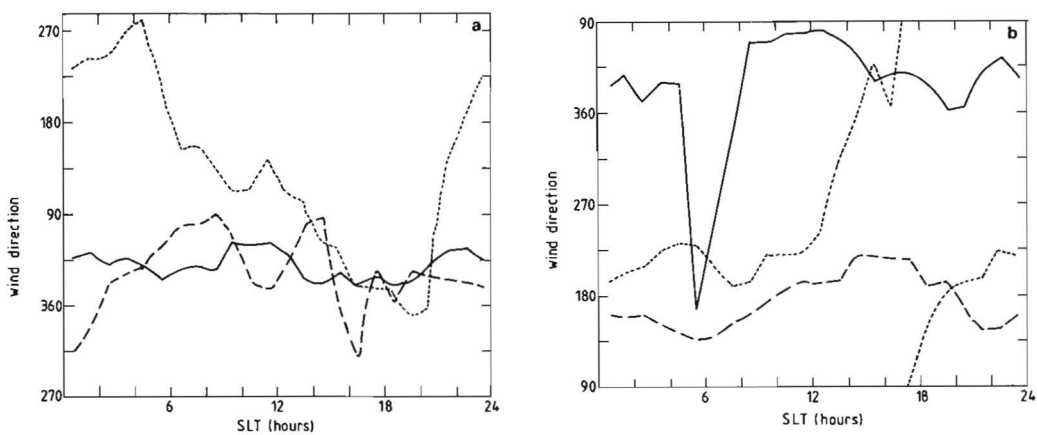
Figure 4.17 The diurnal wind direction for a - May 1984, b - September 1984.
_____ *Atbara,* ..... *Khartoum,* ----- *Wad Madani.*

Table 4.6a Winter

| station (year) | Diurnal course group (potential wind range in m/s) wind direction range | | |
	December	January	February
KHARTOUM 1984	B (3-5.5) NNW-NNE	A (4-7) NNW-NNE	A (4-7) NNW-NNE
1983	B (3.5-6.5) NNW-NNE	B (4.5-6.5) NNW-N	B (3.5-7) NNW-NNE
1982	B (3-5) N-NNE	A (2-4) NNW-N	B (2.5-6) NNW-N
WAD MADANI 1984	A (3-4.5) N-NNE	A (3-5) N-NNE	A (3-5) N-NNE
1983	A (2.5-4.5) N-NNE	A (3-5.5) N-NNE	A (2.5-5) NNE-NE
1982	A (2-4) N-NE	A (2.5-4) NNE-NE	B (2.5-5) NNW-NNE
ATBARA 1984	B (3-6) N-NNE	A (2-4) N-NNE	A (3-6) N-NNE
1983	B (2-4.5) NNE-NE	B (3.5-6.5) N	B (3.5-6) N-NNE
1982	A (3-5) N-NNE	A (1-3) N-NNE	-
EL OBEID 1984	B (1.5-4.5) N-NNE	A (3.5-7) N-NNE	B (3-6.5) N-NNE

Table 4.6b   Advancing Monsoon

station	Diurnal course group (potential windspeed range in m/s) Wind direction range		
	March	April	May
KHARTOUM 1984	B (3-6) N-NE	B (3-7.5) NW-NNE	C (1.5-4.5) *
1983	B (2.5-6) NW-NNE	B (3-6.5) NW-NNE	C (1-4) WNW-NNE
1982	B (2-6) NNW-N	B (1.5-5) WWW-NNE	C (1-4) NNW-NNE
WAD MADANI 1984	A (2.5-5) NNW-NE	A (2-4.5) N-ENE	C (2.5-5) *
1983	B (1.5-4) NNE-NE	B (1.5-3.5) NW-NNE	B (2-4.5) *
1982	A (2.5-5) NW-N	B (1.5-3.5) WNW-NNE	B (2-4.5) SSW-NW
ATBARA 1984	A (2-5) N-NNE	A (2.5-6) N-NNE	C (1-4) NNE-ENE
1983	B (2.5-6) N-NNE	B (2-5.5) N-NNE	C (1.5-4) NNE-ENE
1982	D (1.5-3.5) NNE	-	A (2.5-6) N-NE
EL OBEID 1984	B (2-7) N-NE	B (2-7.5) N-NE	C (2.5-6) *

Table 4.6c Monsoon

station	Diurnal course group (potential wind speed range in m/s) Wind direction range			
	June	July	August	September
KHARTOUM 1984	D (2-4.5) WSW-WNW	C (1-5) SW-NW	D (1.5-4.5) SSW-WNW	D (2-4.5) *
1983	C (2-5.5) SSE-WNW	D (2-5.5) WSW-S	D (2.5-5) SSW-W	D (1-3.5) SSW-NW
1982	C (2-7) NW-SW	D (2-5.5) S-SW	C (2.5-5) SSE-SSW	** SSE-SSW
WAD MADANI 1984	C (2.5-7) WSW-NW	C (2.5-7) SSW-W	C (3-7) S-WSW	C (2-6) SE-SW
1983	C (3-6) S-SW	C (2.5-7) S-SSW	C (2.5-6) S-SSW	C (0.5-4) SSE-WSW
1982	C (2-5) SSW-W	C (2-7) SSW-WSW	C (4-7.5) NW-NNE	C (3-6) W-N
ATBARA 1984	D (1-3) NW-NNW	D (1-4) NW-NNW	C (1.5-5) WNW-NNW	C (1-4) W-ENE
1983	D (1-4) WSW-NE	C (1.5-4) SW-NW	B (2-6) WSW-WNW	** WNW-NE
1982	B (1-6) WNW-NNW	B (1.5-6) WSW-WNW	C (3.5-7) SW-W	B (2-4) *
EL OBEID 1984	D (1.5-4) SWS-WNW	C (2.5-5) SW-SNW	C (1.5-4.5) SSW-W	** SSW-W

63

Table 4.6d   Retreating Monsoon

stations	Diurnal course group (potential wind speed range in m/s Wind direction range	
	October	November
KHARTOUM 1984	C (2-4) N-ENE	B (1.5-4) NNW-NNE
1983	C (2.5-5) NNW-NNE	B (2.5-5.5) NNW-NE
1982	C (2.5-5) NNW-NNE	B (2.5-5.5) NNW-NNE
WAD MADANI 1984	B (1.5-3) WNW-NE	B (3-5) NW-N
1983	– NW-NNE	A (1.5-4)
1982	C (1-3.5) NE-E	A (2-4) W-NW
ATBARA 1984	C (1-5) N-ENE	C (2.5-5) N-NNE
1983	D (1-3) N-ENE	B (2-4) N-NE
1982	C (2-4) N-ENE	C (3.5-4) N-NNE
EL OBEID 1984	A (1-4) N-NE	B (1.5-5) N-NE

Table 4.6   The surface wind regime in Central Sudan for the four seasons.
* = The wind direction cycle shows variation larger than 180°.
** = The wind speed cycle shows a low wind speed with relatively large variations.

4.6.2 _Radiation, humidity and pressure surface data_

The global radiation data from Shambat and Dongola show a diurnal cycle
which can perfectly be described by a half-sine function with a maximum at
about 700 W/m^2 (see chapter 5, fig. 5.2). The relative humidity data from
Shambat, Khartoum and Dongola show a similar diurnal cycle during all months.
The relative humidity is very low during the whole year in Central Sudan. On
the average it varies between 20%-50%, being maximum at about 6 hr SLT and
minimum at about 16 hr SLT. The surface pressure diurnal cycles, available
from Khartoum and Atbara, show a similar behaviour for all months with a
minimum at about 10 hr SLT and a maximum at about 16 hr SLT. The difference
between these extremes is about 4 mb. The temperature diurnal cycles,
available from Khartoum, Dongola, and Atbara, show a large diurnal variation.
The difference between the maximum (at about 16 hr SLT) and the minimum
temperature (at about 7 hr SLT) is about 10°C for the monsoon and about 15°C
for other seasons.

Figure (4.18) shows typical patterns of the relative humidity, pressure,
temperature and wind speed diurnal cycles. From the figure we see that the
sharp increase of the wind speed coincides in time with the maximum pressure.
The figure further shows that the relative humidity cycle is proportional to
the temperature cycle, while that of the pressure behaves like the derivative
of the temperature cycle. The behaviour of these profiles will be discussed in
more detail in chapter 5.
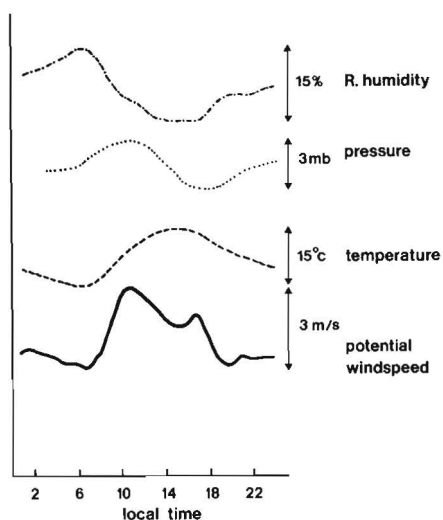
Fig. 4.18
A typical pattern of the relative
humidity, pressure, temperature
and wind speed cycle over the
region.

4.7 Upper air data representation

The upper air data represented here are obtained from Khartoum, Dongola,
El Obeid, Kassala and El Damazin. All observations, except the Khartoum midday
observations, are from pilot balloon ascents (midday and midnight). From El
Damazin only midday data are available. The pilot balloon observations consist
of only wind speed and wind direction measurements. The vertical resolution
has an increment of 500 m up to 3 km (for El Obeid the observations are only
up to 2 km). The midday observations at Khartoum are measured by means of a
Vaisala (Finnish) radiosonde instrument which records the wind speed, wind
direction, humidity, temperature and the pressure. The measurement intervals
are irregular; surface, 900, 850, 800, 700 and 600 mb. The pilot balloon and
radiosonde measurements have a height accuracy of about 200 m.

4.7.1 The wind profile

The general shape of the midday profile of the wind speed in Central
Sudan observed in the four seasons (with the exception of El Damazin) shows a
typical trade wind profile with a jet-like structure from the surface up to
about 2 km. Above 2 km the wind speed increases with height. Figure 4.19 shows
a typical profile. The maximum wind speed observed in the jet-like structure
occurs at about 1 km. The increase of the wind speed from the surface to 1 km
ranges from 1-4 m/s over the region. Among all the wind profiles, that of El
Damazin (which is about 500 km SE of Khartoum) is exceptional, probably
because the region is woodland savannah and its climate is highly influenced
by the tropical climate from the south. Over the whole year the wind speed in
El Damazin increases slightly with height from the surface up to 2.5 km; the
difference is less than 3 m/s.

The wind direction profiles vary with seasons in Central Sudan, except
for Dongola since the I.T.C.Z. hardly reaches this region. The prevailing wind
direction in Dongola varies in the range of NE-NW from the surface to 3 km in
all seasons. In the winter, the advancing monsoon and the retreating monsoon
the prevailing wind direction at the other stations varies between NE to NW
below 1 km. Above 1 km the prevailing wind direction varies between NW to SW.
In the monsoon the prevailing wind direction in the lower kilometer varies
over the region in the range SW-NW, while above 1 km the

prevailing wind varies from SW-NE. Some May and September months show large variations in the wind direction profile. These variations are expected to be caused by the passage of the I.T.C.Z. during these months.

The midnight wind profile in Central Sudan shows a similar behaviour during all seasons. Below 0.5 km the wind speed shows a sharp increase due to the nocturnal jet which is expected to occur in this layer. The increase of the wind speed between the surface and 0.5 km varies in the range 2-9 m/s over the region. The largest increases are observed in El Obeid (see fig. 4.20) while the lowest are observed in Dongola. The wind direction does not show much changes from the surface up to 3 km in contrast with the day profile. The prevailing wind direction in the monsoon varies over the region from SW to NW, while during the other seasons the wind direction varies from NE to NW. Fig. 4.20 gives an example of the midnight wind profile.
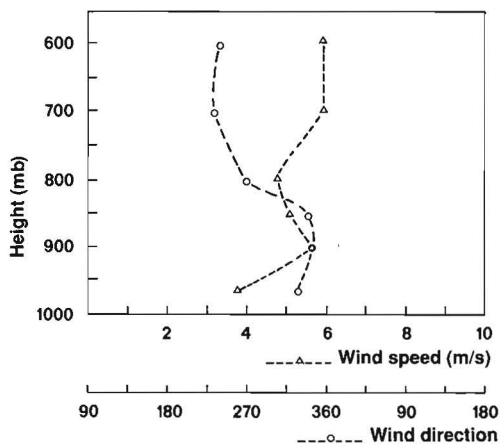
Fig. 4.19
Midday wind profile of Khartoum
for December 1984.
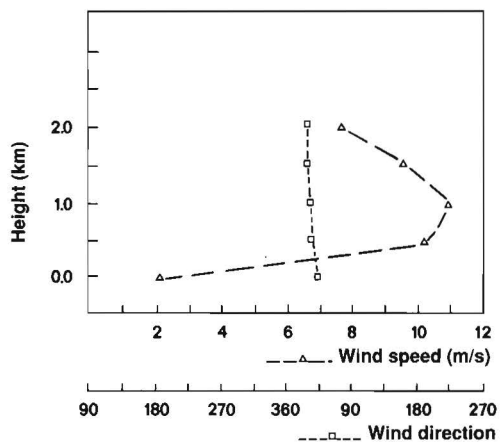
Fig. 4.20
Midnight wind profile of El Obeid
for December 1984.

4.7.2 *Khartoum potential temperature and relative humidity profile*

From the radiosonde temperature data of Khartoum (1983, 1984) we cal-
culated the monthly averaged potential temperature profiles. The potential
temperature profiles as well as the relative humidity profiles are important
variables for estimation of the upper limit of the planetary boundary layer.
Fig. 4.21 and 4.22 show the midday potential temperature profiles and the
relative humidity profiles for the two years. In the winter season the
potential temperature is constant from the surface up to an upper limit at
about 900 mb. The upper limit of constant potential temperature increases in
height as a function of month to a maximum of approximately 800 mb in the
monsoon season. The constant behaviour of the potential temperature and the
change of the relative humidity as a function of height indicates the height
of the convective PBL. Figure 4.21 and 4.22 show that the height of the
boundary layer increases from about 1 km in the winter up to about 2 km in the
monsoon. The relative humidity profiles have a very low average: less than 40%
in the winter and up to at most 60% in the monsoon, indicating that there is,
especially in the winter, a high occurrence of zero cloud-cover. These
profiles will be discussed in more detail in Chapter 6.
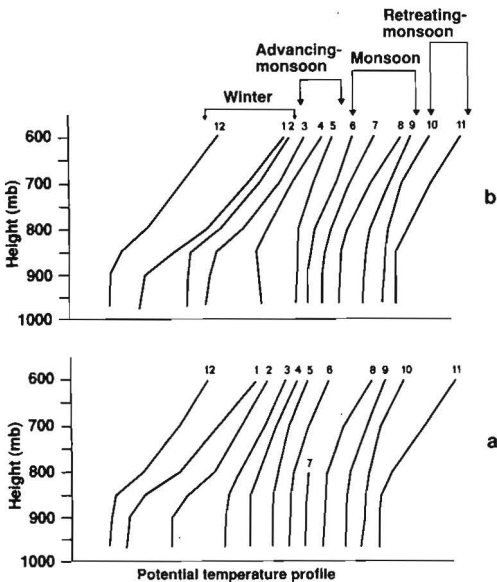
Fig. 4.21
Monthly averaged midday
potential temperature
profiles at Khartoum
a – 1984, b – 1983.
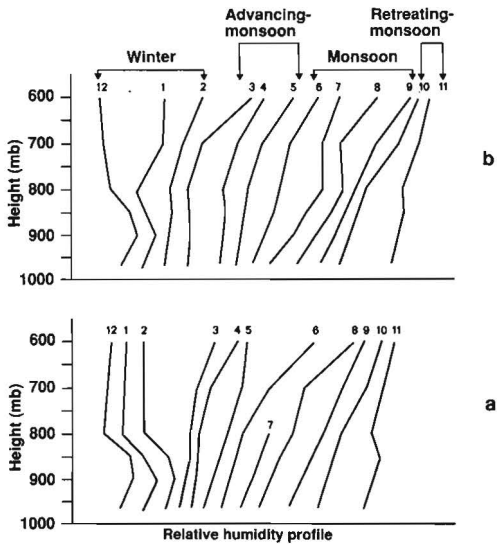
Fig. 4.22
Monthly averaged midday
relative humidity
profiles at Khartoum
a - 1984, b - 1983.

4.8 Conclusions

In most cases meteorological data are considered to be unreliable without
proper checks. In the case of Sudan the wind data from Khartoum, Atbara and
Wad Madani are investigated and corrected for exposure. The results from
Khartoum and Wad Madani are found to be of sufficient quality for wind energy
analysis. The data from Atbara, however, are found to be unreliable because of
the large aerodynamical roughness. Unfortunately, there is no nearby station
in the surroundings of Atbara to check the quality of the data and there is
also no independent check by other means at the station.

A data base is constructed consisting of about 330×10^3 meteorological
observations from eight stations in Central Sudan, which is useful material
for modelling the boundary layer. Using such a data base is more economical
than to install in a new network of measuring equipment to estimate the wind
potential.

69

The diurnal wind course shows a noticeable variable character which is probably due to the large sensible heat flux received. Consequently there is a large difference between the day and night wind speeds, since the temperature difference between the day and night amounts to about 15° C. The wind diurnal cycle shows the unique behavior of reaching its maximum at about 10 hr. (in temperate latitudes the maximum is usually reached at midday). This phenomenon will be discussed in detail in Chapters 5 and 6.

May and September wind data show large variations. This is due to the low wind speed recorded in these months and the influence of the I.T.C.Z. which passes over this region in May northwards and in September southwards. These large variations in May and September are also observed in the wind midday profiles. The frequency distribution is strongly dependent on the seasons, which means that the annual distribution is not representative for each month. This is an important result for wind energy applications in the Sudan (and also for other Sahelian regions which have a similar climate).

The midday wind speed profile shows a wind maximum around 1 km, with a wind speed increase from the surface up to 1 km ranging from 1 to 4 m/s over the region. Such an increase is a typical behaviour of a trade wind profile. The nocturnal profile indicates the presence of a pronounced nocturnal jet since a sharp increase in the wind is observed from the surface up to 0.5 km ranging from 2 to 9 m/s over the region. The midnight wind direction profile shows only small variations from the surface up to 3 km; in some cases the wind direction profile is even constant.

The midday temperature profile of Khartoum shows the typical behaviour of a convective boundary layer. It indicates that the height of the boundary layer increases from about 1 km in the winter to about 2 km in the monsoon. The heights are in agreement with the boundary layer heights indicated by the relative humidity profiles. The relative humidity is very low in Khartoum (at midday) from the surface up to 3 km. It is less than 40% in the winter and reaches a maximum of about 60% in the monsoon season. A more quantitative discussion about the midday and midnight upper air data will be presented in Chapter 6.

C H A P T E R   5

A BOUNDARY LAYER MODEL FOR THE DETERMINATION OF HOURLY SURFACE
WIND CHARACTERISTICS IN A REPRESENTATIVE TROPICAL AFRICAN REGION

CHAPTER 5

A BOUNDARY LAYER MODEL FOR THE DETERMINATION OF HOURLY SURFACE
WIND CHARACTERISTICS IN A REPRESENTATIVE TROPICAL AFRICAN REGION

ABSTRACT

In this article a quantitative transposition model is introduced which
determines hourly wind speeds in a representative tropical region (Central
Sudan). The model consists of two parts. Firstly, a local boundary-layer
model, based on the energy balance equation and the Businger-Dyer equations,
is used to compute the average diurnal cycle of various characteristic
boundary layer parameters. Secondly a horizontal transposition method is
introduced to calculate the wind speed behaviour at an arbitrary station from
that at a reference station. This method is based on assumed spatial constancy
of the turbulence parameter u_* in the period November-April in a region of
about (700×800) km^2 in Central Sudan. The constancy of u_* is concluded from
the very stationary character of the climate. The model-computed hourly wind
speeds are in good agreement with the potential wind speeds (at 10 m over open
country) calculated from the measured data, and provides better results than
the conventional procedure which assumes constant regional hourly wind speeds.

5.1 Introduction

In tropical Africa the density of the meteorological observation stations
is relatively low. Due to lack of maintenance of measuring equipment, the
reliability of the measured meteorological data, such as the surface wind
speed, is often limited. According to Woodhead (1970), wind statistics in
tropical East Africa are estimated to have an observation uncertainty of about
15%. If we consider the additional exposure uncertainty of approximately 10%
(Wieringa, 1983), the maximum error for estimating wind at one station from
another is of the order of 25%. The relatively large uncertainties in
published data, which are mostly presented as monthly averages (e.g. Griffiths

72

and Soliman 1972), do not provide a sufficient basis for analysis requirements for wind engineers, hydrologists and agrometeorologists.

The low station-density, especially in tropical countries, resulted in a rough method (which we will refer to as the "conventional method") of estimating the wind speed. In this method, one assumes a constant regional wind speed in a region of at least (100x100) km^2. In practice it means that the data from a single station are considered as representative for the region (e.g. Hamid and Jansen 1981, Weather Bureau RSA 1975, Reed 1975). The conventional method is still often used when only the wind data are accessible, while good information on station measuring conditions is unavailable. In such cases only height corrections are possible (e.g. Exell and Fook 1986, Duensing et al. 1985).

A better description of the regional surface wind climate requires that some form of atmospheric boundary layer modelling is applied to the station observations. A useful first step to wind information improvement is the application of local-scale azimuth-dependent exposure corrections to the wind observations at partially-sheltered stations (Duchene-Marullaz 1977, Wieringa 1983). However, this does not solve the mesoscale surface wind representativity problem, for which additional modelling is required to extrapolate hourly wind speed to other locations.

In the literature there are only a few publications dealing with models that calculate hourly wind speeds at the surface. Peterson and Parton (1983) computed the diurnal variations of surface wind speeds at 2 m, using a model for simulated diurnal variation in air temperature at short grass prairie sites. This model is limited to regions where the mean monthly diurnal variations of wind speed and air temperature exhibit similar patterns. Bhumralkar et al. (1980) used a non-divergent model for hourly wind speed computation in complex terrain. However, their published figures show a large discrepancy between the wind speeds measured and those calculated. Most of the existing analytical wind climate models (e.g. Simiu 1973) are generally restricted in their applications to near-neutral stability, when roughness and topography are the only dominating boundary conditions. For modelling the wind climate in tropical countries such as the Sudan, however, the extremely large average heat fluxes present an additional boundary condition of major importance. In other words, a tropical wind climate model needs explicit handling of stability. Such an approach is found in some recent models (e.g. Petersen et al. 1984, Gryning and Larsen 1981). These models are based on the

boundary layer resistance laws that require a more detailed meteorological data base than is usually available in tropical countries.

A pioneer study of the wind climate in the Sudan was published by Sutton (1923). He has drawn attention to the peculiar behaviour of the diurnal cycle of the wind, which shows a decrease of the wind speed from the morning to the afternoon with a maximum around 9 hr, Sudan local time (SLT). A firm explanation for this distinctive diurnal wind course has not yet been found. At the present stage of this research we will only give a qualitative description of the behaviour of the diurnal cycle in Central Sudan (see section 5.3.3)

An interesting meteorological field project has been carried out in South West Africa at Tsumeb (19° S, 17° E), where the dry season climate shows much similarity to the Central Sudan climate (Walk 1972, Mayer and Walk 1973, Mayer 1974, for a review see Walk and Wieringa 1988). An important result of this study was the proof of the applicability in low latitudes of the Dyer flux-gradient equations, which were developed for moderate latitude (Dyer 1974).

The main item of this chapter is devoted to a boundary layer wind transposition method to determine the hourly surface wind in Central Sudan. This method is checked with the aid of several years of hourly processed routine meteorological data (about 330×10^3 observations) from Sudanese stations (see section 5.2). The starting point for this method is the stationary character of the climate (see section 5.3) which follows from the following regional characteristics:

1. The regional topography is non-mountainous.
2. The Regional-scale pressure systems (isobar patterns) are steady.
3. The Local boundary-layer parameters generally vary only over 10% - 15%. From this we derive the assumption that at a given time the turbulence parameter u_* shows no systematic variations across the region at a given hour (see section 5.4.4).

The actual modelling is based on the energy balance equation and on the Monin-Obukhov similarity theory (see section 5.4.1). The basic input information consists of data observed at a reference station R. From these data we compute the regional hourly values of u_*. Then for an arbitrary station A in the region, where only pressure and temperature are known or can be estimated, we calculate the wind speed $U(z)$, using a mesoscale regional roughness estimate. In this fashion, typical boundary layer wind climate characteristics, such as the diurnal cycle, can be transposed quantitatively

to an arbitrary regional location (see section 5.4.4).

The sensitivity of the model to various parameters is analysed in section 5.5, using the available data base. Section 5.6 shows that the variation of the friction velocity (u_*) across the region is within the accuracy range of the roughness length estimate and the uncertainty due to the calibration and maintenance of the measuring equipments. The quality of the model is tested in section 5.7 by comparing the computed wind speed to two sets of data: first to those obtained by the conventional procedure (constant regional wind speed) and secondly with the potential wind speed (which is the wind speed at 10 m over open country calculated from the measurements). The model output showed better results than the conventional procedure and good agreement with the potential wind speed data.

In Central Sudan the model gives satisfactory results for the period November-April. As yet the application is unreliable in the monsoon and the months just before and after the monsoon (May, October), because the climate in this season shows large regional variations. These variations are mainly due to the passage of the Inter Tropical Convergence Zone (ITCZ).

As far as we know, this is the first hourly surface wind estimation model for tropical Africa. Moreover, the technique of horizontal application of the Businger-Dyer flux-gradient equations at constant height appears not to have been published before.

The region considered in this investigation measures about (700×800) km^2 and lies between 12°N 30°E and 20°N 36°E in the Central Sudan. The topography of this region is non-mountainous, with a gentle slope towards the valley of the Nile which traverses the centre of the region from south to north. The average terrain slope $\partial z/\partial x$ toward the Nile is about 1.3×10^{-3} from the west and approximately 0.7×10^{-3} from the east, while the Nile valley itself has a south-north slope of 0.1×10^{-3}. In figure 5.1 we picture the region of investigation with some general topographical characteristics.
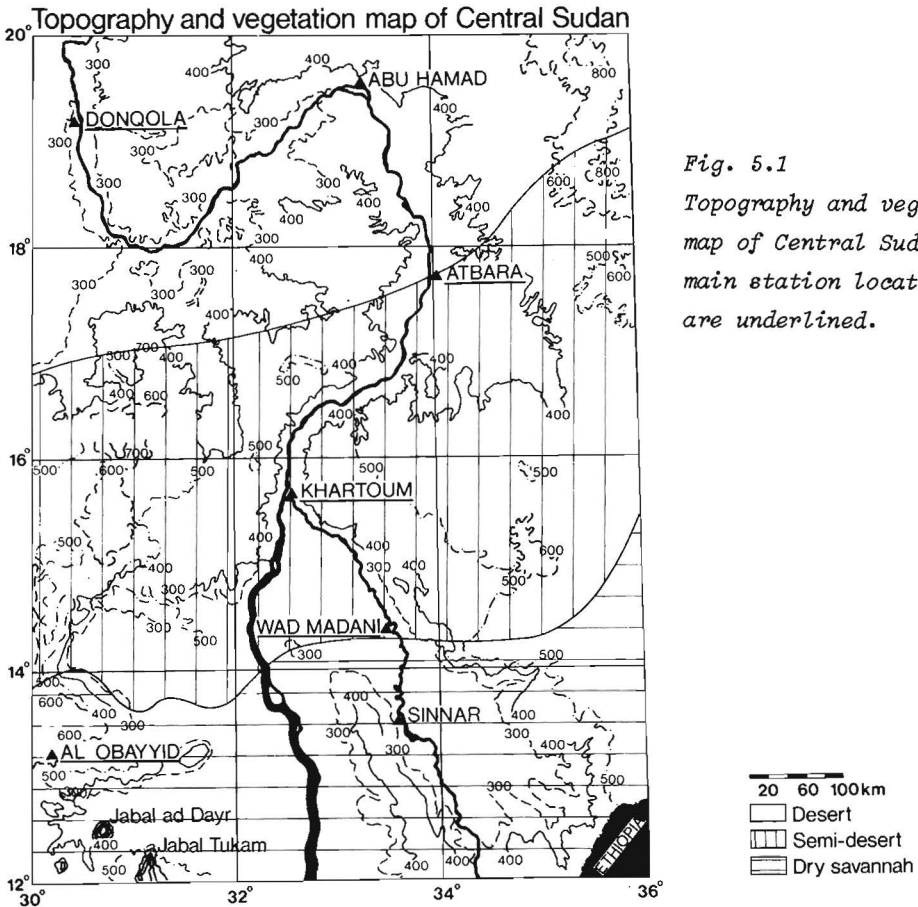
Fig. 5.1
Topography and vegetation
map of Central Sudan. The
main station locations
are underlined.

In this article we define the climate in Central Sudan as a tropical Sahara climate (Sahara is originally an Arabic word meaning "desert"). A tropical Sahara climate combines climate characteristics from a semi-desert with a dry savannah climate; it has large diurnal temperature variations and little rainfall. Physically the climate is dominated by the south-north oscillation of the ITCZ. It crosses the region twice a year; its exact passage time and speed is variable, but on the average the ITCZ crosses the Khartoum region northward around May-June and southward around October-November. Therefore the Sudan has four seasons: (a) winter (December-February); (b) advancing monsoon (March-May); (c) monsoon (June-September) and (d) retreating monsoon (October-November) (see ABu Bakr et al, 1986, ABu Bakr, 1988).

In order to be able to develop a climate model for Central Sudan and check its accuracy, a sufficiently detailed and reliable data base is needed. For this purpose unprocessed data were kindly supplied by the Sudanese Meteorological Department in Khartoum with support from WMO. They are from the following stations:

a. Khartoum (Al Khurtum) airport (15°40'N, 32°32'E 381 m a.s.l.).
b. Shambat agrometeorological station (8 km north of Khartoum airport, 380 m a.s.l.).
c. Wadi-Seidna airport (25 km NNE of Khartoum airport, 385 m a.s.l.).
d. Wad Madani (Wad Medani) agrometeorological station (14°23'N, 33°29'E, 405 m a.s.l.).
e. Atbara (Atbarah) station (17°40'N, 33°58'E 345 m a.s.l.).
f. Dongola (Dunqulah) airport (19°10'N, 30°29'E, 228 m a.s.1)
g. El Obeid (Al Ubayyid) airport (13°10'N, 30°14'E, 570 m a.s.l.).

Table 5.1 reviews the available data and figure 5.1 shows the location of some of the stations. The data were processed by computer and corrected for obvious errors (ABu Bakr, 1988). The wind data were corrected for local exposure deficiencies according to the method proposed by Wieringa (1986). An independent field check of the wind speed data at Shambat station (ABu Bakr, 1988) showed that the less than perfect maintenance and calibration resulted in an uncertainty of about 15%, which is in agreement with the estimate of Woodhead (1970). Statistical correlation analysis of data from nearby stations (Wad Madani, Khartoum, Shambat) showed, that a reliable reference data base was obtained for use in wind potential estimate and climate modelling (ABu Bakr et al., 1986).

Type of the data	Stations	Years
1. Surface-wind hourly data measured by means of Dines pressure tube anemograph. The measurements are at 15 m above the ground level.	Khartoum Atbara Wad Madani El Obeid	1982, 83, 84 1982, 83, 84 1982, 83, 84 1984
2. Surface wind 3-hourly averaged data; period of measurements between (0300-0900) G.M.T. Dines pressure-tube anemograph (10 m. above sea level) is used.	Wadi-Seidna	1984
3. Surface-wind 6 hours mean data. Cup anemometer measurements at 10 m.	Shambat Wad-Madani	1984 1984
4. Surface temperature, hourly data.	Shambat Atbara Dongola Khartoum	1984 1984 1984 1983, 84
5. Surface pressure 3 hourly data	Khartoum Atbara	1983, 84 1984
6. Soil temperature for different depths in the soil (recorded at 06, 12, 18 hours). See section 5.4.2.	Shambat	1984
7. Global radiation recorded hourly	Dongola Shambat	1984 1984
8. Relative humidity recorded hourly	Shambat Dongola Khartoum	1984 1984 1984

Table 5.1 Tabulation of the data obtained from the Khartoum Meteorology Office.

5.3 *The stationary character of the climate*

The diurnal cycle of meteorological surface data in Central Sudan shows that the climate is very stationary. In this context this means that the day-to-day variations are very small and that the average diurnal cycle shows the same behaviour all across the region. This is observed in our data when the data of different stations and years are compared. In particular, the day-to-day variations are relatively small in the winter, advancing monsoon and retreating monsoon seasons (except October and May). In the monsoon the day-to-day variations are much larger. The behaviour of the measured surface boundary layer parameters are discussed below with regard to climatic stationarity.

5.3.1 *Radiation*

In Sudan measurements of global radiation are made with Robitzsch bimetal actinographs, with a typical accuracy of about 15% (Thams, 1953). In the whole country the measured global radiation can be fitted excellently to a half-sine function peaking at noontime (see figure 5.2). Average cloud cover at Khartoum is less than 30% during the period October–April, and around 50% in May–September (see Griffiths and Soliman, 1972). Comparative studies of direct and diffuse radiation (ABu Bakr, 1980) show that more than 80% of the radiation is direct, and the observed average radiation differs little from values obtained from theoretical calculations neglecting the diffuse radiation. Data from the meteorological office in Khartoum show for example that the 1970-1980 annual average global radiation is 252 W/m^2 at Ghazala Gawazat (11°N, 26°E, 485 a.s.l.) and 279 W/m^2 at Dongola (19°N, 26°E, 228 m a.s.l.), showing a maximum geographical variation across the region of about 10%. The monthly averages at Wadi Halfa (22°N, 31°E), Khartoum and El Fasher (14°N, 25°E) vary at most about 12% around the annual average (Griffiths and Soliman, 1972). Day-to-day variations are much less: at Dongola and Shambat in 1984 the standard deviation of single-hour averages around the monthly average for that hour does not exceed 8 W/m^2. Variations of these magnitudes are well within observation accuracy limits, so global radiation can be assumed constant in this region.
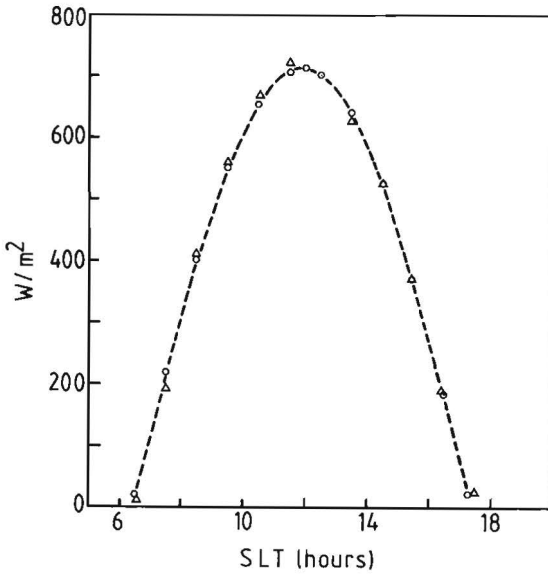
Fig. 5.2
A fit of the global
radiation data from
Shambat (January 1984)
by a half sine function.
SLT represents the Sudan
local time (o the calculated
values, △ the measured
values).

5.3.2 *Temperature, pressure and humidity*

Analysis of the 1984 data from Khartoum shows that standard deviations of single-hour averages around the monthly average for that hour do not exceed 0.55°C for temperature, 0.45 mb for pressure and 2% for relative humidity. So again the day-to-day deviation is very small. Also, for the whole region the diurnal cycle of these parameters show a similar behaviour (see figure 5.3). The diurnal cycle of the air temperature at 2 m shows an average range of 15°C between day and night, typical for the tropical Sahara climate. The pressure shows a diurnal average range of 3 mb, with maximum pressure at about 11 hr (SLT) and minimum pressure at about 18 hr SLT. Relative humidity is on the average less than 50% everywhere.
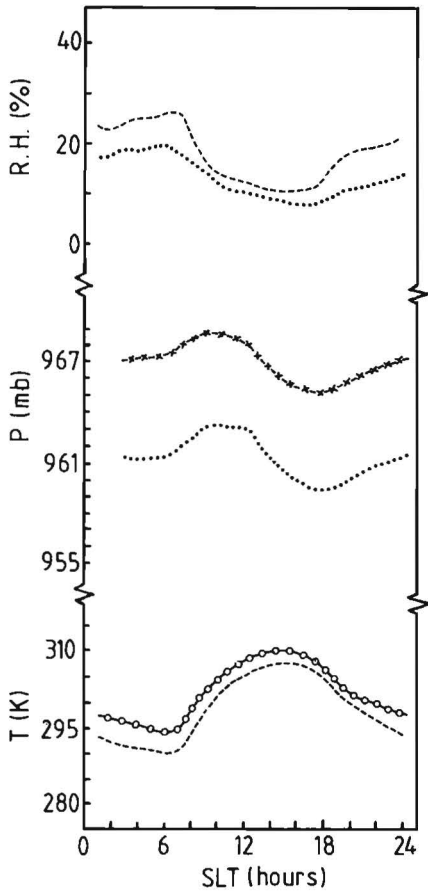
Fig. 5.3

*Comparison between the diurnal course
of the temperature, the pressure and
the relative humidity (R.H.) for March
1984 from the following stations:*
a. ---- Dongola b. -o- Shambat,
c. .... Khartoum d. -x-x- Atbara.

5.3.3 *Wind speed and direction*

The wind displays very stationary characteristics in winter, advancing
monsoon and retreating monsoon (except October and May). This stationarity is
related to the steadiness of the trade wind regime. Isobar maps show that in
the winter the dominating pressure systems are a high-pressure area in Egypt
(oscillating between 25°N and 30°N) and a low-pressure zone which is related
to the ITCZ in southern Sudan. From November until April the isobars in
Central Sudan show a similar pattern, running from Northeast to Southwest,
with a maximal pressure gradient $(\partial p/\partial z) \sim 0.01$ mb/km. As a result, the
diurnal course of wind components generally shows a comparable behaviour
across the whole region, especially in the winter. On the other hand, from May

81

until October the pressure systems show large variations in Central Sudan due
to the movement of the ITCZ. For the wind direction, the diurnal range is
about 25° over the whole region. In the winter, the wind direction varies
between NNW at midnight and NNE at noon. Only during the monsoon, when the
ITCZ passes, large wind azimuth variations are observed for some weeks.

For the wind speed, the day-to-day variations are small. For all stations
it was found that for any individual hour the standard deviation of the mean
of the monthly average wind speed at that hour does not exceed 0.45 m/s. The
monthly averages of wind speed during the winter across the region are in the
range 2-7 m/s (see Table 5.2).

The general shape of the diurnal cycle of the wind speed in central Sudan
does not resemble those published for moderate latitudes. Figure 5.4 shows a
comparison of the diurnal course of January for 1982, 1983 and 1984 for three
stations. The surface wind speed shows a sharp increase after sunrise to a
maximum around 9 hr SLT with subsequently a steady decrease in the early
afternoon. Just before sunset the wind speed exhibits a sharp decrease.
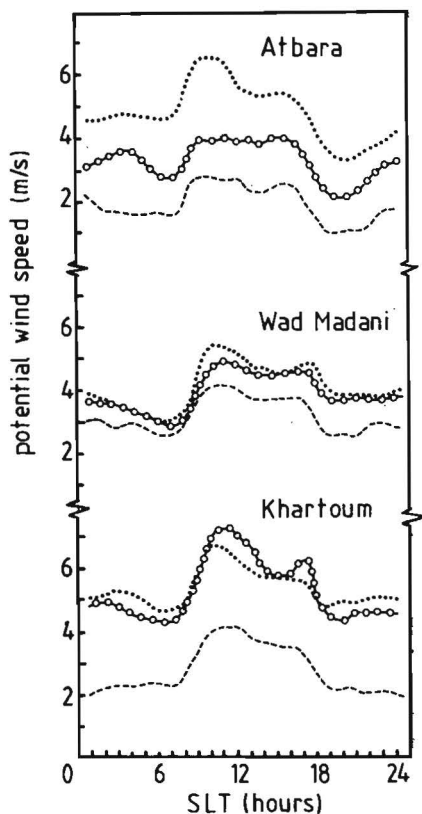
Fig. 5.4
The comparison of the potential
wind diurnal course of January
from Khartoum, Wad Madani and
Atbara for the following years:
a. ---- the 1982 data.
b. .... the 1983 data.
c. -o-o- the 1984 data.

TABLE 5.2

Winter wind regime (s = hourly averaged potential wind speed in m/s)

station	December wind speed	wind direct.	January wind speed	wind direct.	February wind speed	wind direct.
Khartoum						
1984	3<s<5.5	NNW-NNE	4<s<7	NNW-NNE	4<s<7	NNW-NNE
1983	3.5<s<6.5	NNW-NNE	4.5<s<6.5	NNW-N	3.5<s<7	NNW-NNE
1982	3<s<5	N-NNE	2<s<4	NNW-N	2.5<s<6	NNW-N
Wad Madani						
1984	3<s<4.5	NNE-NNW	3<s<5	N-NNE	3<s<5	N-NNE
1983	2.5<s<4.5	N-NNE	3<s<5.5	N-NNE	2.5<s<5	NNE-NE
1982	2<s<4	N-NE	2.5<s<4	NNE-NE	2.5<s<5	NNW-NNE
Atbara						
1984	3<s<6	N-NNE	2<s<4	N-NNE	3<s<6	N-NNE
1983	2<s<4.5	NNE-NE	3.5<s<6.5	N	3.5<s<6	N-NNE
1982	3<s<5	N-NNE	1<s<3	N-NNE	-	-
El Obeid						
1984	1.5<s<4.5	N-NNE	3.5<s<7	N-NNE	3<s<6.5	N-NNE

Sutton (1923) was the first to draw attention to this peculiar phenomenon. His investigation was based on one year's anemograph records at Khartoum (2-hourly data), and Beaufort scale wind force estimates at 8, 14 and 20 hr for 14 stations in Sudan. He observed that the wind speed, after reaching a maximum at 9.00 hr, gradually decreases during the day. He suggested that the region where this phenomenon is observed is located between (9-18)°N and (30-35)°E, but not outside this region, e.g. in Wadi Halfa (22°N), Kassala (36°E) and Al Fasher (25°E).

Observations reported by Farquharson (1939) show that in Central Sudan the wind speed decreases between early morning and noon up to about 1 km above the surface. Farquharson suggested that this distinctive behaviour is not confined to Central Sudan only but also occurs in other regions between 20°N to 20°S. His suggestion was based on a very limited number of stations; Fort Lamy (Chad), Berbera (Somalia), Gulu (03°N, 32°E), Salisbury (18°S, 31°E, Zimbabwe) and Bulawayo (20°S, 28°E, Zimbabwe). A similar diurnal cycle was also observed in Tsumeb (19°S, 17°E), see Walk and Wieringa (1988), and Dodoma (6°S, 35°E, Tanzania), from the data published by Woodhead (1969).

A study by Tetzlaff (1982) shows, that southward of the tropic of Cancer such morning-peaking cycles occur in winter all across the Sahara, from Mali to Sudan. At latitudes higher than ~ 22°N, the time of the wind maximum reverts to 12-13 hr SLT.

In order to explain the peculiar behaviour of the wind diurnal course we are presently investigating the dynamics of the whole boundary layer using the available data from Sudanese radiosonde stations (see chapter 6). In the present context it is sufficient to know, that the qualitative behaviour of the wind is similar across Central Sudan.

Concluding the discussion presented in this section, it was shown that for wind, as well as for other parameters, the Central Sudan shows a similar behaviour of diurnal cycles. The magnitude of cycle averages and amplitudes, however, may exhibit sizeable variations across the region. Still, the stationarity of the climate in the period November to April is beyond doubt. This conclusion is also supported by monthly pressure gradient charts published by Sutton (1923).

5.4 *Model description*

The fundamental equations used here are obtained by combining the Monin-Obukhov similarity theory with the energy balance equation. In order to provide physical insight into our method, we will briefly describe its theoretical background.

Attention is explicitly drawn to the fact, that in the context of this analysis all fluxes, temperatures and wind speeds are averages of all the climatologically available hourly observations, instead of just a selection chosen in order to conform with theoretical requirements. We chose this approach since our purpose is to model the existing wind climate, rather than to develop an idealized model. For reasons of convenience we omitted the notation of time dependence of the parameters; e.g. instead of writing $u_*(t)$ we will only write u_*.

In the following we will first give a review of the basic equations of the model (section 5.4.1). Subsequently, in section 5.4.2 and 5.4.3, we present a detailed discussion of the way the energy balance parameters, net radiation and soil heat flux are handled in the model. Then, in section 5.4.4, we discuss the basic asumptions of the transposition methodology. Finally, in section 5.4.5, we describe how the model computes the regional value of u_* from observations at a reference station (R), which is used to calculate the local values of $U(z)$ at arbitrary stations (A). Parameter notation follows common usage and is specified in appendix A.

5.4.1 *Basic equations*

The main parameter used in the computation of wind speed is the friction velocity u_*, which is obtained from integration of the dimensionless wind shear equation:

$$\frac{\partial U}{\partial z} = \frac{u_*}{\kappa z} \phi_M \left(\frac{z}{L}\right) \tag{5.1}$$

Here L is the Obukhov stability parameter, defined by

$$L = \begin{cases} \dfrac{T_a u_*^2}{\kappa g \theta_*} & \text{for stable conditions (night time)} \quad (5.2a) \\[4mm] \dfrac{-C_L P u_*^3}{g Q_H} & \text{for unstable conditions (day time)} \quad (5.2b) \end{cases}$$

85

where $C_L = MC_P/\kappa R$.

L is negative for unstable conditions (upward net surface heat flux) and positive for stable conditions (downward net surface heat flux). The hours around sunset and sunrise should be considered as transition hours between stable and unstable conditions. For the dependence of the dimensionless wind gradient ϕ_M on (z/L) we use the Businger-Dyer flux-gradient relations according to Paulson (1970) and Dyer (1974):

$$\phi_M(\frac{z}{L}) = \begin{cases} 1 + 5(z/L) & \text{for stable conditions} \quad (5.3a) \\ (1 - 16(z/L)^{-1/4} & \text{for unstable conditions} \quad (5.3b) \end{cases}$$

taking $\kappa = 0.41$, the integrated u_*-equation is given by

$$u_* = \begin{cases} \kappa\ U(z)[\ln(\frac{z}{z_o}) + 5\ \frac{z}{L}]^{-1} & \text{(stable conditions)} \quad (5.4a) \\ \kappa\ U(z)[\ln(\frac{z}{z_o}) - \psi\ (\frac{z}{L}) + \psi(\frac{z_o}{L})]^{-1} & \text{(unstable conditions)} \quad (5.4b) \end{cases}$$

where

$$\psi(\frac{z}{L}) = 2\ \ln\ [\frac{1 + \phi_M^{-1}\ (\frac{z}{L})}{2}] + \ln\ [\frac{1 + \phi_M^{-2}\ (\frac{z}{L})}{2}] \qquad (5.5)$$
$$- 2\ \arctan\ [\phi_M^{-1}\ (\frac{z}{L})] + \frac{\pi}{2}\ .$$

The sensible heat flux parameter Q_H, needed as input parameter for equation (5.2), is obtained from the energy balance equation:

$$Q_H = Q_N - Q_G - Q_E\ , \qquad (5.6)$$

where Q_N is the net radiation and Q_G is soil heat flux. The latent heat flux (Q_E) can be neglected in comparison with the other energy balance components because the humidity is low and the region is arid. Thus the energy balance is

86

reduced to:

$$Q_H = Q_N - Q_G , \tag{5.6a}$$

where

$$Q_N = \begin{cases} Q_{L\downarrow} - Q_{L\uparrow} & \text{for stable conditions} & (5.7a) \\ Q_{L\downarrow} - Q_{L\uparrow} + Q_T & \text{for unstable conditions} & (5.7b) \end{cases}$$

$$Q_{L\downarrow} = \epsilon_s \epsilon_a \sigma T_a^4 , \tag{5.8}$$

$$Q_{L\uparrow} = \epsilon_s \sigma T_s^4 , \tag{5.9}$$

$$Q_T = Q_s (1-A_s) . \tag{5.10}$$

The equations (5.7) - (5.10) are obtained from Munn (1966). The calculation of the input parameters for equation (5.6a) from the limited available data presented some problems, which will be discussed in detail in section 5.4.2 for the soil heat flux Q_G and in section 5.4.3 for the net radiation Q_N.

The temperature scale for turbulent heat transfer (θ_*) is related to the sensible heat flux Q_H by

$$Q_H = - \rho C_p u_* \theta_* . \tag{5.11}$$

For stable condition (nighttime) the value of θ_* was taken equal to 0.08 K (Venkatram, 1980). The constancy of θ_* all through the night was previously concluded from the measurements at Tsumeb where the climate is similar to central Sudan (Abele, 1975; Walk and Wieringa, 1988). In these measurements Q_H showed a constant value during the night, which implies that θ_* is also constant. We shall see in section 5.4.4 that this assumption is confirmed by our computations.

When a constant θ_*-value is used, u_* (solved from equation 5.2a and 5.4a) has a quadratic solution:

$$u_* = \frac{1}{2 X_2} [- X_1 + (X_1^2 - 4 X_2 X_3)^{\frac{1}{2}}] , \tag{5.12}$$

where

$$\chi_1 = \kappa \ U(z),$$ (5.13)

$$\chi_2 = \ln(z/z_o),$$ (5.14)

$$\chi_3 = 5(\kappa \ g \ z \ \theta_*)T_a \ .$$ (5.15)

We note that $U(z) > 1.5$ m/s in the period November-April, which means that $(\chi_1^2 - 4 \ \chi_2\chi_3) < 0$ hardly occurs.

5.4.2 *Soil heat flux* (Q_G)

The soil heat flux is computed using the equation of heat conduction (5.16) (Van Wijk 1963, Mayer and Walk 1973):

$$Q_G(t) = \lambda \ [(\frac{\partial T}{\partial z})_{z'} - \int_o^{z'} (\frac{1}{K_G}) \ (\frac{\partial T}{\partial t}) \ dz] \ ,$$ (5.16)

where z' is the threshold depth, i.e. the depth where the variations in the temperature diurnal cycle approach zero. To solve equation (5.16) we need the thermal conductivity (λ), the thermal diffusitivity (K_G) as well as the diurnal cycle of the soil temperature. The soil temperature in Central Sudan is only measured in Shambat (at 6, 12 and 18 hr SLT at the depths 1, 2.5, 10, 20, 50 and 100 cm). At these observation hours the surface temperature was obtained by extrapolation, using the Lagrangian polynomial method.

From the measured soil temperature at the above mentioned depths and the computed surface temperature we calculated the daily average temperature $T_{av}(z)$ for each depth and at the surface. From the three available measurements, the temperature at 12 hr and 18 hr are considered as the maximum and minimum of the temperature diurnal cycle. This assumption is based on the hourly soil temperature data measured at Tsumeb (Mayer and Walk 1973). Their results show that the temperature time lag increases with depth and that the nighttime temperature variation is at most a few degrees, which implies that $T_{18 \ hr} \approx T_{min}$, since the minimum temperature usually occurs in the early morning. These measurements also show that the difference between the temperature at 12 hr and the maximum temperature is only of the order of a few

degrees. Consequently $T_{av}(z)$ is approximately the average of the temperature at 12 hr and 18 hr. From the extrapolated surface temperature and the measured soil temperature we computed the thermal diffusivity K_G by the help of equation (5.17):

$$K_G = \frac{\omega}{2} \left[\frac{z_1 - z_2}{\ln(\Delta T_{so1}/\Delta T_{so2})} \right]^2 ,$$ (5.17)

where ΔT_{so1} is the soil temperature amplitude at depth z_1. K_G is calculated for different depths from $z = 1$ cm to $z = 20$ cm which proved to be the threshold depth. We derived a value of $K_G = (4.6 \pm 0.2) \times 10^{-5}$ m²/s. From studies by Buursink (1971) we know that in the Khartoum region the soil type is sandy clay loam, with a volumetric heat capacity C_h of about 2.5 MJ/m³K. Then we have a working value of the soil thermal conductivity $\lambda = K_G C_h \approx 1.4$ W/m K, which is in agreement with other calculated values for such type of soils (van Wijk 1963, Ten Berge 1986). To compute the hourly soil and surface temperature we used equation (5.18) (van Wijk 1963),

$$T_{so}(z,t) = T_{av}(z) + \Delta T\, e^{-z/d} \sin\left(\omega t - \frac{z}{d}\right) ,$$ (5.18)

where ΔT is the soil temperature amplitude at $z = 1$ cm assumed constant for all depths, and $d = \left(\frac{2K_G}{\omega}\right)^{1/2}$. From the obtained hourly surface and soil temperature and the estimated λ and K_G values the soil heat flux (Q_G) as expressed by equation (5.16) can be calculated.

5.4.3 Net radiation (Q_N)

For the unstable daytime condition the net radiation is equivalent to the difference between the net short wave radiation at the earth's surface (Q_T) and the net long-wave radiation ($Q_{L\downarrow} - Q_{L\uparrow}$). Q_T is obtained from equation (5.10). Q_s is the measured hourly global radiation obtained from Shambat station, which is considered to be representative for the whole region (see section 5.3.1). The surface albedo A_s is estimated for the region to be about 0.25, which is an acceptable value for a semi-arid savannah region (Budyko, 1956; List, 1966; Kondratyev, 1969).

The surface-emitted long-wave radiation ($Q_{L\uparrow}$) is calculated from equation (9) with $\varepsilon_s = 1$, which is a commonly used value in most applications (Brutsaert, 1982). Because of the lack of observations of the surface temperature T_s we employed an empirical equation (Holtslag and van Ulden, 1985) in which only the surface heat coefficient (c_s) and the air temperature are required:

$$Q_{L\uparrow} = \sigma T_a^4 + 4 \sigma T_a^3 (T_s - T_a) , \qquad (5.19a)$$

where

$$4 \sigma T_a^3 (T_s - T_a) = c_s Q_N . \qquad (5.19b)$$

Typical values of c_s vary from about 0.12 for moist grass to approximately 0.38 for bare dry soil. For Sudan conditions, at Shambat, by comparison of air temperatures with surface temperatures (from the diurnal cycle of the soil temperature, calculated in section 5.4.2) we derived $c_s = 0.28 \pm 0.05$.

The long-wave radiation received by the surface from the atmosphere ($Q_{L\downarrow}$) is calculated by equation (5.8). Since the latent heat of evaporation is negligible in Central Sudan, $Q_{L\downarrow}$ is calculated using the $\varepsilon_a(t)$ from an empirical equation (5.20) given by Idso and Jackson (1969):

$$\varepsilon_a = 1 - 0.261 \exp [- 7.77 \times 10^{-4} (273 - T_a)^4] . \qquad (5.20)$$

Such an estimate depends on the fact that the long-wave-emission from the atmosphere originates mainly from CO_2 and water vapour in the lower troposphere, with generally an effective black-body emission correlated

strongly to screen temperature, particularly at the low humidities prevalent
in the Central Sudan.

We now can compute Q_N for stable and unstable conditions (with equation
(5.7) - (5.10) by using equation (5.19), (5.20), the surface albedo value (A_s
= 0.25), and the measured global radiation (Q_s).

In the following paragraph we will derive a relation between the sensible
heat flux (Q_H) and the net radiation (Q_N) for unstable conditions in the
region by assuming the soil heat flux of Shambat as representative. Since
Shambat station is the only station where both Q_N and Q_G are known, a
proportionality constant (C_G) between the two heat fluxes can be determined
($Q_G = C_G \, Q_N$). This proportionality constant is assumed to be representative
for the whole region, which means that in the model computation the value Q_G
for the other stations (where no soil temperature data are available) can be
substituted by $C_G \, Q_N$. The same approach has been used earlier for the
computation of heat fluxes for temperate latitudes (Van Ulden and Holtslag
1985, De Bruin and Holtslag 1982). From monthly hourly average data for a
whole year C_G was found to be equal to 0.32 ± 0.08, which is a very reasonable
value for a Sahara tropical climate (Menenti 1984, Ten Berge 1986). With this
value equation (5.6a) for unstable conditions can be written as:

$$Q_H = 0.68 \; Q_N \; . \tag{5.21}$$

We finally calculate the value of θ_* (temperature scale for turbulent heat
transfer) for stable conditions using equation (5.6a) and (5.11). The average
value of θ_* obtained is 0.07 ± 0.05 K which is in agreement with the
assumption of the nighttime constancy of u_* (see section 5.4.1) and with the
value of 0.08 K given by Venkatram (1980).

Though the calculation of the diurnal cycle of the surface temperature
(section 5.4.2) is rather rough, still the results are reasonable for our
purpose. For the model computation we used the values $\theta_* = 0.08$ K for stable
and $Q_H = 0.68 \; Q_N$ for the unstable condition.

5.4.4 *Basic assumptions of the transposition methodology*

The fundamental assumption made in the transposition of the hour-to-hour
wind speed across Central Sudan is the constancy of large-scale average
friction velocity in this region, at least during the period from November to

April. This assumption is based on two arguments, namely the homogeneity of the pressure gradient and the lack of regional variation in the boundary layer fluxes.

Firstly, the stationarity of the climate (which was discussed in section 5.3) implies a steady isobar pattern. This implication is supported by the isobar maps for the region published by Sutton (1923). A steady isobar pattern results in very small variations in the geostrophic wind $(G(t))$ across the region at any given daytime hour. In addition, also our upper-air data (Khartoum, Dongola and El Obeid) show relatively small variations in the free atmospheric wind (above 800 mb) across the region (see chapter 6).

Secondly, in this climate strong buoyant convection prevails in daytime because of the large upward heat flux and strong instability. The convection does not vary significantly across the region, so the turbulence in the boundary layer is uniform at any given hour. For the nighttime the clear sky, characteristic of the region, results in a low constant turbulence temperature scale (θ_*).

We now turn to terrain effects on the momentum flux. It was already remarked that topographic effects are small and systematic, may be generating bias but no random variations between stations. This leaves us with the necessity to account for mesoscale roughness, in principle by using integral roughness classifications (Davenport, 1960 and Wieringa, 1986) and the landscape characteristics of the region (ABu Bakr, 1988). The region shows a high degree of homogeneity and the vegetation varies between semi-desert and dry savannah. From representative landscape photos for the region the estimated mesoscale roughness is about 0.25 m (see chapter 4, fig. 4.9), somewhat increasing in the monsoon season due to the extra growth of some vegetation in this season.

Summarizing this section we can say that at any given hour there is little regional variation in the turbulent fluxes in the mixing layer, resulting in an approximately constant regional geostrophic drag coefficient C_g ($= u_* /G$). Since the variations of the geostrophic wind (G) are small (except during the monsoon) u_* will only exhibit minor variations across the region. On this approximate constancy of u_* we base the introduced methodology of transposition of the surface wind speed across central Sudan. A summary of the basic concepts and assumptions used in the model is given in Figure 5.5.

| THE LOCAL BL PARAMETERS HAVE MEAN STANDARD DEVIATION <15% | THE REGIONAL SCALE ISOBARS ARE STEADY | NON COMPLEX REGIONAL TOPOGRAPHY |
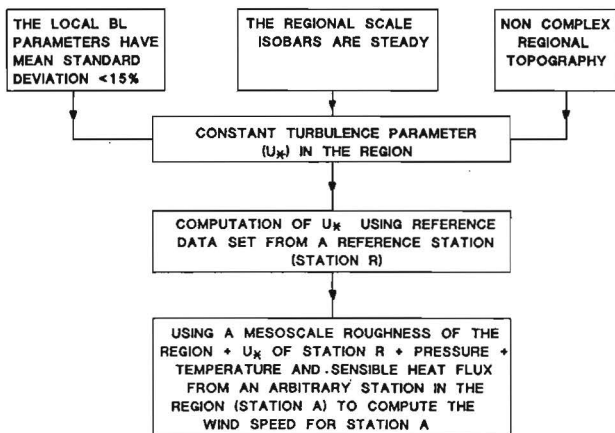
Fig. 5.5
Block diagram of the
model methodology.

5.4.5 *Methodology*

The basic computations of the transposition method are carried out in two steps. First, the friction velocity (u_*) is computed for a reference station in the region, where hourly wind measurements are available. Second, for other stations (where there is a lack of detailed wind speed information) the wind speed is computed, using u_* of the reference station. These computations are carried out every hour and are carried out separately for unstable and stable conditions. In the following subsections we will explain in detail the computation of the transposition methodology.

5.4.5.1 *Unstable conditions*

In order to compute u_* for daytime conditions, an iteration process is applied to solve equations (5.2b) and (5.4b). In these calculations z is constant (15 m). Starting from an estimated value of u_* and L, the iteration process is repeated until the readjustment of u_* is less than 1.26% (criterion chosen so that the change in L-values in a subsequent iteration is not more than 2%). To determine a proper 'starting' value for the iteration, it is important that the function ϕ_M in equation (5.3b) must not be less than zero, otherwise ϕ_M will have a complex value. To satisfy this condition, L should be less than zero or greater than 240. Another limitation for the starting value of L is the value of u_*. Since the value of u_* should be greater than zero,

93

the starting value of L should be less than zero. So when a negative L value is used, both conditions are satisfied. For this model we have used a starting value of L = -5. The iteration process shows a fast convergence, within at most 6 steps, and the convergence factor is nearly always less than 0.5. The iteration is stopped when $|x_{i+1} - x_i|/x_{i+1} < 0.0125$, where x_i = ith solution-approximation.

The accuracy of the iteration result is checked as follows;

a. The wind speed is computed using different starting values of L (L = -1, -2, ..., -20). The maximum difference obtained for the computed wind speeds is 1%.

b. The computed values of u_* and L are used to compute the wind speed for the same station, which is numerically the same measured wind speed as used in the computation of L and u_*. This check is repeated for four stations for each month. The largest difference found between the computed and measured wind speeds is 0.2%.

As a result of these two checks we can conclude that the iteration process gives reliable results. The computed value of $u_*(t)$, using data from a given reference station (station R), is considered constant over the region. The routine meteorological data (T(t), P(t), and $Q_H(t)$) of an arbitrary station (station A) and the value of u_* from station R are used for computing the Monin-Obukhov length and the wind speed by application of equation (5.2b) and (5.4b).

5.4.5.2 *Stable conditions*

For stable conditions u_* is calculated from equation (5.12), using $\theta_* = 0.08$ K, and the routine meteorological data from the reference station. Since equation (5.12) is a quadratic equation, there are two solutions for u_*. From the climatological point of view the value of one of them is not realistic, since it is always < 0.1 m/s. The routine meteorological data of station A and u_* from the reference station are used for computing the Monin-Obukhov length and the wind speed, applying equation (5.2a) and (5.4a).

In the computation of the unstable and stable conditions two types of roughness are used; for the reference station the local azimuth-dependent roughness is used, and for the other stations a mesoscale roughness is used. The mesoscale roughness (z_o^m = 0.25 m) was estimated from the landscape characteristics of the whole region (see section 5.4.4). In fact, the

computation of the Monin-Obukhov length and the wind speed is carried out for every subsequent hour for the three arbitrary stations (e.g. Atbara, Wad Madani and El Obeid) using a single reference station (e.g. Khartoum).

5.5 *Sensitivity of the parameters used in the computation of U(z)*

In order to present a clear picture of the applicability of the model, it is necessary to have information about the sensitivity of the input parameters to the final computed quantities. We therefore analysed the sensitivity of all parameters on U(z) which is computed as a function of a variation of the hourly data of the parameter considered (L, z or u_*). Figures 5.6, 5.7, and 5.8, which are discussed in the following sections, present the monthly averages of the increase or decrease of the hourly values of U(z) as the other parameters vary.

5.5.1 *Sensitivity of U(z) to the Monin-Obukhov length*

Under the condition of constant u_*, according to equation (5.2), the Monin-Obukhov length must be linearly dependent on the temperature, the pressure and the sensible heat flux. Figure 5.6 shows the variation of U(z) as a function of L, when L is computed from the hourly measured data while all other parameters are kept constant. From figure 5.6 we see, that as L decreases as much as 30% the wind speed shows a decrease of only 3% under unstable conditions and an increase of 6% under stable conditions. An increase of 30% in L results in even smaller changes in U(z) for unstable condition and a decrease of U(z) by 3%, under stable conditions.

From these results it is clear that the variation of L in this region has only a very limited influence in the computation of the wind speed. Practically this implies that if either the temperature, pressure or heat flux varies by about 30%, the computation of the wind speed is still reliable.
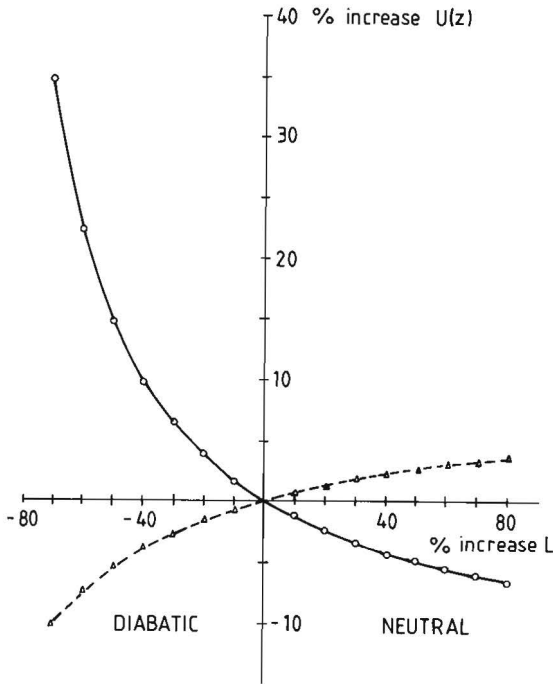
Fig. 5.6
Sensitivity of the average
U(z) as function of L.
-o-o- stable conditions data.
----Δ---Δ- unstable
conditions data.

5.5.2 *Influence of the roughness estimate on U(z)*

It is evident from equation (5.4) that the $U(z)$-values computed for some arbitrary regional station A will be strongly dependent on the used values of the roughness length. There are two roughness lengths involved; the local roughness z_0^R at the reference station, where u_* is computed and the mesoscale roughness z_0^m used to estimate $U(z)$ at station A. The first set of curves in figure 5.7 (with triangular points) assume a constant mesoscale roughness z_0^m for station A. Increasing the roughness at the reference station will increase u_*, and consequently also $U(z)$ at station A.

For the illustrated case an increase of z_0^R from 0.2 m to 0.5 m results in a $U(z)$ increase of about 15%, slightly more for unstable than for stable conditions. The second set of curves in figure 5.7 (with circular points) assumes z_0^R at the reference station to be constant, so the u_*-values are

constant for the given data set. An increase in the mesoscale roughness at station A then results in a decrease of U(z)-values at that station. For a z_o^m -change from 0.2 to 0.5 m, the value of U(z)-decreases about 15% as can be seen from the figure. The figure also shows, that for both sets of curves the sensitivity of U(z) to changes in roughness increases significantly when the roughness values are smaller than 0.2 m.

Because the computation of U(z) is very sensitive to errors in the roughness length, the estimate of the roughness length should be very accurate. In practice, for estimate of roughness lengths < 0.4 m the best accuracy is about 20%.
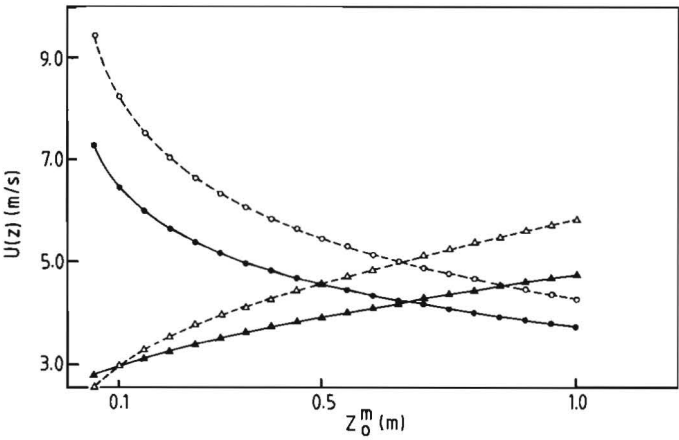
Figure 5.7 Wind speed as a function of the roughness length, for the daytime (o,Δ) and the nighttime (•,▲). The symbols Δ, ▲ represent the computed speed for station A as a function of z_o^R (roughness of the reference station) while the mesoscale roughness of station A is constant. The symbols o, • represent the computed wind speed for station A as the function of the mesoscale roughness, while the roughness length of the reference station is constant.

5.5.3 The influence of u_* on the computed U(z)

Obviously, the computed U(z) will be strongly dependent on the value of u_*. Figure 5.8 shows the variation of U(z) as u_* varies. The figure shows that a variation of about 30% of u_* results in a variation of about 20% (35%) for stable (unstable) condition. For unstable conditions, U(z) and u_* show a linear relation. In the case of stable conditions, U(z) and u_* are linearly

related for increase and for small decrease of u_*, but as u decreases more than 50% the curve increasingly departs from its original linearity (see figure 5.8). The reason for this departure is not yet understood. Nevertheless, for this stationary climate the variation in u_* values does not exceed 40% on average, so our analysis is restricted to the linear region.
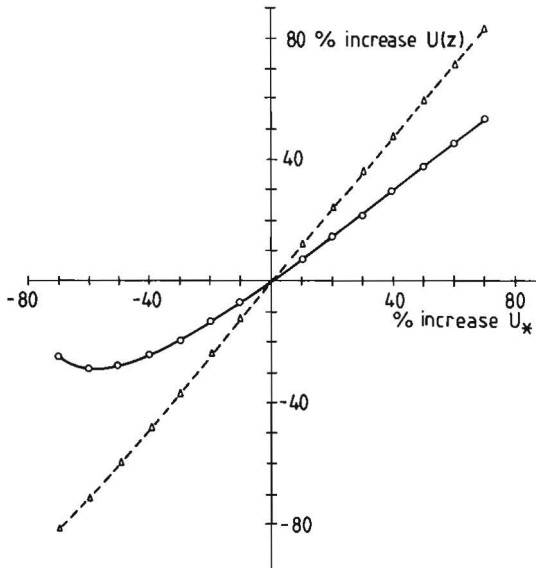
Fig. 5.8
Sensitivity of average $U(z)$
as a function of u_*.
-o-o- stable conditions data.
--Δ--Δ--- unstable
conditions data.

5.6. Check on the assumption of regional constancy of the friction velocity

To check the basic assumption of the constant u_* value in the region numerically, we compared the value of u_* from four stations in the region (Khartoum, Atbara, Wad Madani and El Obeid), using the routine meteorological data for the seasons of 1984 with stationary climate (winter, advancing monsoon and retreating monsoon).

For each station the roughness length of the immediate surroundings was estimated by ABu Bakr (1988). At Khartoum and Wad Madani, z_0 for various azimuths is in the range 0.2 m to 0.5 m. At El Obeid, z_0 varies little around an average of 0.25 m. The observation height is 15 m at all stations. The surroundings of Atbara station are not only very rough (z_0 = 1 m), but there are also displacement effects due to surrounding obstacles with a typical height of about 6 m. Their influence has been accounted for by using a

displacement height of 4 m (Brutsaert, 1975), which means that u_* at Atbara was actually calculated for z = 11 m and corrected to z = 15 m. According to equation (5.3), computed values of u_* decrease 11% for stable condition and 5% for unstable conditions as z increases from 11 m to 15 m.

Figure 5.9 shows the percentage difference (u_*^{AR}) of the monthly averages of u_* between Khartoum u_*^R and the other stations u_*^A for stable and unstable

conditions: $u_*^{AR} = (\dfrac{u_*^R - u_*^A}{u_*^R})$ x 100. From the figure we see, that the difference

on the average is less than 25%, except for the nighttime data at Atbara because of the high local roughness length (z_0 = 1 m) which has a stronger influence in stable condition than unstable condition.

Considering that for the estimate of z_0 the best accuracy attainable is about 20% (see section 5.2) and that the uncertainty due to lack of maintenance and calibration is in the order of 15%, (ABu Bakr 1988, Woodhead 1970), u_* can be assumed constant within experimental limits for these seasons.
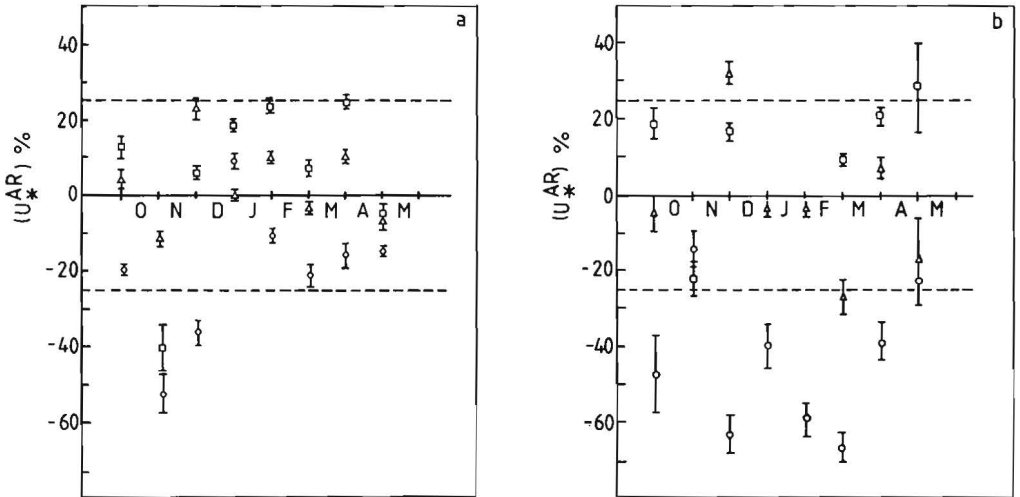
Figure 5.9. Percentage difference u_*^{AR} between the friction velocity at
        Khartoum and the friction velocity at other stations as function
        of month (October - May)
        a. daytime u_*^{AR}, b. nighttime u_*^{AR}.
        o Atbara, □ Wad Madani, Δ El Obeid. The dashed lines indicate the
        boundary limits according to the text.

5.7. *Validation of the model results*

To test the model results we will compare the computed wind speed with the following sets of data:

a. the wind speed estimated by the conventional method in regions of very few stations

b. the potential wind speed calculated from the measured wind speed.

5.7.1 *Comparison between the model and the conventional method*

We will first discuss the conventional method and its applicability in this region. This method, still often applied in regions of very few stations, is based on the assumption that the wind data of one station in a region of at least 100x100 km^2 is the representative wind speed for the whole region (e.g. Exell and Fook 1986, Duensing et al. 1985, Hamid and Jansen 1981). To check the reliability of such an approach in Central Sudan we will compare the measured data of the available four stations, using the Khartoum station as a comparison reference. We calculated the percentage difference,

$$U^{AR} = (\frac{U^A - U^R}{U^A}) \times 100, \quad \text{where } U^A \text{ is the measured wind speed at an arbitrary}$$

station (Atbara, Wad Madani or El Obeid) and U^R is the measured wind speed of the reference station, which in this case is Khartoum.

For the conventional method to be reliable, the difference should not exceed the estimated accuracy of 25%. Figure 5.10 shows the percentage difference between Khartoum and the other 3 stations. The figure shows that on the average U^{AR} is greater than 40%. From this comparison we can conclude that the assumption of constant wind speed in the whole region is not reliable.

To compare the model with the conventional method we calculate the percentage difference (U^A_{MC}) of the measured data (U^A) and the computed wind speed (U^A_C) for station A using the reference station (R),

$$U^A_{MC} = (\frac{U^A - U^A_C}{U^A}) \times 100. \quad \text{Then we compare } U^A_{MC} \text{ to the percentage difference}$$

(U^{AR}). The comparison is carried out for the different reference stations. One has to keep in mind, that the computed wind speed (U^A_C) is corrected for the terrain roughness, while the measured wind speed (U^A) is uncorrected. For a reliable model result the two inequalities: $U^A_{MC} < U^{AR}$ and $-25\% < U^A_{MC} < 25\%$ should hold. Figure 5.11 shows typical examples of the comparison

100

between U^{AR} and U^A_{MC} for different data sets computed from different stations. From the comparison of all data sets it is observed that the two inequalities hold for all months on the average except in some cases for October, November and May, which are the months when the stationarity of the climate is less pronounced. In conclusion, the model on the average is successful, especially if we take into consideration that the measured wind is not corrected for the terrain roughness. To avoid the roughness correction argument we will compare the computed data with a data set which is corrected for the roughness in the following section.
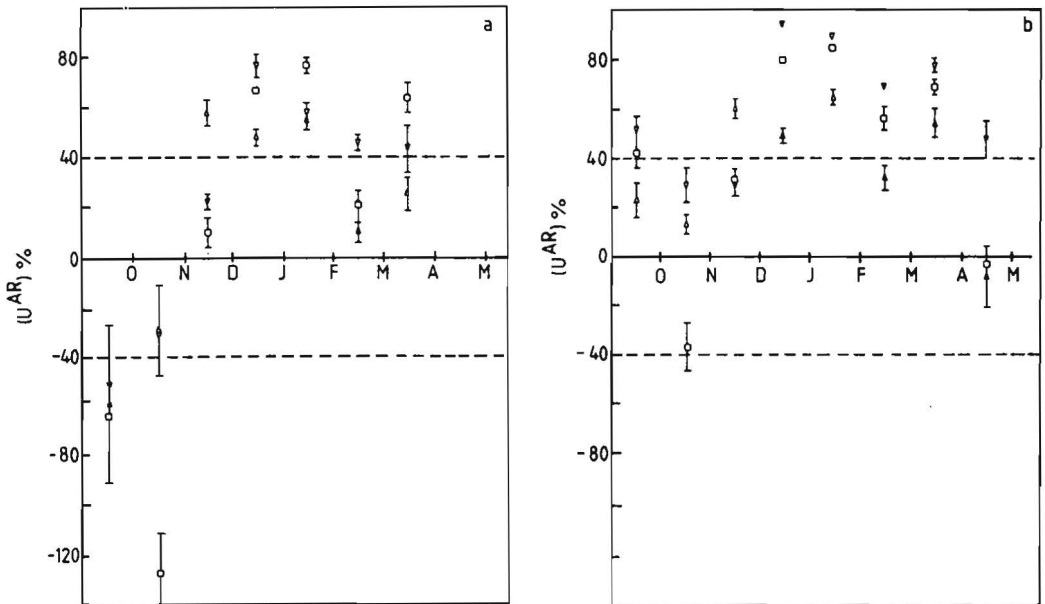
Figure 5.10 Percentage difference U^{AR} between wind at station A and that at Khartoum as function of month (October - May).
a. nighttime U^{AR}, b. daytime U^{AR}.
▽ Atbara, □ Wad Madani, Δ El Obeid. It can be seen that most of the U^{AR} values are well above ± 40% (dashed lines).
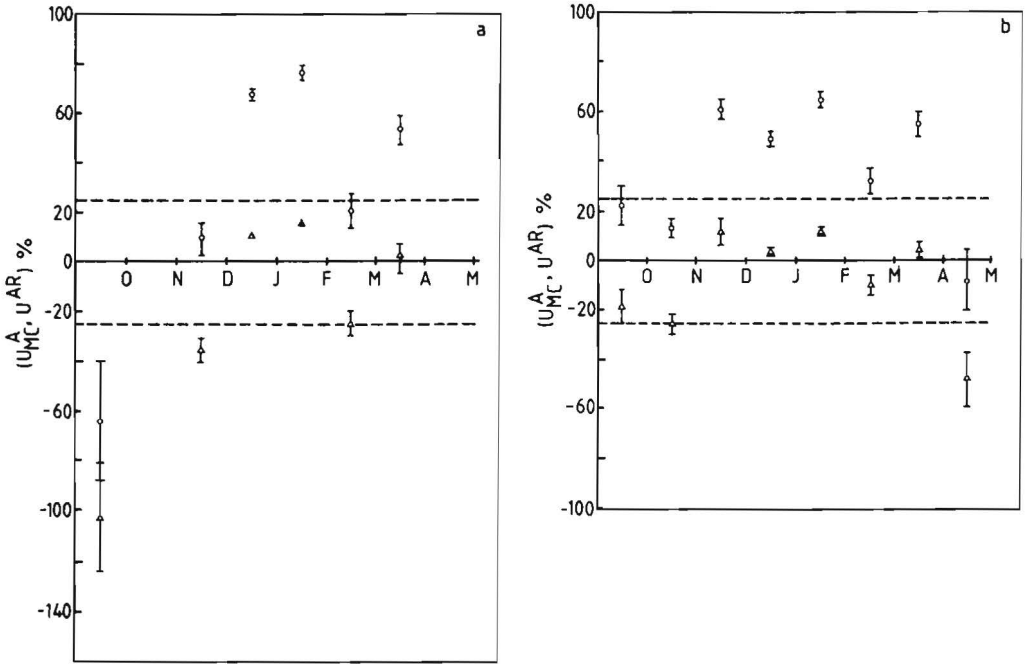
Fig. 5.11 Comparison between the percentage difference $U^A_{MC}(\triangle)$ *(of the
measured wind (station A) to the computed wind (station A)) and
the percentage difference* U^{AR} *(o) (of the measured wind from
station A to the measured wind from station R) as a function of
month (October - May).
a. Wad Madani reference station, b. El Obeid reference station.
The dashed line indicate the boundary limit of the inequality*
$(-25\% < U^A_{MC} < 25\%)$.

5.7.2 *Comparison between the computed wind speed and the potential*
wind speed

The solution of the roughness correction argument mentioned above is to
compare the computed wind speed U^A_C with the potential wind speed U_P. The

potential wind speed is the measured wind speed corrected only for local terrain roughness and obstructions, and for an unobstructed station in open country U_P^A is identical to the wind measured at 10 m height (Wieringa, 1986). It is calculated according to

$$U_P^A = 0.76 \ U^A \ \ln \left(\frac{60}{z_o}\right) \left[\ln\left(\frac{z}{z_o}\right)\right]^{-1} \ , \qquad (5.22)$$

where z is the station measuring height. For the stations data we calculate

the percentage difference U_{CP} between U_C^A and U_P^A: $U_{CP} = \left(\dfrac{U_C - U_P}{U_C}\right)$ x 100. Taking

into consideration the best accuracy of the roughness length estimation, which is about 20% (see section 5.5.2), we define the boundary conditions of the model. If the model is to be successful, then the inequality $-25\% < U_{CP} < 25\%$ must hold.

Figure 5.12 shows a typical example of the monthly averages of U_{CP} for some stations, using different reference stations. From U_{CP} values for all stations the criterion $-25\% < U_{CP} < 25\%$ holds on the average, except in the case when Atbara is the reference station (see also figure 5.13b), which is due to the high roughness length ($z_o = 1$ m) of the close surroundings of Atbara station, as mentioned in section 5.6.

The achievement of the inequality $-25\% < U_{CP} < 25\%$ on the average proves the validity of our model. Figure 5.13 shows the comparison between the hourly averaged computed wind speed and the hourly potential wind speed for El Obeid (January 1984) and Khartoum (March 1984), using three reference stations. From the figure we see that the agreement between the model calculations and the potential wind speed is good for the reference stations El Obeid, Khartoum and Wad Madani. Using Atbara as a reference station, the variation between the model results and the potential wind speed is somewhat larger due to its large roughness. It is clear from the figure, that the model correctly reproduces the morning peak in the diurnal wind cycle, mentioned in section 5.3.3.

This model can also be used to determine the diurnal temperature cycle for an arbitrary station in case the wind speed of the arbitrary station is known. Moreover the model is expected to be applicable in all regions which have a large scale flat topography and small variations in the regional pressure system satisfy the model conditions are: e.g. Chad, Niger, Saudi Arabia, Tsumeb (south west Africa), Northern Mexico, maybe also North Canada and Siberia where the pressure systems does not show much variation in some seasons.
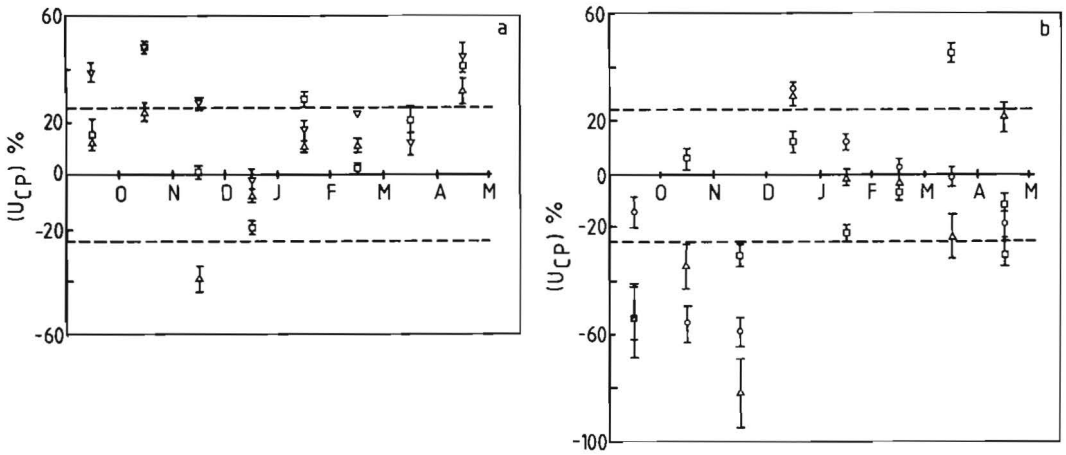
Figure 5.12 The percentage difference (U_{CP}) between the computed wind speed and the potential wind speed as a function of the month (October – May) for three stations.
a. nighttime U_{CP} using Khartoum as reference station, b. daytime U_{CP} using Atbara as reference station.
o Khartoum, □ Wad Madani, ∇ Atbara, △ El Obeid. The dashed line indicates the boundary limit of the inequality (-25% < U_{CP} < 25%).
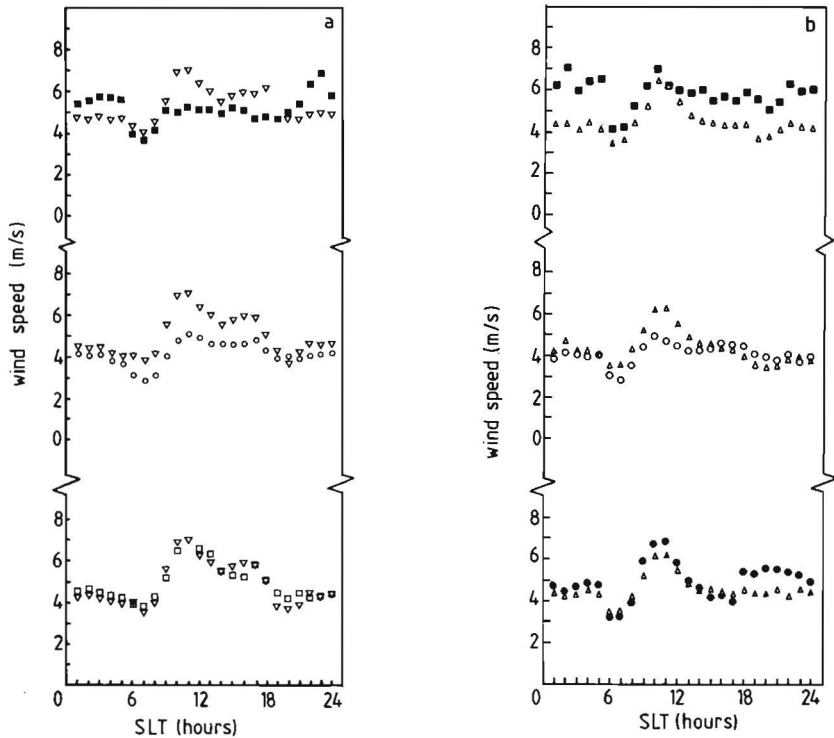
*Figure 5.13 a. Comparison between El Obeid (January 1984) potential wind
speed (∇) and the computed wind speed for El Obeid using three
reference stations, b. Comparison between Khartoum (March 1984)
potential wind speed (Δ) and the computed wind speed for
Khartoum, using three reference stations.*
□ wind speed computed using Khartoum as a reference station.
o wind speed computed using Wad Madani as a reference station.
■ wind speed computed using Atbara as a reference station.
● wind speed computed using El Obeid as a reference station.

5.8. *Conclusion*

A local boundary layer model, based on the energy balance equation and on
the Businger-Dyer equations, is used to compute the average diurnal cycle of
various boundary layer parameters. A horizontal transposition method is
introduced to compute the wind speed behaviour at an arbitrary station. This

method is based on the relatively homogeneous characteristics of the climate and the topography in the region, and developed with the use of about 330×10^3 processed routine meteorological data from seven stations in Central Sudan.

The main assumption of the model is the constancy of the turbulence parameter u_* across the region at a given hour. This assumption is concluded from the following regional characteristics:

a. The stationary character of the climate, which means that day-to-day variations of the boundary layer parameters are very small and that their average diurnal cycle shows the same behaviour across the region.

b. The regional homogeneity of the topography and the pressure field.

From the diurnal cycle of the wind, temperature, radiation, pressure, and relative humidity data it was shown, that the stationarity of the climate in the period November to April is remarkably good.

The diurnal cycle of the wind speed shows a peculiar behaviour: a sharp increase after sunrise to a maximum around 9 hr SLT, with subsequently a steady decrease in the early afternoon and a sharp decrease just before sunset. According to the literature such a diurnal cycle is also observed some other inland regions on the African continent between 20°N and 20°S. To provide a solid explanation for this anomalous phenomenon one needs detailed upper air data from a large number of stations in a representative region (such as Central Sudan) within 20°N to 20°S.

It is shown numerically that the percentage difference of u_* over the region is less than 25% in the period November to April. Since the best attainable accuracy in the estimate of z_0 (for $z_0 < 0.4$ m) is about 20% and the uncertainty due to lack of maintenance and calibration is in the order of 15%, the assumed constancy of u_* is within the experimental error.

The model results (computed wind speed for three arbitrary stations) are tested by comparisons to two sets of data:

a. The wind speed estimated by the conventional method in regions of very few stations.

b. The potential wind speed calculated from the measured wind speed.
   The model shows better results than the conventional method and is
   in good agreement with the measured wind speed.

This model is thought to be the first model for hourly surface wind estimation for tropical African regions and the technique of horizontal application of the Businger-Dyer flux-gradient equations at constant height

seems not to have been discussed before in literature. Additionally we think
that this methodology is very promising in all regions which have a large
scale flat topography and only small variations in the regional scale pressure
system; in other words, typical pressure gradient variations should not exceed
about 0.01 mb/km.

ACKNOWLEDGEMENT

C H A P T E R 6

CHARACTERISTICS OF THE DIURNAL COURSE OF THE
UPPER AIR WIND IN CENTRAL SUDAN

CHAPTER 6

CHARACTERISTICS OF THE DIURNAL COURSE OF THE
UPPER AIR WIND IN CENTRAL SUDAN

6.1 *Introduction*

In literature only a very limited number of articles deal with the
understanding of the physical and dynamical processes causing the wind flow in
the inland PBL in tropical African regions (between 20°N and 20°S). In these
regions, the distinctive behaviour of the wind flow differs in some aspects
from those in moderate latitudes (see chapters 4 and 5). At the surface the
nighttime wind speed is relatively low and steady, as expected from stability
effects. The higher wind speed during the day is slightly decreasing in the
course of the day. Just after sunrise there is a sharp increase of the wind
speed and just before sunset a sharp decrease is observed (see section 5.3.3).
        A first question towards understanding the dynamical processes in the
tropical African PBL is how the above mentioned distinctive behaviour of the
diurnal cycle in the surface wind relates to other diurnal cycles of the PBL.
As a first step in finding a solution for this problem we investigate in this
chapter a number of meteorological upper air measurements obtained from four
stations in Central Sudan.
        Although publications related to the central problem of this chapter are
very scarce, there are some interesting suggestions published by Farquharson
(1939), Krishna (1968) and Tetzlaff (1982). Farquharson (1939) observed from
his upper air measurements in Khartoum that the distinctive behaviour of the
diurnal wind cycle is not only confined to the surface but extends up to 1 km.
His morning and midday measurements show a decrease of upper PBL wind speed
from morning to midday. He assumed this decrease to be related to the position
and the associated temperature gradient of the ITCZ.
        Krishna (1968) disagreed with the argument of Farquharson; from the
results of his numerical one-dimensional PBL model study of the diurnal
variation of the wind he suggested that even without the temperature gradient,

the rotation of the earth alone is sufficient to account for the fall of the
wind speed from the morning to midday. The results of his numerical model
computations showed that the time of occurrence of the low level wind maxima
shifts with the latitude; it occurs before midnight at 55°N, gradually
approaches midnight at 30°N, occurs at sunrise near 17°N, and at more southern
latitudes it occurs after sunrise. In his article the Khartoum data were taken
as an example.

Tetzlaff (1982) made an extensive study of the trade wind in North
Africa. His investigation is based on six-hourly upper air data from 22
stations. He also observed the distinctive behaviour of the wind cycle up to
about 1 km in regions between 20°N - 12°N. It was found that the maximum wind
speed of the nocturnal jet occurs in the early morning in the lower 500 m
above the surface. He suggested that the morning maximum of the surface wind
speed is related to this nocturnal upper wind maximum. After the early morning
maximum of the nocturnal jet, when after sunrise the height of the vertical
mixing increases, layers with increasingly higher wind speed are assumed to
transport their momentum downwards. Then the layers with the largest wind
speed in the PBL reach the surface at late morning and afterwards the wind
speed decreases at the surface. From the diurnal course of the wind vector
Tetzlaff estimated the trade wind inversion height, assuming that the level at
which the diurnal course disappears is equivalent to the inversion height. For
latitudes 26°, 21° and 16°N he thus found inversion heights of 1, 1.2 and
1.6 km respectively. In order to calculate the wind divergence he used a large
scale grid model. The results of this model showed that for latitudes 26, 16,
and 11°N the large scale subsidence is 20, 50 and 100 mb/day, respectively.

In this chapter we discuss some interesting aspects of the PBL which may
contribute to the understanding of the diurnal wind course behaviour. First we
calculated the diurnal course of the height of PBL. For the daytime we adopted
the inversion rise model of Tennekes (1973a) in the form used by Van Dop et
al. (1982). For the nighttime we applied the diagnostic equation of
Zilitinkevich (1972). The input parameters in these calculations are only the
measured surface data and the midday temperature profile (midnight radiosonde
observations are not available in Sudan). The results of our computations are
in agreement with those estimated from the upper air data in the Sudan region.
They are also comparable with the PBL heights estimated for the Sahel region
by Tetzlaff (1982). The influence of the cumulative large scale subsidence on
the computation of height of the PBL is implicitly included since the measured

temperature profile is used as input parameter (see section 6.2).

The comparison between the profile of the daytime wind direction and that of the nighttime wind direction for Khartoum and Kassala shows that there is not only a diurnal course up to about 1.5 km, but surprisingly also above 2 km (see section 6.3.1). From the hodographs we obtained the type of thermal advection aloft (above the PBL), while the advection within the boundary layer is estimated using the horizontal surface temperature gradient of the region and the actual wind in the PBL. The upper air thermal advection shows the same behaviour over the region during the day. The thermal advection during the night is not similar over the whole region (see section 6.3.2).

6.2 *Computations of the diurnal cycle of the height of the PBL*

The height of the PBL is strongly influenced by the characteristics of the earth's surface. When the sun shines, the heating of the earth's surface results in large differences between the temperature of the surface and that of the air layer just above the surface. The increase of the upward surface heat flux as a function of time during the day results in a vertical growth of the convective turbulence layer or the mixed layer. The upper limit of the mixed layer is where the rising convective plumes reach the stable non-turbulent upper air. Just after sunset the effect of convective mixing is suppressed, and the nighttime height of the PBL is determined by surface friction, geostrophic wind and the radiational cooling during the night (see e.g. Garratt, 1982).

The diminishing of the shear stress generates an inertial oscillation which together with the geostrophic wind produces a layer of maximum wind, the so-called low level jet (Blackadar, 1957). The maximum of this low level jet is theoretically expected to occur at a time $T \approx \frac{\pi}{f}$ after sunset. For low latitude regions such as the Khartoum region this time will therefore be 22 hrs after sunset, which cannot be considered as a realistic value since sunrise (12 hours after sunset) will interrupt this oscillation. Tetzlaff (1982) observed that the actual jet maximum for such latitudes occurs in the early morning between 2-5 hr GMT (which is 4-7 hr SLT), which is about half of the time estimated by the Blackadar expression.

To compute the diurnal course of the height of the boundary layer we use a prognostic approach for the daytime and a diagnostic approach for the nighttime calculation. As a result we will discuss the stable conditions

(nighttime) and the unstable conditions (daytime) separately.

6.2.1 *Stable conditions*

In literature there are various estimation formulas for the height of the nocturnal boundary layer (h_n) (e.g. Karacin and Berkowicz, 1988; Nieuwstadt, 1984; Caughey et al., 1982). For the Khartoum h_n computation we will use the well known diagnostic formula by Zilitinkevich (1972) in which it is assumed that h_n is proportional to the surface stability parameters;

$$h_n = C_N \left(\frac{u_* L}{f}\right)^{1/2} .$$

(6.1)

Published values of the proportionality constant C_N vary from 0.22 to 0.7 (e.g. Wyngaard, 1975; Brost and Wyngaard, 1978; Nieuwstadt, 1984). In our computation we used the most recent result $C_N = 0.35$, which is obtained from accurate observations by Nieuwstadt (1984). The values of u_* and L are computed by an iteration process (see Chapter 5) using equation (6.2) and (6.3):

$$L = \frac{T_a u_*^2}{\kappa g \theta_*} ,$$

(6.2)

$$u_* = \kappa\, U(z)\, \left[\ln \left(\frac{z}{z_0}\right) + 5\, \frac{z}{L}\right]^{-1} .$$

(6.3)

The temperature scale for turbulent heat transfer (θ_*) is taken as a constant which equals 0.08 K (Venkatram, 1980). For more information about the iteration process and the parameters used see Chapter 5, section 5.4.1. Using equation (6.1) the hourly values for h_n are computed for the winter season.

6.2.2 *Unstable conditions*

Many theoretical and observational studies of the growth of the convective boundary layer have been published (see e.g. Driedonks, 1982). It was found that the hourly mixing depth is strongly dependent on the variation of the upward heat fluxes as a function of time. For the computation of the daytime boundary layer height (h_d) for Central Sudan we need a convective PBL model which neglects the cloudiness complications, since in the winter season there is hardly any cloud-cover (more than 95% of the synoptic observations

indicate cloudless sky). For this reason we adopted for our computation the model of Van Dop et al. (1982) which is based on the Tennekes (1973a) model of the time evolution of a cloud-free convective boundary layer, starting from an accurate estimate of the initial conditions (see section 2.7). The equation used is:

$$h_d (t + \Delta t) = h_d(t) + \Delta t \frac{\partial h_d}{\partial t} , \qquad (6.4)$$

where

$$\frac{\partial h_d}{\partial t} = \frac{\overline{\theta w}_o}{\gamma h_d [1 - \frac{c_2 \kappa L}{c_1 h_d}]} [1 + 2c_1 [1 + (\frac{c_2 \kappa L}{c_1 h_d})^2]] , \qquad (6.5)$$

and

$$\overline{\theta w}_o = \frac{Q_H}{\rho C_p} , \qquad (6.6)$$

$$\gamma = \frac{\partial \theta}{\partial z} . \qquad (6.7)$$

$\overline{\theta w}_o$ is the turbulent kinematic flux of sensible heat at the earth's surface. Q_H is the sensible heat flux which is computed from the individual hourly global radiation measurements (see chapter 5) and γ is the lapse rate of the potential temperature above the inversion base. The fact that we have only measurements of a single temperature profile (midday data) during the day forces us to assume, that γ is constant during the day and equal to its calculated value from the midday sounding. Though such an assumption cannot be justified completely (γ normally is a function of time) we intuitively expect the variation of γ not to be large in a stationary climate like Central Sudan. Acceptable values for the proportionality constants are $c_1 = 0.2$ and $c_2 = 5$ (see Driedonks, 1982).

For the computation the time step Δt is taken equal to 3600 s, since all the stability parameters used are calculated from the hourly routine meteorological data. The starting value for the computation of equation (6.5) is taken as the boundary layer height at the last hour of the night. The starting hour of the computation is at 7 hr. SLT, since in the winter the sun rises in Central Sudan at about 6.30 hr SLT, and the net heat flux usually

changes sign about one hour later (Van Ulden and Holtslag, 1985). As a result the height of the boundary layer at t = 6 hr is computed using the nocturnal boundary layer (NBL) height equation (equation 6.1). The starting value for the daytime computation of BL height at t = 7 hr SLT is taken as the height of the nighttime boundary layer at t = 6 hr SLT.

In this computation the effect of the subsidence on the BL growth is implicitly included in the value of γ which is obtained from the measured daytime temperature profile. The cumulative large scale subsidence in the Sahel (which is related to the descending part of the Hadley cell) results in a large stability aloft (large value of γ). Moreover, Tetzlaff (1982) found that in the layer (850-700) mb the subsidence is about 250 m/12 hrs at 16°N, which means that the subsidence reduces the height of the daytime PBL by at most 250 m. From this we can conclude that our computation of the PBL height is not much biased by the subsidence. We expect that this influence should be considered only explicitly, when the subsidence is greater than 100 mb/day.

The computer program is written in such a way that it computes the hourly PBL heights for the 24 hours. For the nighttime (18-06 hr SLT) equation (6.1) is used and for the daytime (07-17 hr SLT) we applied equation (6.4). The height of the PBL is computed for the winter season (December, January and February); the results of the three months do not show much differences.

A representative result of the diurnal course of the height of the PBL is shown in fig. 6.1. From the figure we observe that just after sunset h_n decreases to a minimum at about 20 hr SLT, after which it shows a quasi steady-state value, about 400 m. This value is compatible with those observed
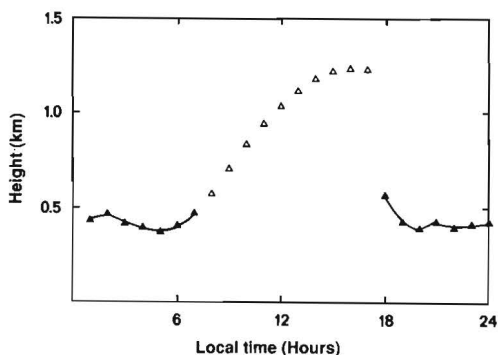
Fig. 6.1
The computed diurnal course of the height of the boundary layer.

in mid-latitudes (e.g. Thorpe and Guymer, 1977). The decrease of h_n after sunset is discussed in literature by many authors (e.g. Deardorff, 1974; Smeda, 1979); from physical point of view this behaviour can be viewed as a relaxation process in which h_n reaches an equilibrium height.

6.2.3 *Validation of the BL height computations*

To test the computation results, we compared the computed BL height with the BL height estimated from the upper air data. For checking the computed height of the daytime boundary layer (h_d) we used the midday Khartoum radiosonde data. From the temperature as well as from the humidity profile we can roughly estimate h_d. Fig. 6.2 shows a representative winter profile of the potential temperature and the relative humidity. The average surface pressure level is 970 mb. The potential temperature shows an adiabatic constant behaviour from the ground up to 900 mb ($Y = 10°K/km$), which is a characteristic of convective boundary layers indicating the presence of a mixed layer. We expect that the lower limit of the mixing layer is only a few tens of meters above the ground. The wind profile of the region (from the four stations) shows that the surface wind is about 85% of the average geostrophic wind speed (up to 850 mb). The layer 800-700 mb shows a steady increase of the potential temperature, which indicates a stable free atmosphere with a Y of about (15.5 ± 1.7) K/km. The transition (inversion) layer lies between turbulent air from the convective mixed layer below and the non-turbulent air from the stable layer. In this layer entrainment is caused by turbulent eddies entering into the stable layer. Though the absolute humidity at Khartoum is very low, its relative change still roughly does indicate the height of the PBL. Due to the insufficient vertical resolution of the data (increments of 500 m), we cannot give an accurate estimate of h_d. The accuracy of the height of the measurements is ± 0.2 km. The value of the height h_d is usually estimated from the middle of the transition layer (Deardorff, 1972). This leads us to estimate an h_d of about 1.1 ± 0.2 km. The computed value of h_d, 1.2 ± 0.1 km is thus in good agreement with the value estimated from the measurements. As the upward heat flux increases in the course of the day, the mixed layer is deepened until a maximum height of about 1.3 km at about 16 hr SLT.
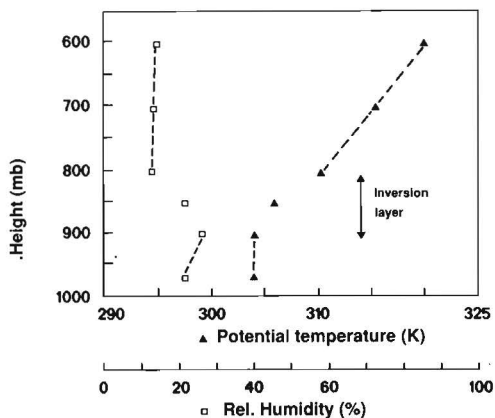
Fig. 6.2
Khartoum midday profile
of the potential tempe-
rature (▲) *and relative*
humidity □ *of January 1984.*

Unfortunately no temperature profiles for the nighttime in Khartoum are available to check the height of the turbulent mixed layer (h_n). As an alternative we consider the height of the wind maximum (which can be obtained from the available wind profiles) to back our model results. Clarke (1970) defined the top of the nocturnal boundary as equivalent to the height of the wind maximum, since this is the maximal height at which shear-induced turbulence can be generated. Beyrich and Klose (1988), however, found from their non-stationary two-layer model results that h_n should be about 20% smaller than the height of the wind maximum. The only data available to check the computed value of h_n are the Khartoum midnight pilot balloon measurements, which show a weak maximum at about 500 m, see figure 6.3. A more precise position of the maximum cannot be estimated because of the insufficient vertical resolution of the data, the increment of which is 500 m. However, the Farquharson (1939) pilot balloon data (in the period 4-7 hr SLT) for the winter do show a better resolution (increments of about 300 m with surface observation at about 150 m) than that of our data. From his data it can be concluded that the maximum is at about 300 m (fig. 6.3). From the two data sets and the nocturnal profiles published by Tetzlaff (1982) we roughly expect that the wind maximum is between 300 and 500 m. In conclusion we can say that the computed h_n (400m) is in good agreement with the height of the maximum wind speed observed from the measurements.

One of the aspects that our computation cannot produce is the variation of the magnitude of the wind maximum as a function of time. This would be of great importance, especially in the very early morning when the jet structure reaches its maximum, because it can give an indication of the maximum horizontal momentum stored in the jet, which we think is strongly related to the surface wind morning-peak.
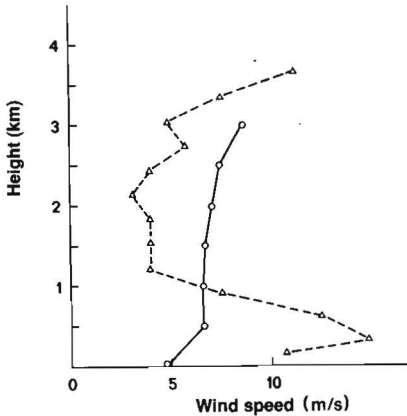
Fig. 6.3
Nocturnal wind profile at Khartoum.
-o- Khartoum midnight data of
  January 1984.
-Δ- Khartoum data in the period
  (4-7) hr. SLT of January
  1936 (Farquharson, 1939)

6.3 *Analysis of the upper wind observations*

In this section we will give a qualitative discussion about the measured wind profiles (see chapter 4) in Central Sudan. The analysis presented here is based on the midday (13 hr SLT) and midnight (24 hr SLT) monthly averaged wind profiles for the winter season of 1984 from the stations Khartoum, Dongola, Kassala and El Obeid. With exception of the Khartoum midday data the observations are pilot balloon measurements with a vertical resolution of 500 m, from the surface up to 3 km. The Khartoum midday data are radiosonde measurements for the following heights: surface, 900, 850, 800, 700 and 600 mb.

We are aware that the information available to us is too little to draw definite conclusions about the behaviour of the PBL wind diurnal course in Central Sudan. We therefore will concentrate our discussion on the behaviour

of the measured wind profile, the veering of the wind and the thermal
advection over the region.

6.3.1 *The behaviour of the measured wind profile*

The general shape of the wind profile in Central Sudan is comparable with
those measured in other Sahelian regions (Tetzlaff, 1982). It exhibits a
behaviour which is typical for the trade winds (Riehl, 1979).

The midday wind speed increases from the surface up to a maximum at about
1 km above which it starts decreasing to a minimum at about 2 km. The wind
direction changes from northeasterly to southeasterly with increasing height.
Fig. 6.4 gives an example of the wind profiles in central Sudan. Throughout
the winter season the midday wind profiles show from the surface up to 1 km an
increase of the wind speed ranging from 1 to 4 m/s over the region. Such
behaviour may not be explained by convective PBL theory alone, since for a
convective PBL the wind speed should be constant above the surface layer
because of the strong mixing (see chapter 2). We are convinced that this
behaviour is related to the trade wind.
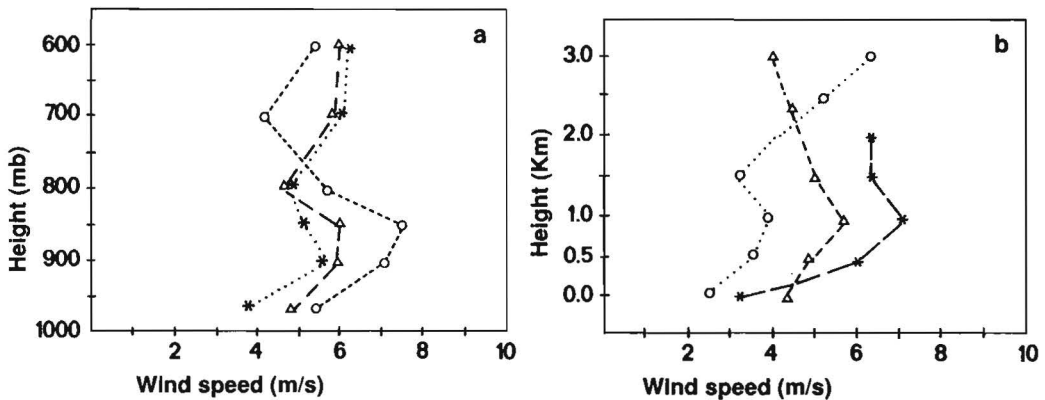
Fig. 6.4 Midday wind profile 1984.
    a - Khartoum; --△-- January, --o-- February, ... December*
    b - Dongola; --△-- January, Kassala; ..o.. January,
    El Obeid, ---- December.*

The midnight pibal profile shows a nocturnal jet in the lowest 500 m, and
the difference between the wind at the jet peak and the surface wind varies in
the range from 2 to 8 m/s for the four stations. The largest difference is
observed at El Obeid. The differences observed from our data are comparable
with those at other Sahelian regions described by Tetzlaff (1982). The maximum
difference observed by him is 12 m/s at En Nahud (which is 200 km west of El
Obeid).

The behaviour of the wind profile from the late night (about 5 hr) to the
mid morning (about 10 hr) indicates that there is a continuous redistribution
downward of the momentum which is stored in the nocturnal jet, due to the
mixing below the rising inversion. This is illustrated schematically in fig.
6.5. In this figure the late night wind profile is drawn as a solid curve,
which reaches a maximum wind speed of $U_1(z_m)$ at height z_m (which is equivalent
to the PBL height h_n) and a surface wind speed of $U_1(z_1)$. The wind profile at
about 10 hr. is depicted by the dashed curve showing a maximum wind speed
$U_2(z_m)$ at height z_m, and a surface wind speed $U_2(z_1)$. According to Tetzlaff
(1982) the surface wind maximum is due to a downward transport of the full
momentum stored in the nocturnal jet.
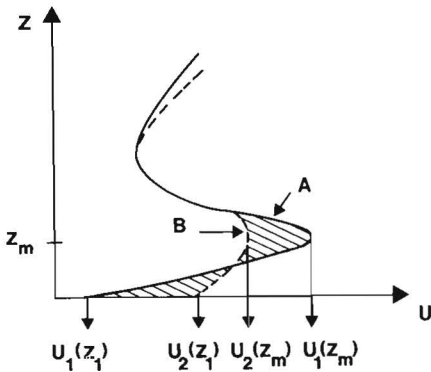
Fig. 6.5
Schematic behaviour of the wind profile
at about 5 hr. SLT (profile A) and
10 hr. SLT (profile B).

To check this argument we used the Khartoum wind profiles 1936
(Farquharson 1939) and the surface wind data of 1983, '84. The combined use of
the 1983, '84 data with those of Farquharson from 1939 is justified by the
stationarity of the climate (see chapter 5). Fig. 6.6 shows a representative
winter profile (January 1936, from Farquharson's data) where we consider the
morning profile (in the period 4-7 hr. SLT) to be equivalent to the late night

profile (profile A in fig. 6.5). The afternoon profile (in the period 11 to 15 hr. SLT) can probably represent the wind profile at about 10 hr. (profile B in fig. 6.5) since in advance we do not expect large changes in the wind profile after 10 hr. According to Farquharson's data for the winter the difference between the early morning and the afternoon wind speed is 7.5 m/s at 300 m and 5 m/s at 150 m height. Since Farquharson's lowest observation is at 150 m we used the winter season surface data of 1983, '84 to obtain the difference between the wind speed at 5 hr. and 10 hr. at the surface, which is about - 2 m/s. This indicates that the decrease in the wind speed at height z_m results in an increase of the surface wind. However, the increase is about a factor 3 smaller than would be the case if the total momentum stored in the jet would be transported to the surface.
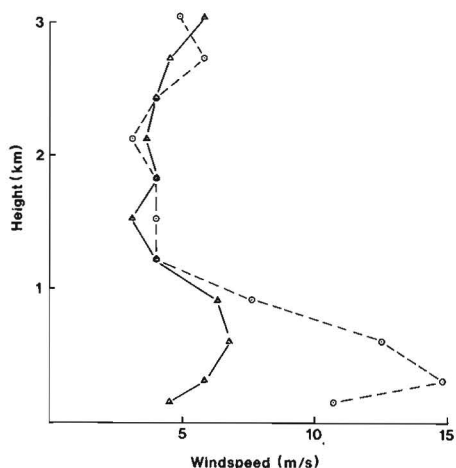
Fig. 6.6
Mean monthly wind profile for
January 1936 (Farquharson, 1939).
--o-- Observation in the period
(4-7) hr. S.L.T.
- Δ - Observation in the period
(11-15) hr. S.L.T.

From the data it seems that there are two important processes:
(a) There is a vertical redistribution of the momentum stored in the nocturnal jet. This process takes place just after sunrise and may explain the maximum of the surface wind. (b) There is a diurnal course in the circulation of the PBL which has a larger time scale than the momentum redistribution in the morning. We think that the change in total momentum of the PBL from the late night to the mid morning as shown in fig. 6.6 is related to this process. The combination of these two processes can account for the observation of the change in momentum as mentioned above.

A comparison between the wind direction profiles for midday and midnight from the four stations indicates that the Khartoum and Kassala data show strong variations while those at Dongola and El Obeid show no variation. Fig. 6.7 depicts the Khartoum wind direction profile for midday and midnight in the winter season. A strong change of direction is seen between the day and night data; about 45° eastwards in the PBL and about 90° westwards in the layer above 2 km. Consequently there is a transition layer, at about 1.5-2 km, where the wind direction is stable. In Kassala similar variations are observed. In the 1984 data they are most pronounced in December and less pronounced, but clearly observed, during the other winter months. This variation in the wind direction suggests that there also exist a diurnal course in the circulation well above the PBL. The diurnal course above 2 km is, to our knowledge, not reported before in the Sahelian region.
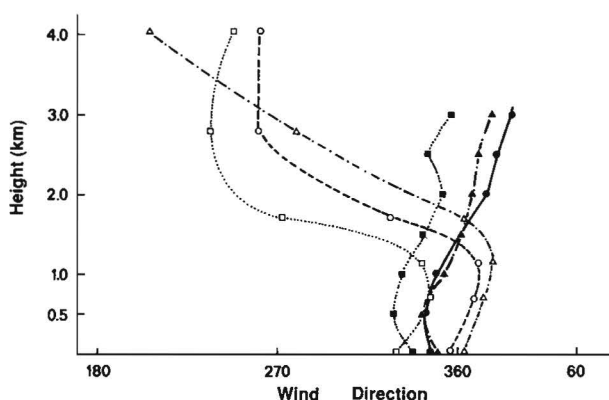
Fig. 6.7 Monthly averaged wind direction profile from Khartoum for the winter season 1984.

···□···, ···■···· December midday and midnight profiles
--o--, -●- January midday and midnight profiles
-.-Δ-.-, -.-▲-.- February midday and midnight profiles.

6.3.2 *Thermal advection in Central Sudan*

In this section we present a qualitative discussion of the thermal advection since there is a clear distinction in the wind direction above the PBL with respect to that within the PBL. Therefore, we will separately discuss the thermal advection in the PBL and the thermal advection above the PBL. To determine the thermal advection in the PBL we use the surface temperature gradient maps and the average wind direction in the PBL. For the thermal advection above the PBL we use the upper air data of the region. The analysis of the thermal advection is carried out both for the day and night data.

To determine the average winter time advection in the lower PBL (below $\approx$ 0.5 km height) we combine the average PBL wind vector with the layer-average horizontal temperature gradient $\nabla_h T$. For this purpose we used 30 years (1950-1980) of monthly average maximum and minimum temperatures for January from 20 stations, rather than the limited temperature data from 1984. In making actual $\nabla_h T$-evaluations we had to exclude six of these stations, because they are physically separated from the Central Sudan by mountains: Port Sudan and Tokar at the Red Sea coast, Yambio in the far south, and El Fasher, El Geneina and Nyala in the mountaineous western Jebel Marra region.

The surface-layer extreme temperatures T_{max} and T_{min} are taken to be representative of local average PBL temperatures at midday, respectively midnight, for determination of large-scale horizontal temperature gradients in that layer. In daytime the temperature lapse rate in the well-mixed PBL layer will be adiabatic, apart from a shallow superadiabatic surface layer which in this homogeneous region (see chapter 5) will have a similar height everywhere. Therefore a truly horizontal daytime $\nabla_h T$ at a single height a.s.l. can be obtained by transforming local temperatures to that reference height, using the adiabatic lapse rate. In this correction the obtained $\nabla_h T$ is not dependent on the choice of a reference height, and the elevation of Khartoum was arbitrarily chosen as reference. For the nighttime evaluations, elevation correction will be discussed further below.

The average horizontal daytime gradient was calculated from the T_{max} values of 14 stations through least-square fitting of a simple flat model plane, taking $z = T_{max}$ (elevation-corrected) and x,y the coordinates on a km grid. Fig. 6.8 shows the result, $\nabla_h T_{day} = 10.9 \times 10^{-3}$ K/km in direction 139°. In the central region between 27° and 37° longitude the deviations of individual stations, plotted in 0.1 °C units, vary randomly around this model

plane within $\approx 1°$, showing satisfactory representativity of the gradient. Large systematic deviations are seen at the Red Sea and in Jebel Marra, testifying to the separate geographical status of these areas.

In the region between 31°E – 36°E and 9°N – 21°N the terrain is very flat, with elevation differences less than 20 m/100 km relative to Khartoum. From the 8 stations in this flat region we get $\nabla_h T_{day}$ = 13.0 x 10^{-3} K/km in direction 130°, not differing significantly from the 14-station result.
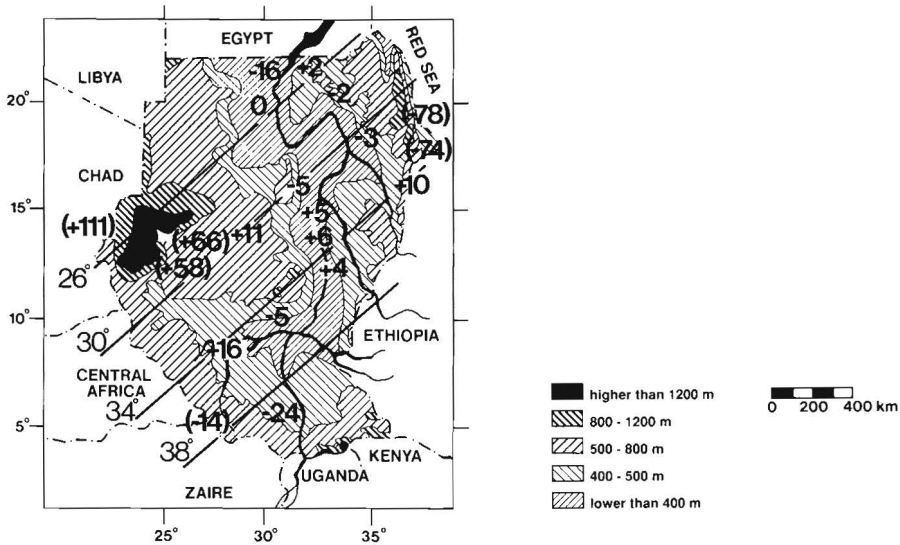
Fig. 6.8 Large-scale daytime temperature gradient for January. The model plane is indicated by the linear isotherms. Digits at the stations indicate $\Delta T = T_{max}$ (observed, corrected to Khartoum elevation) – T_{max} (modelled), in units of 0.1 C. Stations with bracketed digits were not used in calculating the average gradient.

For nighttime $\nabla_h T$ calculations, representativity of T_{min} for the average PBL is less certain because of insufficient mixing. Moreover, transformation to a common elevation requires some assumption about the climatological average nighttime lapse rate in the lower PBL, which is hardly feasible from the limited local data. Pielke and Mehring (1977) found, that in complex

terrain the 24-hour lapse rate has a regional average value of 5.4°C/km in moderate latitudes; assuming the daytime lapse rate to be adiabatic, this would indicate that at night the average lapse rate is approximately isothermal there. In the Sudan the nighttime stability might be larger.

For assessing the sensitivity of the calculated nighttime $\nabla_h T$ to these assumptions, calculations were done both for adiabatic elevation correction, similar to the daytime procedure, and with unchanged T_{min} data, which should be applicable for the isothermal situation. The plane-model method was again used, and obtained gradient slopes and directions are tabulated below.

Elevation correction:	Adiabatic	None (isothermal)
Flat region (8 stations)	6.2×10^{-3} K/km, 159°	5.8×10^{-3} K/km, 163°
Extended (14 stations)	9.5×10^{-3} K/km, 139°	7.7×10^{-3} K/km, 141°

It appears that the result of nighttime horizontal gradient calculation does not depend significantly on the choice of elevation correction, but that its dependence on the used calculation region is stronger than in daytime. For the four night cases the average gradient is 7.3×10^{-3} K/km, direction 150°.

Because $\nabla_h T_{day}$ = 12.0×10^{-3} K/km, direction 135°, is the average for the two region sizes, it follows that the direction of average PBL temperature gradients in the Sudan is continuously southeasterly. However, gradient magnitude varies between day and night by a factor two. Tetzlaff (1982) gets $\nabla_h T$ = (7 to 12) $\times 10^{-3}$ K/km, southerly, from gridpoint calculations for the entire Sahel region, which agrees with these Sudanese gradients.

In the Sudan the PBL wind vector varies from NE to NW, so we conclude that in the PBL cold advection occurs both during the day and the night.

To determine the thermal advection above the PBL we present the data as wind hodographs for ease of interpretation. In our construction and interpretation of the hodographs we follow the convention used by the Weather Forecasting Handbook of the British Meteorological Office (1975). In such a hodograph the wind vector is plotted in a two dimensional plane of concentric circles, the radius of which is linearly related to the velocity of the wind. The wind direction plotted along the circles is directly equivalent to the measured direction. In this convention the wind vector is drawn as a vector which ends at the origin (a difference of 180° with some other conventions). The direction of the thermal wind is indicated in such a way that the "flow" is from higher to lower layers (indicated by an arrow in figures 6.9-6.10).

The great advantage of a hodograph is that it shows from observations at a single location the warm and cold air advection relative to the station. In the northern hemisphere the thermal wind flow is such that the cold air is to the left of the flow and the warm air to the right of it. Moreover, the hodograph indicates the direction in which warmer or colder air is blowing in any layer, i.e. baroclinic behaviour (warm or cold advection). If the wind direction does not change with height this means barotropic behaviour (for more details see chapter 2).

Hodographs for the winter months were constructed using the monthly average wind vector. The behaviour of the hodographs for the winter months proves to be very similar. Typical profiles of the winter season (January data) from the four above mentioned stations are depicted in figures 6.9-6.10.

From the figures 6.9a,b we see that the daytime thermal wind over the region, except at El Obeid, in the layer 0.5-3.0 km varies from SW to NW, showing cold advection. The data from El Obeid, however, do not clearly show advection but this might be related to the limited heights of the measurements (only up to 2 km).
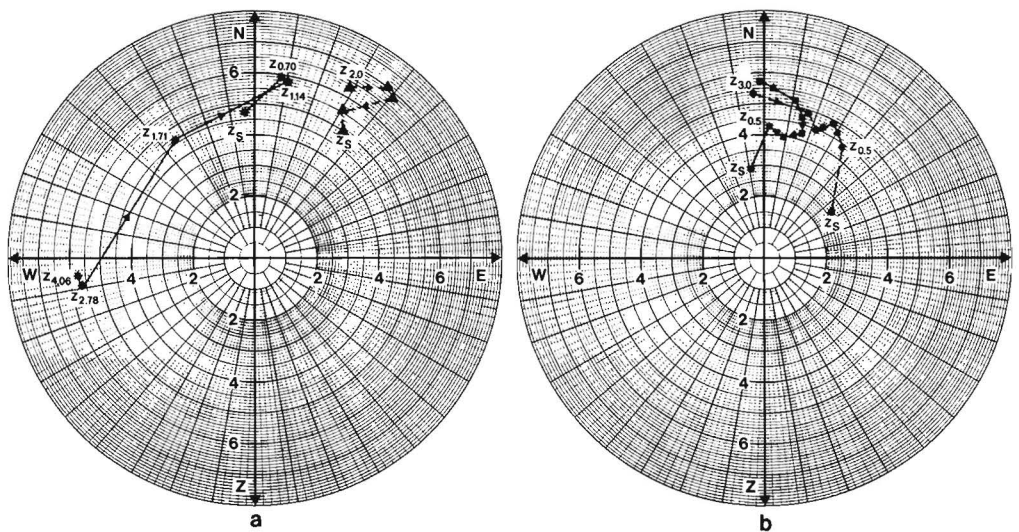
Figure 6.9 January 1984 midday hodograph a - -*- Khartoum data, -▲- El Obeid data, b - -●- Kassala data, -■- Dongola data.

In fig. 6.10a,b the midnight hodographs are presented. The thermal wind direction (in the layer 0.5 to 3.0 km) varies as function of height from NE to E in Khartoum while the El Obeid thermal wind is SE, so both stations show warm advection (see fig. 6.10a). From fig. 6.10b we see that the thermal wind direction varies as a function of height from SW to WNW in Kassala, while in Dongola the thermal wind is WSW. Both stations indicate cold advection.
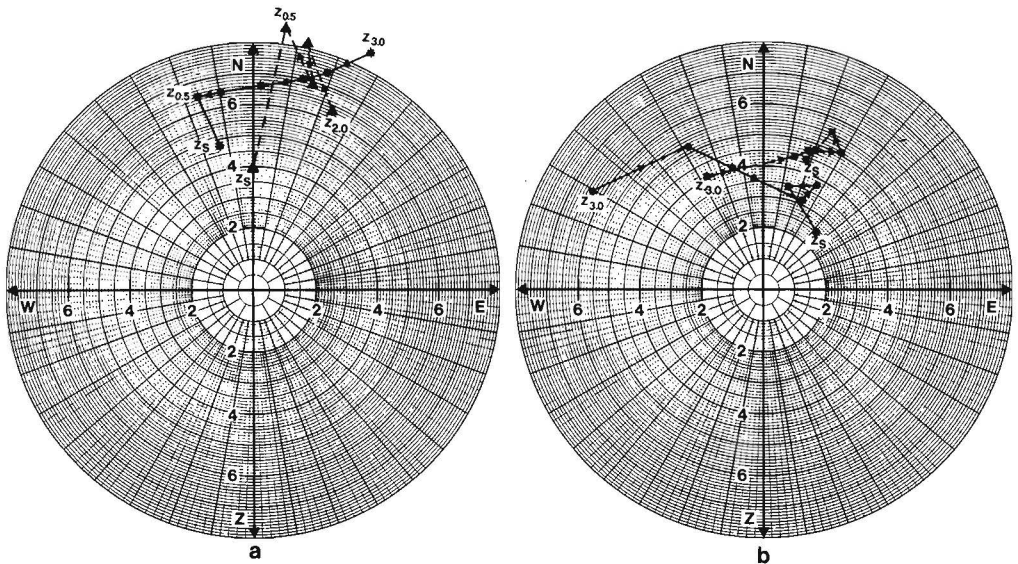
Figure 6.10 January 1984 midnight hodograph a- -*- Khartoum data, -▲- El Obeid data. b- -●- Kassala data, -■- Dongola data.

In conclusion, the thermal advection over the region shows a cold advection during the day both in the PBL and above it. During the night there is cold advection in the PBL over the region, while above the PBL Khartoum and El Obeid indicate warm advection and Dongola and Kassala show cold advection. The reason for the variation of the thermal advection during the night above the PBL is not yet clear to us. We intuitively suggest that this behaviour is due to either a local or mesoscale circulation.

The height of the PBL also can be roughly estimated from the hodograph, since it should be indicated by a clear wind direction shift. In the figures 6.9, 6.10 we observe that the wind vector shows a clear shift and decrease in

magnitude at about 0.5 km for the night profile and at about 1 km for the day profile, in agreement with the results obtained in the previous section.

6.4 *Conclusions*

For the understanding of the diurnal wind course behaviour in the PBL in Central Sudan, four essential aspects of the PBL have been investigated:

(i) The diurnal course of the height of the PBL is computed, applying a version of the inversion rise model of Tennekes (1973a) and using the surface observations and the midday temperature profile. The large scale subsidence, which is an important cumulative phenomenon in this region, is implicitly included in the computation since the measured potential temperature gradient above the inversion is used as an input parameter. The nocturnal BL height obtained from the model is 0.4 km and that of midday is 1.1 km. The computed height from the upper air data in the region shows good agreement with the estimated height from the upper air data in the region and with those published in literature for other Sahelian regions.

(ii) From our Khartoum surface data and Farquharson's (1939) wind profile data for Khartoum, it is found that the decrease from early morning to midday of the wind speed at height h_n results in an increase of the surface wind, which is about a factor 3 smaller than would be the case if the energy stored in the jet were transferred completely to the surface. This behaviour is thought to be due to two processes: (a) The downward transport of the horizontal momentum stored in the nocturnal jet. (b) The diurnal course of the circulation in the PBL which takes place on a larger time scale than that of the redistribution of the momentum in the early morning.

(iii) The behaviour of the measured wind profile up to 3 km in the region is analysed and compared with profiles from other Sahelian regions. The general shape of the wind profile in Central Sudan shows a typical trade wind behaviour. The comparison between midday and midnight wind direction profiles from Kassala and Khartoum stations shows that also a diurnal course in the circulation exist above the PBL. This diurnal course in the circulation above 2 km has, to our knowledge, not been reported before for other Sahelian regions.

(iv) From hodographs of the midday and midnight profiles and the horizontal surface temperature gradient over Sudan the thermal advection over the region has been estimated. During the daytime the thermal advection is homogeneous over the region, showing cold advection in the PBL and above it. During the night the thermal advection shows a clear variation over the region. This is suggested to be due to either a local or mesoscale circulation. For a quantitative understanding of this phenomenon we need more detailed upper air data base than what is presently available.

APPENDIX A

Notation

A_s	= surface albedo
c_h	= volumetric heat capacity $[J/m^3K]$
C_L	= $\frac{MC_p}{R\kappa}$ (= 8.52)
C_p	= specific heat at constant pressure (1003 J/kg K)
d	= damping depth of soil temperature diurnal cycle $(\frac{2\,K_Q}{\omega})^{\frac{1}{2}}$
g	= gravitational force (10 m/s^2)
K_G	= thermal diffusivity $[m^2/s]$
L	= Monin-Obukhov length [m]
M	= molecular weight (0.028966 kg/mol)
P	= pressure [mb]
Q_E	= latent heat flux $[W/m^2]$
Q_G	= soil heat flux $[W/m^2]$
Q_H	= turbulent transfer of sensible heat to the atmosphere (upward flow is positive) $[W/m^2]$
$Q_{L\uparrow}$	= scattered and ground-reflected longwave radiation $[W/m^2]$
$Q_{L\downarrow}$	= direct longwave radiation received by the earth surface from the atmosphere $[W/m^2]$
Q_N	= net radiation $[W/m^2]$
Q_s	= short wave length radiation from the sun and sky $[W/m^2]$
Q_T	= net short wave radiation at the earth surface $[W/m^2]$
R	= universal gas constant (8.314 J/mol K)
T	= absolute temperature [K]
T_a	= air temperature at 2 m [K]
T_{av}	= average temperature during a diurnal cycle [K]
T_s	= surface temperature [K]
T_{so}	= soil temperature [K]
$\overline{V}$	= wind speed vector [m/s]
v	= south-north wind component [m/s]
v_g, u_g	= component of the geostrophic wind [m/s]
$\vec{v}_g$	= geostrophic wind vector [m/s]
U_p	= potential wind speed [m/s]
U(z)	= measured wind speed at height z [m/s]
u	= west-east wind component [m/s]

$\overline{u'w'}, \overline{v'w'}$ = turbulent momentum transports $[m^2/s^2]$

u_* = frictional velocity $[m/s]$

w = vertical wind component $[m/s]$

z = height at which wind speed is measured (15 m)

z_o = roughness length $[m]$

z' = threshold soil depth for the diurnal course of the temperature $[m]$

ΔT = amplitude of the air temperature $[K]$

γ = gradient of potential temperature above the mixed layer $[K/km]$

Γ_d = dry adiabatic lapse rate $[10\ K/km]$

ε_a = atmospheric emissivity under clear sky

ε_s = emissivity of the surface

θ = potential temperature $[K]$

$(\overline{\theta\omega})_h$ = vertical kinematic heat flux $[Km/s]$

$(\overline{\theta\omega})_o$ = surface kinematic heat flux $[Km/s]$

θ_* = turbulent temperature scale $[K]$

κ = von Kàrmàn constant (0.41)

λ = thermal conductivity $[W/m\ K]$

ρ = air density $[kg/m^3]$

ν = molecular viscosity $[m^2/s]$

σ = Stefan-Boltzmann constant ($5.67 \times 10^{-8}\ W/m^2\ K^4$)

$\tau_{x,y}$ = local kinematic momentum flux in the x and y directions, respectively $[m^2/s^2]$

ω = angular frequency $[s^{-1}]$

Ω = rotation frequency of the earth $[s^{-1}]$

Appendix B

Hourly potential wind speed and wind direction from Khartoum airport and Wad
Madani station for 1983, '84.

B.1 Khartoum potential wind speed (m/s) 1983

L.TIME	JAN	FEB	MAR	APR	MAY	JUN	JUL	AUG	SEP	OCT	NOV	DEC
0030	5.2	3.9	3.5	3.6	2.0	3.8	3.7	3.5	2.9	4.9	4.4	4.3
0130	5.5	4.2	3.8	3.9	2.3	4.6	4.6	3.7	3.4	4.9	4.5	4.4
0230	.5.4	4.4	3.7	3.6	2.5	4.2	4.3	3.6	3.1	4.9	4.2	4.4
0330	5.4	4.1	3.9	3.6	2.5	4.0	4.2	3.5	3.0	4.5	4.0	4.4
0430	5.2	4.1	3.6	3.4	2.3	4.1	4.4	3.5	3.0	4.3	4.0	4.4
0530	4.8	4.1	3.7	3.3	2.2	3.6	4.4	3.4	2.8	3.9	3.8	4.1
0630	4.8	3.8	3.4	3.4	2.2	3.7	4.2	3.5	3.1	3.8	3.9	4.1
0730	5.0	4.3	4.2	4.2	2.9	4.6	5.0	3.9	3.6	4.2	4.1	4.7
0830	5.9	5.5	5.7	5.6	3.6	5.2	5.3	4.4	3.4	4.5	5.1	6.4
0930	6.7	6.7	6.3	6.1	4.2	5.5	5.3	4.6	3.5	5.1	5.6	6.5
1030	6.6	7.3	6.1	5.9	3.8	5.4	5.2	4.6	3.2	5.2	5.7	6.5
1130	6.2	7.0	5.3	5.1	3.2	5.1	4.8	4.3	3.1	5.0	5.1	6.2
1230	6.0	6.6	4.9	4.7	2.8	4.7	4.2	4.0	2.5	4.7	4.6	6.0
1330	5.8	6.3	4.8	4.2	2.6	4.3	4.0	3.8	2.6	4.4	4.3	5.8
1430	5.8	5.9	4.9	4.3	2.5	4.2	3.7	3.8	2.3	4.2	4.1	5.6
1530	5.7	5.9	4.8	4.3	2.3	3.7	3.5	3.5	2.1	4.0	4.1	5.6
1630	5.6	5.9	4.7	4.2	1.9	3.3	2.8	3.1	1.8	3.6	3.8	5.3
1730	5.1	4.8	4.2	3.5	1.7	2.8	2.8	3.0	1.8	3.1	3.0	4.3
1830	5.0	3.9	3.4	2.8	1.4	2.4	2.5	3.0	1.4	3.0	3.1	3.8
1930	5.0	3.8	3.2	2.8	1.6	2.2	2.5	3.4	2.2	3.7	3.4	3.9
2030	5.1	3.6	3.2	3.1	1.7	2.9	3.1	3.9	2.6	4.0	3.9	3.8
2130	5.3	3.8	3.4	3.4	1.6	3.7	3.8	3.8	3.1	4.1	4.2	4.1
2230	5.3	3.8	3.5	3.5	2.0	3.2	4.7	3.8	3.0	4.4	4.4	4.4
2330	5.2	3.8	3.6	3.6	2.0	3.2	3.6	3.7	3.2	5.0	4.6	4.2

B2 Khartoum potential wind speed (m/s) 1984

L.TIME	JAN	FEB	MAR	APR	MAY	JUN	JUL	AUG	SEP	OCT	NOV	DEC
0030	4.8	4.6	3.6	4.0	2.8	3.9	3.1	4.4	3.1	2.9	2.7	3.9
0130	5.2	4.8	3.8	4.3	3.1	4.3	3.2	4.0	3.2	3.0	2.8	4.0
0230	4.7	4.6	3.6	4.7	3.0	4.0	3.5	3.6	3.4	3.1	2.7	4.2
0330	4.7	4.7	3.7	4.7	2.7	3.8	3.4	3.2	3.3	3.3	2.5	4.2
0430	4.5	4.8	3.6	4.6	2.8	4.0	3.2	3.0	3.0	3.1	2.3	4.3
0530	4.5	4.6	3.5	4.4	3.0	3.7	3.2	2.9	3.0	2.7	2.4	4.2
0630	4.2	4.7	3.6	4.0	2.8	3.5	3.2	3.0	3.0	2.5	2.3	4.0
0730	4.8	4.9	4.2	5.1	3.4	3.5	4.0	3.5	3.3	2.8	2.8	4.1
0830	5.8	6.3	5.2	6.0	4.2	4.2	4.6	4.2	4.2	3.6	3.8	4.9
0930	6.9	6.9	6.1	7.0	4.6	4.0	4.3	4.0	4.3	4.3	4.2	5.5
1030	7.3	7.1	6.1	7.4	4.5	3.8	3.8	4.1	4.1	4.5	3.9	5.5
1130	7.0	7.1	5.4	6.8	4.3	3.9	3.5	3.9	3.9	4.5	3.6	5.1
1230	6.6	6.8	4.8	6.4	4.0	3.8	3.3	3.5	3.5	3.9	3.2	4.6
1330	6.0	6.8	4.6	6.0	3.6	3.9	3.0	3.5	3.4	3.5	3.1	4.5
1430	5.8	6.7	4.5	5.8	3.5	3.7	2.9	3.4	3.2	3.1	3.0	4.5
1530	5.8	6.4	4.4	5.6	3.5	3.9	2.7	3.4	2.8	3.0	2.8	4.6
1630	6.3	6.3	4.4	4.9	2.9	3.6	2.3	2.8	3.4	2.8	2.6	4.4
1730	5.4	5.8	3.8	3.9	2.5	3.2	1.8	2.3	3.1	2.5	2.0	3.8
1830	4.6	4.5	3.1	3.1	2.0	2.6	1.7	1.8	2.9	2.6	1.7	3.5
1930	4.4	4.5	3.3	3.2	2.0	2.5	1.9	1.7	3.3	2.5	1.8	3.5
2030	4.7	4.2	3.5	3.6	1.9	2.6	2.8	2.3	3.2	2.4	2.0	3.6
2130	4.7	4.2	3.6	3.9	2.9	3.0	2.8	2.9	3.3	2.5	2.2	3.7
2230	4.8	4.2	3.5	3.9	2.8	3.8	2.9	3.5	3.0	2.6	2.3	3.9
2330	4.8	4.2	3.6	3.9	2.7	4.1	2.9	4.1	2.6	2.7	2.5	4.1

B3 Khartoum wind direction 1983

L.TIME	JAN	FEB	MAR	APR	MAY	JUN	JUL	AUG	SEP	OCT	NOV	DEC
0030	333	332	332	326	321	193	212	225	253	332	351	355
0130	332	332	334	329	338	195	199	218	251	224	352	355
0230	333	332	333	326	335	217	204	219	254	332	355	357
0330	337	330	336	329	333	215	201	223	233	336	355	360
0430	338	335	339	334	340	214	203	230	217	335	357	002
0530	337	336	342	338	336	211	204	233	222	339	358	003
0630	339	344	345	341	343	202	207	225	226	335	360	009
0730	340	350	352	353	004	205	214	233	239	336	005	014
0830	354	004	004	006	015	224	218	242	257	358	016	028
0930	004	019	013	011	023	241	238	255	278	025	023	034
1030	004	021	018	009	028	243	238	256	283	033	033	040
1130	002	019	013	360	025	248	243	260	282	032	032	041
1230	355	016	004	347	015	265	246	263	286	030	016	038
1330	351	015	352	337	341	285	244	263	300	022	002	031
1430	349	356	349	329	333	294	252	262	301	357	359	022
1530	347	349	344	327	332	304	253	264	294	349	357	012
1630	347	348	342	329	328	296	242	266	327	349	356	011
1730	341	350	343	332	327	298	245	261	321	352	351	005
1830	335	344	339	329	316	291	217	233	250	347	345	003
1930	334	339	336	324	319	246	211	228	235	338	339	001
2030	333	336	332	322	310	218	195	216	241	333	336	360
2130	334	330	334	322	304	164	188	218	241	330	337	355
2230	333	331	332	326	304	187	203	220	235	331	342	353
2330	333	332	331	324	306	194	220	221	241	332	346	351

B4 Khartoum wind direction 1984

L.TIME	JAN	FEB	MAR	APR	MAY	JUN	JUL	AUG	SEP	OCT	NOV	DEC
0030	337	345	354	001	232	276	257	252	197	353	333	335
0130	340	347	355	005	242	274	249	254	207	347	337	336
0230	340	350	356	007	245	275	246	263	231	356	340	340
0330	346	354	360	010	269	272	238	242	228	002	340	338
0430	346	353	001	008	282	265	230	255	236	006	342	342
0530	348	355	005	009	219	257	222	240	232	012	348	342
0630	348	001	008	015	157	254	221	236	210	010	351	345
0730	352	005	017	021	159	256	223	229	192	022	002	352
0830	006	019	027	033	141	268	235	238	197	035	014	006
0930	021	031	033	040	115	277	259	272	223	055	022	015
1030	033	035	038	043	115	288	271	281	222	058	024	021
1130	035	035	033	045	146	289	275	283	224	060	019	022
1230	030	029	028	034	116	288	279	290	244	050	009	014
1330	018	022	017	027	104	293	287	284	310	044	004	007
1430	001	016	009	017	064	299	300	301	353	022	356	001
1530	351	014	360	016	057	296	301	307	051	009	350	356
1630	359	011	356	011	019	297	308	311	006	004	348	347
1730	358	009	358	008	016	295	312	313	101	004	343	346
1830	354	358	356	002	015	298	277	318	154	011	336	342
1930	348	360	355	359	351	299	266	306	184	359	336	338
2030	346	355	355	355	355	295	249	266	193	352	331	338
2130	342	352	356	357	137	300	259	246	197	347	332	332
2230	340	349	356	359	185	304	250	259	224	350	332	335
2430	339	344	354	001	226	266	256	253	219	351	333	333

B5 Wad Madani potential wind speed (m/s) 1983

L.TIME	JAN	FEB	MAR	APR	MAY	JUN	JUL	AUG	SEP	OCT	NOV	DEC
0030	4.1	3.2	2.4	2.1	3.3	5.2	4.3	3.8	2.3	/	2.6	3.1
0130	4.0	3.4	2.3	2.1	3.3	5.6	4.7	3.7	2.4	/	2.4	3.2
0230	3.8	3.1	2.4	2.2	3.1	5.2	4.5	3.3	2.3	/	2.4	3.1
0330	3.6	3.0	2.4	1.9	2.7	5.0	4.3	3.4	2.1	/	2.3	3.2
0430	3.5	3.0	2.2	1.8	2.6	4.2	4.0	3.1	2.0	/	2.1	3.4
0530	3.2	3.2	2.1	1.7	2.7	4.0	3.6	2.8	1.6	/	2.1	3.1
0630	3.2	3.0	2.1	1.8	2.9	3.6	3.7	2.9	1.5	/	2.0	3.0
0730	3.6	3.4	2.5	2.4	3.4	4.6	4.5	4.0	2.1	/	2.2	3.3
0830	5.1	4.5	3.6	3.3	4.3	5.4	5.6	5.0	3.4	/	3.2	4.2
0930	5.6	5.0	4.0	3.5	4.5	6.0	6.5	5.6	4.1	/	3.6	4.5
1030	5.4	5.2	3.9	3.3	4.6	5.9	6.6	5.8	3.8	/	3.5	4.6
1130	5.3	4.9	3.7	3.0	3.6	5.4	6.2	5.3	3.5	/	3.3	4.2
1230	4.9	4.5	3.3	3.0	3.3	5.2	5.4	5.1	3.2	/	3.0	3.9
1330	4.8	4.4	3.4	2.9	3.5	4.7	4.7	4.7	2.8	/	2.9	4.0
1430	4.7	4.4	3.4	2.8	3.3	4.2	4.3	4.5	2.3	/	3.1	3.9
1530	4.8	4.4	3.3	3.0	3.4	3.9	4.3	4.2	2.2	/	3.4	4.1
1630	5.0	4.3	3.3	2.9	3.4	3.6	3.7	3.5	1.8	/	3.4	3.9
1730,	4.5	3.9	3.0	2.5	3.3	3.7	3.9	3.4	1.2	/	2.4	3.1
1830	4.0	3.0	2.4	2.0	2.8	3.7	3.4	2.5	0.7	/	2.1	2.8
1930	4.0	3.0	2.2	1.9	3.0	3.9	2.7	2.6	1.1	/	2.2	2.9
2030	4.1	3.2	2.3	2.1	3.3	3.8	3.3	2.6	1.4	/	2.5	3.0
2130	3.9	3.3	2.3	2.1	3.3	3.4	3.3	3.1	1.8	/	2.5	2.9
2230	4.0	3.2	2.4	2.1	3.1	4.0	3.6	3.0	2.3	/	2.7	3.1
2330	4.2	3.3	2.4	2.1	3.2	4.8	3.6	3.6	2.2	/	2.6	3.0

B6 Wad Madani potential wind speed (m/s) 1984

L.TIME	JAN	FEB	MAR	APR	MAY	JUN	JUL	AUG	SEP	OCT	NOV	DEC
0030	3.9	3.4	3.4	3.4	3.4	4.9	4.8	5.1	3.8	2.2	3.6	3.5
0130	3.9	3.8	3.4	3.5	3.4	4.8	5.1	4.6	3.5	2.4	3.7	3.6
0230	3.8	3.8	3.5	3.3	3.6	4.4	4.9	4.0	3.6	2.1	3.6	3.7
0330	3.6	3.9	3.3	3.0	3.1	4.3	4.9	3.3	3.5	2.2	3.4	3.6
0430	3.5	3.6	3.3	2.9	2.8	4.2	5.1	3.4	3.2	2.3	3.5	3.5
0530	3.3	3.3	3.2	2.7	2.8	4.3	4.7	3.6	3.6	2.1	3.2	3.3
0630	3.2	3.1	2.9	2.5	3.3	4.3	5.2	3.7	3.6	1.9	3.2	3.1
0730	3.4	3.5	3.5	3.0	4.2	6.3	6.3	4.9	4.7	2.3	3.7	3.6
0830	4.2	4.4	4.4	3.9	4.9	7.0	7.2	6.5	5.8	2.8	4.7	4.4
0930	5.0	4.8	4.9	4.5	5.3	7.1	7.3	6.9	5.8	3.0	4.9	4.9
1030	5.2	5.0	4.7	4.6	5.1	6.4	6.4	6.4	5.3	3.1	4.9	4.7
1130	5.0	5.1	4.4	4.4	4.6	6.0	6.0	5.8	4.7	3.1	4.4	4.5
1230	4.8	4.8	4.3	4.4	3.9	5.7	5.3	5.0	4.3	3.0	4.3	4.3
1330	4.8	4.7	4.4	4.3	3.7	5.6	5.1	4.6	3.9	2.8	4.4	4.4
1430	4.7	4.6	4.4	4.2	3.6	5.1	4.5	4.1	3.7	2.8	4.5	4.5
1530	4.8	4.7	4.8	4.3	3.4	4.9	4.2	3.7	3.2	3.1	4.4	4.4
1630	4.9	4.6	4.6	4.2	3.2	4.1	4.4	3.9	3.2	2.8	4.4	4.3
1730	4.3	4.0	4.2	4.0	3.2	4.1	3.7	3.7	3.1	2.5	3.5	3.6
1830	3.9	3.3	3.3	2.9	3.0	4.0	3.4	3.5	2.8	2.0	3.3	3.5
1930	4.1	3.3	3.4	2.8	3.1	3.0	3.1	3.4	2.9	2.0	3.4	3.6
2030	4.1	3.3	3.3	3.1	3.5	3.4	3.3	3.9	3.2	1.9	3.3	3.6
2130	4.0	3.4	3.3	3.1	3.5	4.2	3.4	3.9	3.0	2.1	3.5	3.5
2230	4.0	3.5	3.3	3.2	3.4	4.4	4.0	4.6	3.4	2.3	3.4	3.5
2330	4.0	3.5	3.5	3.2	3.6	4.8	4.7	5.0	3.6	2.3	3.6	3.7

B7 Wad Madani wind direction 1983

L.TIME	JAN	FEB	MAR	APR	MAY	JUN	JUL	AUG	SEP	OCT	NOV	DEC
0030	008	029	038	345	330	195	181	193	199	///	345	008
0130	011	029	039	347	341	191	180	195	198	///	348	008
0230	017	032	041	352	348	200	182	200	204	///	348	012
0330	016	035	041	355	010	208	186	200	192	///	354	019
0430	016	038	043	358	020	206	190	196	179	///	001	018
0530	016	040	046	003	039	204	196	185	169	///	011	019
0630	020	043	051	008	097	203	191	182	183	///	010	019
0730	023	045	058	017	110	212	186	192	191	///	016	026
0830	034	051	060	025	099	231	195	201	203	///	028	035
0930	037	051	060	027	107	220	202	208	210	///	031	040
1030	036	050	060	022	118	221	214	218	229	///	038	035
1130	035	048	056	014	164	230	214	220	232	///	029	026
1230	029	042	045	355	265	233	215	222	238	///	018	009
1330	022	040	033	339	284	232	212	222	242	///	349	002
1430	014	032	032	333	298	234	216	222	246	///	332	353
1530	009	028	028	327	292	238	221	225	254	///	326	352
1630	005	025	028	325	314	238	217	226	253	///	325	348
1730	002	025	024	331	318	247	212	214	235	///	325	344
1830	358	020	023	334	293	221	199	198	215	///	327	341
1930	357	022	027	329	305	204	191	198	184	///	333	348
2030	004	021	031	332	291	222	190	192	170	///	334	350
2130	005	026	031	332	298	216	190	187	187	///	340	354
2230	009	030	033	334	302	195	187	186	190	///	342	358
2330	009	031	037	341	305	215	187	188	194	///	344	004

B8 Wad Madani wind direction 1984

L.TIME	JAN	FEB	MAR	APR	MAY	JUN	JUL	AUG	SEP	OCT	NOV	DEC
0030	353	001	003	025	315	287	237	216	163	248	319	340
0130	355	002	005	032	341	272	230	218	161	320	318	341
0230	356	006	010	037	021	293	213	217	162	328	324	347
0330	359	012	013	038	032	308	208	216	152	333	324	348
0430	360	016	016	041	039	288	209	208	143	334	327	347
0530	002	020	021	045	058	286	216	193	137	354	332	351
0630	007	023	023	046	077	295	218	200	140	346	333	355
0730	011	026	032	053	080	304	216	207	154	018	336	354
0830	023	035	039	061	090	318	227	221	162	033	345	011
0930	028	034	041	063	061	325	241	228	175	046	356	018
1030	025	035	038	053	023	318	254	239	186	018	352	023
1130	022	033	033	064	026	323	259	244	194	030	345	013
1230	022	027	012	022	042	306	262	248	193	349	333	355
1330	005	019	360	021	079	329	276	250	195	322	320	346
1430	001	010	353	014	085	349	275	249	218	307	320	338
1530	357	003	347	011	357	319	278	250	217	292	320	336
1630	351	359	347	017	308	323	279	248	215	293	313	334
1730	347	359	342	017	034	320	275	245	214	278	309	333
1830	345	353	344	020	003	284	239	239	187	278	308	332
1930	345	352	347	019	033	323	235	234	193	294	308	334
2030	348	356	347	018	029	304	232	228	164	306	310	337
2130	351	356	355	020	026	257	231	214	143	309	316	337
2230	352	357	358	021	022	271	234	211	146	315	316	336
2330	355	350	002	023	010	267	240	208	159	324	318	338

B9 Potential wind seasonal standard deviation for Khartoum and Wad Madani

Station	Standard deviation of the potential wind							
	Winter		Advancing Monsoon		Monsoon		Retreating Monsoon	
	day	night	day	night	day	night	day	night
Khartoum	1.8	1.3	1.8	2.0	1.9	2.2	1.1	1.7
Wad Madani	1.0	0.9	1.8	2.0	2.0	2.3	1.0	0.9

Appendix C

Monthly potential wind frequency distribution from Khartoum and Wad Madani for 1983, '84.

C1 Khartoum potential wind frequency distribution 1984

RANGE	JAN	FEB	MAR	APR	MAY	JUN	JUL	AUG	SEP	OCT	NOV	DEC
0-1	000	000	013	020	077	017	061	074	067	057	049	007
1-2	002	006	063	041	155	065	163	122	122	119	192	098
2-3	028	051	151	082	186	167	206	169	101	277	228	149
3-4	123	111	137	125	111	191	121	166	216	131	141	110
4-5	206	164	153	127	057	094	068	077	069	065	060	085
5-6	168	107	107	094	128	065	107	056	066	064	046	027
6-7	084	092	094	065	022	020	014	028	025	024	012	110
7-8	055	084	024	077	024	018	022	018	024	021	006	055
8-9	050	042	011	024	017	009	014	019	014	003	003	019
9-10	022	027	003	009	002	002	001	003	004	000	000	001
10-11	005	012	001	014	001	001	003	000	004	000	000	003
11-12	000	000	000	004	000	000	002	000	002	000	000	000
12-13	000	000	000	000	000	000	000	000	002	000	000	000
13-14	000	000	000	004	001	000	000	000	000	000	000	000
14-15	000	000	000	000	000	000	000	000	000	000	000	000
15-16	000	000	000	000	000	000	000	000	000	000	000	000
16-17	000	000	000	000	001	000	000	000	000	000	000	000

C2 Khartoum potential wind frequency distribution 1983

RANGE	JAN	FEB	MAR	APR	MAY	JUN	JUL	AUG	SEP	OCT	NOV	DEC
0-1	000	004	004	019	099	031	073	029	071	021	000	000
1-2	005	012	058	087	254	139	094	078	189	045	020	003
2-3	030	092	159	131	185	125	121	151	191	090	100	087
3-4	108	135	186	137	107	133	158	171	120	177	246	174
4-5	158	119	093	133	030	098	059	103	047	186	124	147
5-6	164	120	072	115	025	078	088	137	035	094	150	136
6-7	137	090	086	056	006	039	032	036	012	064	051	095
7-8	114	078	060	027	009	038	037	015	012	045	018	072
8-9	017	016	019	007	001	011	056	003	009	017	004	019
9-10	006	005	004	008	001	007	012	002	003	001	000	008
10-11	005	001	000	000	001	009	006	001	006	001	000	003
11-12	000	000	002	000	000	005	003	000	000	000	000	000
12-13	000	000	000	000	000	001	001	000	001	000	000	000
13-14	000	000	000	000	000	003	003	000	000	000	000	000
14-15	000	000	000	000	000	000	000	000	000	000	000	000
15-16	000	000	000	000	000	001	000	000	000	000	000	000
16-17	000	000	000	000	000	001	000	000	000	000	000	000
17-18	000	000	000	000	000	000	001	000	000	000	000	000
18-19	000	000	000	000	000	000	000	000	000	000	000	000
19-20	000	000	000	000	000	001	000	000	000	000	000	000

C3 Wad Madani potential wind frequency distribution 1983

RANGE	JAN	FEB	MAR	APR	MAY	JUN	JUL	AUG	SEP	OCT	NOV	DEC
0-1	000	001	016	072	064	043	050	036	219	///	026	007
1-2	002	037	155	204	118	088	091	067	174	///	146	066
2-3	077	133	296	233	209	130	106	168	071	///	203	179
3-4	259	261	178	149	145	119	130	164	064	///	054	276
4-5	202	146	070	050	082	076	095	116	041	///	005	140
5-6	130	064	018	011	027	065	076	098	015	///	000	056
6-7	066	026	011	001	032	062	078	048	010	///	000	016
7-8	005	002	000	000	032	052	055	026	060	///	000	004
8-9	000	000	000	000	013	028	036	013	000	///	000	000
9-10	000	001	000	000	009	015	014	001	001	///	000	000
10-11	000	000	000	000	005	009	008	002	000	///	000	000
11-12	000	000	000	000	000	009	001	000	000	///	000	000
12-13	000	000	000	000	000	007	002	000	000	///	000	000
13-14	000	000	000	000	000	004	001	000	000	///	000	000
14-15	000	000	000	000	000	005	000	000	000	///	000	000
15-16	000	000	000	000	000	002	000	000	000	///	000	000
16-17	000	000	000	000	000	000	000	000	000	///	000	000
17-18.	000	000	000	000	000	001	000	000	000	///	000	000
18-19	000	000	000	000	000	000	000	000	000	///	000	000
NR	003	001	000	000	008	005	001	005	001	///	000	000

C4 Wad Madani potential wind frequancy distribution 1984

RANGE	JAN	FEB	MAR	APR	MAY	JUN	JUL	AUG	SEP	OCT	NOV	DEC
0-1	000	001	007	003	070	049	017	013	070	072	000	000
1-2	011	022	032	053	104	081	077	074	077	163	016	014
2-3	104	111	179	211	183	102	102	140	184	310	151	134
3-4	257	265	265	231	144	087	115	144	121	153	255	243
4-5	201	084	120	125	071	087	109	106	064	028	169	249
5-6	047	045	064	051	062	060	066	071	073	016	114	094
6-7	016	006	059	042	032	063	111	074	046	020	012	006
7-8	001	000	015	003	027	080	068	062	038	000	003	003
8-9	000	000	002	001	030	044	048	040	016	000	000	001
9-10	000	000	000	000	011	034	013	012	008	000	000	000
10-11	000	000	000	000	004	020	006	003	007	000	000	000
11-12	000	000	000	000	001	040	001	003	005	000	000	000
12-13	000	000	000	000	001	080	000	001	004	000	000	000
13-14	000	000	000	000	002	000	000	000	001	000	000	000
14-15	000	000	000	000	001	001	000	000	000	000	000	000
15-16	000	000	000	000	000	000	000	000	000	000	000	000
NR	001	000	000	000	001	000	000	001	006	000	000	000

REFERENCES

Abele J.: 1975 'Der Energiehaushalt der Erdoberfläche in der Regen- und
    Trockenzeit (Tsumeb/SWA, Mitt. 9)', Meteor. Rundschau 28, 139-147.

ABu Bakr, E.H.: 1980, 'Study of a cylindrical parabolic concentrator',
    B.Sc.Thesis, Phys. Dept., Univ. Khartoum, Sudan.

ABu Bakr, E.H., Rutten, M., Smulders, P.T., Vossers, G., Wieringa, J.: 1986,
    'A method to obtain a wind model for the boundary layer in a
    representative tropical region', Proc. Europ. Wind Energy Conf., Rome,
    Vol. 1, 213-218.

ABu Bakr, E.H.: 1988, 'Central Sudan surface wind data and climate
    characteristics', Sci. Rep. 88-1, Roy. Neth. Meteor. Inst. (KNMI), De Bilt

Barbour, K.M.: 1961, 'The Republic of the Sudan regional geography',
    University of London Press, U.K..

Beyrich, F., Klose, B.: 1988: 'Some aspects of modelling low-level jets',
    Bound. Layer Meteor. 43, 1-14.

Bhalotra, Y.P.R.: 1963, 'Meteorology of Sudan', Memoir no. 6, Sudan
    Meteorological Service

Bhumralkar, C.M., Mancuso, R.L., Ludwig, F.L. , Renne, D.S., 1980: 'A
    practical and economic method to estimate wind characteristics at
    potential wind energy conversion sites', Solar Energy 25, 55-65.

Blackadar, A.K.: 1957, 'Boundary-layer wind maxima and their significance for
    the growth of nocturnal inversions, Bull. Am. Meteor. Soc. 38, 283-290.

Brost, R.A., Wyngaard, J.C.: 1978, 'A model study of the stable stratified
    planetary boundary layer', J. Atmos. Sci. 35, 1427-1440.

Brutsaert, W.: 1975, "Comments on surface roughness parameters and the height
    of dense vegetation', J. Meteor. Soc. Japan 53, 96-97.

Brutsaert, W.: 1982, 'Evaporation into the atmosphere: theory, history and application', Reidel, Dordrecht, Netherlands, 229 pp.

Budyko, M.I.: 1956, 'The heat balance of the earth's surface' (in Russian; Gidrometeoizdat, Leningrad), English transl. (1958) by N.A. Stepanova: U.S. Dept. Commerce, Washington D.C..

Buursink, J.: 1971, 'Soils of Central Sudan', Ph.D. Thesis, Univ. Utrecht, Netherlands

Caughey, S.J.: 1982, ' Observed characteristics of the atmospheric boundary layer'. In: F.T.M. Nieuwstadt and H. van Dop (eds.), 'Atmospheric Turbulence and Air Pollution Modelling', Reidel, Dordrecht, Netherlands, pp. 107-158.

Clarke, R.H.: 1970, ' Observational studies in the atmospheric boundary layer', Quart. J. Roy. Meteor. Soc. 96, 91-114.

Costa, J.: 1985, 'Wind energy project Sudan proposal', Report CWD/DHV, Amersfoort, Netherlands.

Davenport, A.G.: 1960, 'Rationale for determining design wind velocities', J. Am. Soc. Civ. Eng. ST-86, 39-69.

Deardorff, J.W.: 1974, 'Three-dimensional numerical study of the height and mean structure of a heated planetary boundary layer', Bound.-Layer Meteor. 7, 81-106.

Deardorff, J.W.: 1972, 'Parameterization of the planetary boundary layer for use in general circulation models', Monthly Weath. Rev. 100, 93-106.

De Bruin, H.A.R., Holtslag, A.A.M.: 1982, 'A simple parameterization of the surface fluxes of sensible and latent heat during daytime compared with the Penman-Monteith concept', J. Appl. Meteor. 21, 1610-1621.

Driedonks, A.G.M.: 1981, 'Dynamics of the well-mixed atmospheric boundary layer. Ph.D. Thesis, Univ. Amsterdam, (KNMI Sc. Rep. 81-2, pp. 189.

Duchêne-Marullaz P.: 1977, 'Distributions statistiques et cartographie des vitesse moyennes de vent en France; applications a l'énergie éolienne', Centre Scient. Techn. Bâtiment (Nantes) Rep. EN-CLI-77-1.

Duensing, G., Grunewald, G., Martens, G.: 1985, 'Die Windverhaltnisse in überseeischen Landern in Hinblick auf die Windkraftnutzung (Africa)', Einzelveroff, Seewetteramt Deutscher Wetterd. (Hamburg) 111, 115 pp.

Dyer, A.J.: 1974, 'A review of flux-profile relationships'. Bound.-Layer Meteor. 7, 363-372.

Dutton, J.A.: 1986, 'An introduction to the theory of atmospheric motion'. Publ. Constable Ltd., U.K.

Exell, R.H.B., Fook, C.T.: 1986, 'The wind energy potential of Malaysia', Solar Energy 36, 281-289.

Farquharson, J.S.: 1939, 'The diurnal variation of wind over tropical Africa', Quart. J. Roy. Meteor. Soc. 65, 165-183 and 452-454.

Garratt, J.R.: 1982, 'Surface fluxes and nocturnal boundary-layer height; J. Appl. Meteor. 21, 725-729.

Griffiths, J.F., Soliman, K.H.: 1972, 'The Northern desert (Sahara)'. In: 'Climates of Africa', World Survey of Climatology 10 (Elsevier, Amsterdam) 75-131.

Gryning, S.E., Larsen, S.E.: 1981, 'Relation between dispersion characteristics over surfaces with dissimilar roughness and atmospheric stability, under conditions of equal geostrophic winds', Atm. Env. 15, 983-987.

Hamid, Y.H., Jansen, W.A.M.: 1981, 'Wind energy in Sudan', Report CWD 81-2, Amersfoort, Netherlands.

Handbook of Weather Forecasting, 1975 U.K. Meteorological Office Rep. no. Met.0.875.

Holton, J.P.: 1972, 'An introduction to dynamic meteorology', Academic Press, New York, pp. 319.

Holtslag, A.A.M., Van Ulden, A.P.: 1983, 'A simple scheme for daytime estimates of the surface fluxes from routine weather data', J. Clim. Appl. Meteor. 22, 517-529.

Idso, S.B., Jackson, R.D.: 1969, 'Thermal radiation from the atmosphere', J. Geophys. Res. 74, 5397-5403.

Kondratyev, K.Y.: 1969, 'Radiation processes in the atmosphere', WMO No. 309.

Krishna, K.: 1968, 'A numerical study of the diurnal variation of meteorological parameters in the planetary boundary layer-diurnal variations of winds', Monthly Weath. Rev. 96, 269-276.

Koracin, D., Berkowicz, R.: 1988, 'Nocturnal boundary-layer height: observation by acoustic sounders and prediction in terms of surface-layer parameters. Bound.-Layer Meteor. 43, 65-83.

Lawson, T.: 1971, 'Haboob structure at Khartoum', Weather 26, 105-112.

List, R.J.: 1966, 'Smithsonian meteorological tables', Smithsonian Institution, U.S.A.

Mayer, H., Walk, O.: 1973, 'Bodentemperaturen und Bodenwärmestrom in der Trockenzeit (Tsumeb/SWA, Mitt. 2)', Meteor. Rundschau 26, 18-23.

Mayer, H.: 1974, 'Statistische Bearbeitung der Windgeschwindigkeits- und Windrichtungs-daten (Tsumeb/SWA, Mitt. 6)', Meteor. Rundschau 27, 181-187.

Menenti, M.: 1984, 'Physical aspects and determination of evaporation in desert, applying remote sensing technique', Ph.D. Thesis and Rep. 10 of Inst. for Land and Water Management Research, Wageningen, Netherlands.

Munn, R.E.: 1966, 'Descriptive micrometeorology', Academic Press, New York.

Monin, A.S., Yaglom, A.M.: 1971, 'Statistical fluid mechanics: mechanics of turbulence', Vol. 1, MIT Press, Cambridge, U.S.A.

Nieuwstadt, F.T.M.: 1981, 'The nocturnal boundary layer'. Ph.D. Thesis Univ. Amsterdam (KNMI Sc. Rep. 81-1).

Nieuwstadt, F.T.M.: 1984, 'Some aspects of turbulent stable boundary layer', Boundary Layer Meteor. 30, 31-55.

Noordwijk, M. van: 1984, 'Ecology textbook for Sudan', Khartoum University Press.

Oke, T.R.: 1978, 'Boundary layer climates'. Methuen, London, U.K., 372 pp.

Paulson, C.A.: 1970, 'The mathematical representation of wind speed and temperature profiles in the unstable atmospheric surface layer', J. Appl. Meteor. 9, 857-861.

Petersen, E.L., Troen, I., Wieringa, J.: 1984, 'Development of a method for wind climate analysis for non-mountainous terrain in Europe', Proc. Europ. Wind Energy Conf., Hamburg, 6-12.

Petersen, E.L., Troen, I., Frandsen, S., Hedegaard, K.: 1981, 'Windatlas for Denmark', Risø National Laboratory R-428, Denmark.

Peterson, W.C.T., Parton, W.J.: 1983, 'Diurnal variations of wind speeds at short grass prairie sites ,- a model', Agric. Meteor. 28, 365-374.

Pielke, R.A., Mehring, P.: 1977, 'Use of mesoscale climatology in mountaineous terrain to improve the spatial representation of mean monthly temperature', Monthly Weath. Rev. 105, 108-112.

Plate, E.: 1982, 'Engineering meteorology', Elsevier, Amsterdam, 740 pp.

Reed, J.W.: 1975, 'Wind power climatology', Weatherwise 27, 237-242.

Riehl, H.: 1979, 'Climate and weather in the tropics', Academic Press, N.Y., U.S.A.

Simiu, E.: 1973, 'Logarithmic profiles and design wind speeds', J. Am. Soc. Civ. Engin. EM-99, 1073-1083.

Smeda, M.: 1979, 'Incorporation of planetary boundary layer processes into numerical forecasting models', Bound.-Layer Meteor. 16, 116-129.

Stevens, M.J.M., Smulders, P.T.: 1979, 'The estimation of the parameters of the Weibull wind speed distribution for wind energy utilization purposes', Wind Engineering 3, 132-145.

Sutton, L.J.: 1923, 'The climate of Khartoum', Min. Publ. Works, Egypt Physical Dept. Pap. 9.

Ten Berge, H.F.M.: 1986, 'Heat and water transfer at the bare soil surface', Ph.D. Thesis, Agric. Univ. Wageningen, Netherlands.

Tennekes, H.: 1973a, 'A model for the dynamics of the inversion above a convective boundary layer, J. Atmos. Sci. 30, 558-567.

Tennekes, H.: 1973b, 'The logarithmic wind profile', J. Atmos. Sci. 30, 234-238.

Tetzlaff, G.: 1982, ' Nordafrikanische Passat im Winter', Berichte des Inst. Meteor. Klim. Univ. Hannover 22, F.R. Germany.

Thorpe, A.J., Guymer, T.H.: 1977, 'The nocturnal jet', Quart. J. Roy. Meteor. Soc. 103, 643-654.

Thams, J.C.: 1953, 'Erfahrungen mit einem neuen Uberzug der Lamellen des Bimetallaktinographen Fuess-Robitzsch', Geof. Pura Applic. 24, 115-124.

Van Dop, H., De Haan, B.J., Engeldal, C.A.: 1982, 'The KNMI mesoscale air pollution model', KNMI Sc. Rep. 82-6.

Van Ulden, A.P., Holtslag, A.A.: 1985, 'Estimation of atmospheric boundary layer parameters for diffusion applications', J. Clim. Appl. Meteor. 24, 1196-1207.

Van Wijk, W.R.: 1963, 'Physics of plánt environment', North Holland Publ., Amsterdam

Venkatram, A.: 1980, 'Estimating the Monin-Obukhov length in the stable boundary layer for dispersion calculations', Bound.-Layer Meteor. 19, 481-485.

Walk, O.: 1972, 'Beiträge zur Meteorologie eines Steppengebiets (Tsumeb/SWA, Mitt. 1)', Meteor. Rundschau 25, 163-170.

Walk, O., Wieringa, J.: 1988, 'Tsumeb studies of the tropical boundary-layer climate synopsis of publications on a savannah observation project of Karlsruhe University', Wiss. Ber. Meteor. Inst. Univ. Karlsruhe 11.

Weather Bureau RSA: 1975, 'Climate of South Africa, Part 12: Surface winds'. Report WB-38, Pretoria, R.S.A.

Wieringa, J.: 1983, 'Description requirements for assessment of non-ideal wind stations - for example Aachen', J. Wind Engin. Ind. Aerod. 11, 121-131.

Wieringa, J.: 1986, 'Roughness-dependent geographical interpolation of surface wind speed averages', Quart. J. Roy. Meteor. Soc. 112, 867-889.

Wieringa, J. and Rijkoort: 1983, ' Windklimaat van Nederland', Staatsuitgeverij, Den Haag, Netherlands.

Woodhead, T.: 1969, 'The diurnal variation of mean wind speed at four locations in Kenya and Tanzania', E. Afr. Agric. For. J. 35, 160-165.

Woodhead, T.: 1970, 'Mapping potential evaporation for tropical East Africa: the accuracy of Penman estimates derived from indirect assessments of radiation and wind speed', Intern. Ass. Sc. Hydrol. Publ. 92, 232-241.

Wyngaard, J.C.: 1975, 'Modeling the planetary boundary layer extension to the stable case', Bound.-Layer Meteor. 9, 441-460.

Zhang S.F., Oncley S.P., Businger, J.A.: 1988, 'A critical evaluation of the von Kárman constant from a new atmosphere surface layer experiment', 8th Am. Meteor. Soc. Symp. on Turbulence and Diffusion, 148-150.

Zilitinkevich, S.S.: 1972, 'On the determination of the height of the Ekman boundary layer', Bound.-Layer Meteor. 3, 141-145.

SUMMARY

This thesis is a contribution to solve the outstanding problem of
reliable assessment of wind energy potential in tropical African countries
without a sufficient number of meteorological stations. One solution for this
problem is the development of some models to interpolate horizontally between
the few available stations with surface wind and/or upper wind data. Such
models have been developed in the last decade for temperate-latitude
countries. However, they are based on geostrophic similarity principles,
assuming reasonably high Coriolis forces, while in the tropics such forces are
much smaller. Moreover, in the tropics the air flow is dominated by other
mechanisms, such as large stability variations in the atmosphere and the
monsoon phenomena, which cause the above mentioned models to be inappropriate.

To understand the physical processes of the tropical boundary layer wind
regime a representative tropical region is considered, which measures about
$(700 \times 800)km^2$ and lies between 12°N 30°E and 20°N 36°E in the Central Sudan.
We made a detailed study of the climatological and geographical
characteristics of the region. The topography of the region is relatively
flat. The climate of this region is semi-desert, and is strongly dependent on
the Inter Tropical Convergence Zone (I.T.C.Z.), the high pressure belts and
the low pressure belts.

In order to be able to develop a climate model for Central Sudan and to
check its accuracy, we constructed a sufficiently detailed and reliable data
base. For this purpose unprocessed meteorological data (about 330×10^3
observations) from eight Sudanese stations, consisting of surface data and
limited upper air soundings, were supplied by the Sudanese Meteorological
Department in Khartoum. For the used stations we described the station
surroundings and the quality of the observations. The data were processed by
computer and corrected for obvious errors. The wind surface data are further
corrected for local exposure deficiencies.

Statistical correlation analysis of the data showed that the constructed
data base is a reliable source for use in wind potential estimate and climate
modelling. From the frequency distribution analysis we found that the annual
wind frequency distribution gives unreliable estimates of the available wind
energy, and that separate seasonal distributions are required.

In a first step of climate modelling a so-called horizontal transposition

model is developed which deals with the surface wind. This quantitative transposition model consists of two parts. Firstly, a local boundary layer model, based on the energy balance equation and the Businger-Dyer flux-gradient equations, is used to compute the average diurnal cycle of various characteristic boundary layer parameters. Secondly, a horizontal transposition method is introduced to calculate the wind speed behaviour at an arbitrary station from that at a reference station. This method is based on the assumed spatial constancy of the turbulence parameter (u_*) in the period November – April in the region. The constancy of u_* is concluded from the very stationary character of the climate. The model-computed hourly wind speeds are in good agreement with the measured wind speed and provides better results than the conventional procedure, which assumes constant regional hourly wind speeds.

The diurnal cycle of the surface wind in the Sudan shows a distinctive behaviour; the wind speed shows a decrease from the morning to the afternoon, with a speed maximum around 10 o'clock Sudan local time. In literature this phenomenon is hardly investigated. This peculiar diurnal course is not only observed at the surface but up to 1 km above the surface, and it is not confined to Central Sudan but it is also observed in some other African countries between 20°N and 20°S.

In a later stage of this study the diurnal course of the height of the PBL is computed by applying a version of the inversion rise model of Tennekes (1973a), using the surface observations and the midday temperature profile. The computed height of the PBL shows good agreement with the estimated height from the upper air data in the region and with those published in literature for other Sahelian regions.

From the midday and midnight hodographs and the horizontal temperature gradient over Sudan we estimated the thermal advection over the region. During the day the thermal advection is homogeneous over the region, while during the night the thermal advection is variable across the region. Moreover, the comparison between the day and night wind profiles in Khartoum and Kassala stations indicate a diurnal wind course both within the PBL and above it. As far as we know, the diurnal course of the circulation above 2 km has not been reported before in Sahelian regions. This behaviour is suggested to be due to either local or mesoscale circulation. To understand such phenomena a more elaborate data base is indispensible.

The main accomplishments of this dissertation are the following:

i   It is shown that the construction of a data base from the available
    meteorological data results in useful material, both for wind energy
    potential estimates and for climate model development. A necessary
    preliminary job is the collection of sufficient information about
    observation procedures and the surroundings of the considered stations.
    Constructing a data base in this way is reliable as well as both faster
    and more economical than assembling a data base using a new network of
    measuring equipment.

ii For estimation of wind energy in Sahelian regions it is erroneous to rely
    upon the annual frequency distribution. Monthly frequency distributions
    give more accurate estimates because of the large seasonal variation of
    the wind speed in these regions.

iii The stationary character of the climate over the inland Sahelian region
    (except in the monsoon season) is a very favourable condition for
    modelling the surface boundary layer.

iv A transposition boundary layer model is developed, which computes the
    average diurnal cycle of the surface wind speed for an arbitrary location
    where no wind data are available. The model results are in good agreement
    with the measured wind speed.

v   The diurnal course of the height of the PBL is modelled using only the
    surface observations and the midday temperature profile. The computed
    height of the PBL is in good agreement with the estimated PBL height from
    the upper air data.

vi The uncommon morning maximum in the diurnal cycle of the surface wind
    might be partly explained by the momentum downward transfer from a
    dissipating nocturnal low level jet. Analysis of the role of the diurnal
    course of the circulation needs more detailed upper air data than those
    available for this study.

SAMENVATTING

Dit proefschrift draagt bij aan het oplossen van een bestaand probleem:
de betrouwbare schatting van beschikbare windenergie in de landen van tropisch
Afrika, waar onvoldoende weerstations zijn. Een mogelijke oplossing van dit
probleem is de ontwikkeling van modellen voor horizontale interpolatie tussen
de weinige stations, waarvan windgegevens beschikbaar zijn aan de grond en/of
in de hogere atmosfeer. Dergelijke modellen zijn in de afgelopen decade
ontwikkeld voor landen in gematigde breedten. Ze zijn evenwel gebaseerd op
geostrofische similariteitsbeginselen met aanname van aanmerkelijke Coriolis-
krachten, terwijl in de tropen deze krachten geringer zijn. Bovendien wordt in
de tropen de luchtstroming beheerst door andere factoren, zoals grote
variaties in verticale stabiliteit, of optreden van moessons, zodat boven-
genoemde modellen slecht toepasbaar zijn.

Voor bestudering van natuurkundige aspecten van het windgedrag in de
luchtlaag nabij de bodem in de tropen is een representatief gebied genomen ter
grootte van omstreeks 700 x 800 km^2, gelegen tussen 12°NB 30°OL en 20°NB 36°OL
in Soedan. De klimatologische en geografische eigenschappen van de streek zijn
in detail bestudeerd. Het gebied heeft een relatief vlakke topografie. Het
klimaat van het gebied is woestijnachtig en is sterk afhankelijk van de
Intertropische Convergentiezone (ITCZ) en van de gordels van hoge en lage
druk.

Om voor het centrale gebied van Soedan een klimaatmodel te kunnen
ontwikkelen en toetsen, werd een betrouwbaar en voldoende gedetailleerd
gegevensbestand opgebouwd. Voor dit doel werden door de Soedanese
Meteorologische Dienst omstreeks 330.000 onbewerkte meteorologische gegevens
verstrekt, zowel oppervlaktewaarnemingen als een beperkt aantal bovenlucht-
sonderingen. Van gebruikte stations zijn de omgeving en de kwaliteit van de
waarnemingen nagegaan. De gegevens werden in de computer gebracht en
gecontroleerd op duidelijke fouten. De windmetingen van de oppervlaktestations
werden bovendien gecorrigeerd voor effecten van plaatselijke beschutting.

Een statistische correlatie-analyse toonde aan, dat het voltooide
gegevensbestand betrouwbaar is voor gebruik bij schattingen van windpotentieel
en bij modellering van het klimaat. Uit een analyse van frequentieverdelingen
bleek, dat uit de jaarverdeling van de windfrequenties slechts onbetrouwbare
schattingen van beschikbare windenergie te maken zijn. Voor goede energie-

schattingen zijn afzonderlijke verdelingen nodig voor de verschillende
seizoenen.

Als eerste stap bij de klimaatmodellering werd een zogenaamd horizontaal
transpositie-model ontwikkeld, dat betrekking heeft op de oppervlaktewind. Dit
kwantitatieve transpositiemodel bestaat uit twee delen. Ten eerste wordt een
grenslaagmodel, gebaseerd op de energiebalansvergelijking en de Businger-Dyer
flux-gradiënt-vergelijkingen, gebruikt om de gemiddelde dagelijkse gang van
verscheidene karakteristieke grenslaagparameters te berekenen. Ten tweede
wordt een horizontale transpositie-methode ingevoerd om het windgedrag op een
willekeurig station te berekenen uit dat op een referentie-station. Deze
methode is gebaseerd op de aanname, dat in de periode November-April de
turbulentieparameter u_* over dit gebied ruimtelijk niet varieert. De
constantheid van u_* wordt afgeleid uit het zeer gelijkmatige karakter van het
klimaat. Plaatselijke uurgemiddelde windsnelheden, die met het model berekend
zijn, stemmen beter overeen met waargenomen windsnelheden dan het resultaat
van de gewoonlijke aanname, dat de windsnelheid in een gegeven uur over het
hele gebied dezelfde is als die van het weerstation.

De dagelijkse gang van de oppervlaktewind in Soedan vertoont een
bijzonder gedrag: vanaf halverwege de morgen tot het eind van de middag neemt
de windsnelheid af, nadat een maximale waarde is bereikt omstreeks 10 uur
plaatselijke tijd. In de literatuur is dit verschijnsel slechts terloops
bestudeerd. Deze merkwaardige dagelijkse gang treedt niet alleen op aan het
oppervlak maar ook tot op 1 km hoogte, en het verschijnsel beperkt zich niet
tot Soedan maar wordt ook waargenomen in sommige andere Afrikaanse landen
tussen 20°NB en 20°ZB.

In het vervolg van deze studie wordt de dagelijkse gang van de hoogte van
de atmosferische grenslaag berekend door toepassing van een versie van het
inversiestijgingsmodel van Tennekes (1973a), met gebruikmaking van de
oppervlaktewaarnemingen en van het temperatuurprofiel midden op de dag. De
berekende grenslaaghoogte stemt goed overeen met schattingen uit de regionale
bovenlucht-waarnemingen en met gepubliceerde hoogten uit andere gebieden in de
Sahel.

De warmte-advectie in Soedan is geschat uit de middernacht- en middag-
hodografen en uit de regionale horizontale temperatuurgradiënt. Overdag is de

warmte-advectie regionaal homogeen, terwijl 's nachts de advectie varieert over het gebied. Bovendien blijkt uit de vergelijking van dag- en nacht-windprofielen te Khartoum en te Kassala, dat een dagelijkse gang niet alleen optreedt in de grenslaag, maar ook daarboven. Voorzover wij weten is voor de Sahel niet eerder gerapporteerd, dat boven 2 km hoogte de circulatie een dagelijkse gang vertoont. De oorzaak van dit gedrag wordt gezocht in lokale of mesoschaal-circulatie, en om dergelijke verschijnselen te begrijpen zal een uitgebreider gegevensbestand noodzakelijk zijn.

De belangrijkste resultaten van dit proefschrift zijn de volgende:

(1) Aangetoond wordt, dat het opbouwen van een gegevensbestand uit beschikbare weergegevens nuttig materiaal oplevert, zowel voor schatting van beschik-bare windenergie als voor ontwikkeling van klimaatmodellen. Noodzakelijk is, dat vooraf voldoende informatie wordt vergaard over de waarnemings-procedures en de omgeving van de aanwezige weerstations. Bestandsopbouw langs deze weg is betrouwbaar, en zowel sneller als goedkoper dan de aanmaak van een gegevensbestand met behulp van een nieuw waarnemings netwerk.

(2) Voor schatting van de windenergie in de Sahel is het onjuist om de wind-frequentieverdeling van het gehele jaar te gebruiken. Maandelijkse frequentieverdelingen geven betrouwbaarder schattingen vanwege de grote seizoensvariaties in de regionale wind.

(3) Het gelijkmatig karakter van het klimaat in het binnenland van de Sahel (uitgezonderd de moessontijd) schept een gunstige situatie voor het modelleren van de atmosfeer nabij de grond.

(4) Een transpositiemodel voor de grenslaag is ontwikkeld, dat de gemiddelde dagelijkse gang van de oppervlaktewind kan berekenen voor een willekeurige plaats waar geen windgegevens beschikbaar zijn.

(5) De dagelijkse gang van de grenslaaghoogte in Soedan is gemodelleerd, slechts uitgaande van de oppervlaktewaarnemingen en van het temperatuur-profiel in de planetaire grenslaag (PGL) midden op de dag. De berekende grenslaaghoogten stemmen goed overeen met schattingen van de PGL-hoogte uit bovenlucht-waarnemingen.

(6) Het merkwaardige ochtendmaximum in de dagelijkse gang van de oppervlakte wind kan gedeeltelijk worden verklaard uit neerwaarts impulstransport vanuit een dissiperend nachtelijk grenslaag-windmaximum. Analyse van de rol van dagelijkse variaties van de circulatie vereist uitgebreidere bovenlucht-gegevens dan beschikbaar waren voor deze studie.

CURRICULUM VITAE

13 July 1959	Born at Atbara (Sudan)
1970-1976	High School; Camboni Sister's School (Khartoum), finished with an Oxford O-level Certificate
1976-1981	Study Physics at University of Khartoum. Finished with a B.Sc. Honour's Degree
1981-1984	Doctoraal Study in experimental physics in the group of Prof. dr. N. Poulis at University of Leiden
1984-1988	Ph.D. Study at the technical University of Eindhoven in the Laboratory of Fluid Dynamics and Heat Transfer under the supervision of Prof. dr. G. Vossers and Prof. dr. J. Wieringa (KNMI).

STELLINGEN (propositions)

I

The understanding and modelling of the observed low-level-jet of the wind in the Sahel region, especially during the day, is an important aspect for prediction of locust swarm-migration.

Pedgley, E.E., 1981, Vol. 1, C.O.P.A., London (U.K.).

II

For wind energy application in tropical regions, the estimation of the wind potential from the annual or 24-hour averages results in erroneous estimates.

Chapter 4 of this thesis.

III

For the purpose of wind potential evaluation, the construction of a wind data base, using the available hourly meteorological observations, is reliable and more economical than installation of new net-work of wind measuring equipment.

Chapter 4 and 5 of this thesis.

IV

The sandstorms in the Sahel regions which may reach a maximum gust of about 50 m/s with unpredictable wind direction should be taken into consideration in windmills safety design.

Lawson, T., 1981, Weather 26, 105-112.

V

The present state of the available information from the European Centre for Medium Range Weather Forecasts (ECMWF) does not allow an accurate estimate of the wind potential for the tropical African region.

VI

In the absence of understanding local cooking practices, the transfer of woodstove techniques among developing countries is counter-productive.

Bussmann, P.J.T., 1988, Ph.D. Thesis, Eindhoven.

VII

The theoretical work of the clarinet by Benade and Kouzoupis (1988) and Schumacher (1981) is based on an empirical formula proposed by Backus (1963) which has not been confirmed neither theoretically nor experimentally.

Benade, A.H. and Kouzoupis, S.N., 1988, J. Acoust.
Soc. Am. 83, 1, p. 292.
Schumacher, R.T., 1981, J. Acustica, 48, 2, p.71.
Backus, J., 1963, J. Acoust. Soc. Am. 35, 3, p. 305.

VIII

Given a Blasius boundary-layer in incompressible fluid with temperature-independent transport properties. If a harmonic oscillation is imposed on the (constant) main flow, then the relative correction of the time average heat flux (Q) in the limit of high frequencies is given by:

$$\frac{Q(\omega) - Q(\omega = \infty)}{Q(\omega = \infty)} = - \left[\frac{\alpha}{\omega x}\right]^2 \left[\frac{3P}{8(1+P)(1+\sqrt{P})^2}\right],$$

where α and ω are the maximum velocity and circular frequency of the oscillator vibration, x represents the downstream distance from the beginning of the boundary layer and P is the Prandtl number.

IX

Modelling of the neural structure with binary elements, comparable to the spin of electrons in spin glasses, oversimplifies the functioning of the actual neural structure.

Hopfield, J.J. and Tank, W., 1987, Science, 233, 625-633.

X

Participation in top-level sporting competition is both physically and psychologically harmful.

Seoul Olympics, 1988.

E.H. ABu Bakr

Eindhoven, 20th December 1988